

ACTA GEO TECHNICA S LOVENICA

2014/1

mirko grošič & željko arbanas
TIME-DEPENDENT BEHAVIOUR OF REINFORCED CUTS IN
WEATHERED FLYSCH ROCK MASSES

osman sivrikaya et al.
EFFECTS OF GROUND GRANULATED BLAST-FURNACE SLAG ON THE
INDEX AND COMPACTION PARAMETERS OF CLAYEY SOILS

dipova nihhat et al.
SETTLEMENT OF WEAKLY CEMENTED TUFAS

jože kortnik et al.
HIGH SAFETY PILLARS STABILITY CONTROL USING EL BEAM
DISPLACEMENT SENSORS IN LIPICA II QUARRY

j.w. li & h.b. wang
ANALYTICAL SOLUTIONS TO ONE-DIMENSIONAL CONSOLIDATION IN
UNSATURATED SOILS CONSIDERING NON-DARCY LAW OF WATER FLOW

bhagwanjee jha & d. n. singh
FORMATION OF MESO- AND MICRO- PORES IN FLY-ASH ZEOLITES BY
THREE-STEP ACTIVATION

ustanovitelji **founders**

Univerza v Mariboru, Fakulteta za gradbeništvo
University of Maribor, Faculty of Civil Engineering

Univerza v Ljubljani, Fakulteta za gradbeništvo in geodezijo
University of Ljubljana, Faculty of Civil and Geodetic Engineering

Univerza v Ljubljani, Naravoslovnotehniška fakulteta
University of Ljubljana, Faculty of Natural Sciences and Engineering

Slovensko geotehniško društvo
Slovenian Geotechnical Society

Društvo za podzemne in geotehniške konstrukcije
Society for Underground and Geotechnical Constructions

izdajatelj **publisher**

Univerza v Mariboru, Fakulteta za gradbeništvo
University of Maribor, Faculty of Civil Engineering

odgovorni urednik **editor-in-chief**

Bojana Dolinar University of Maribor

uredniki **co-editors**

| | |
|-------------------|-------------------------|
| Jakob Likar | University of Ljubljana |
| Janko Logar | University of Ljubljana |
| Borut Macuh | University of Maribor |
| Stanislav Škrabl | University of Maribor |
| Helena Vrecl Kojc | University of Maribor |
| Bojan Žlender | University of Maribor |

posvetovalni uredniki **advisory editors**

| | |
|-----------------------|--|
| Heinz Brandl | Vienna University of Technology |
| Chandrakant. S. Desai | University of Arizona |
| Pedro Seco e Pinto | National Laboratory of Civil Engineering |

lektor **proof-reader**

Paul McGuinness

naklada **circulation**

300 izvodov - issues

cena **price**

25 EUR/letnik - 25 EUR/vol.; (50 EUR for institutions/za institucije)

tisk **print**

ROLGRAF tiskarna Medvode d.o.o.

uredniški odbor **editorial board**

| | |
|-----------------------|---|
| Amin Barari | Aalborg University |
| Theodoros Hatzigogos | Aristotle University of Thessaloniki |
| Vojkan Jovičič | IRGO-Ljubljana, President of the SloGeD |
| Rolf Katzenbach | Technical University Darmstadt |
| Nasser Khalili | The University of New South Wales, Sydney |
| Bojan Majes | University of Ljubljana |
| Milan Maksimović | University of Belgrade |
| Svetlana Melentijevic | RodioKronsa, Soletanche-Bachy Group, Spain |
| Borut Petkovšek | Slovenian National Building and Civil Engineering Institute |
| Mihael Ribičič | University of Ljubljana |
| César Sagaseta | University of Cantabria |
| Patrick Selvadurai | McGill University |
| Stephan Semprich | University of Technology Graz |
| Devendra Narain Singh | Indian Institute of Technology, Bombay |
| Abdul-Hamid Soubra | University of Nantes |
| Kiichi Suzuki | Saitama University |
| Antun Szavits-Nossan | University of Zagreb |
| Ivan Vaniček | Czech Technical University in Prague |

naslov uredništva **address**

ACTA GEOTECHNICA SLOVENICA
Univerza v Mariboru, Fakulteta za gradbeništvo
Smetanova ulica 17, 2000 Maribor, Slovenija
Telefon / Telephone: +386 (0)2 22 94 300
Faks / Fax: +386 (0)2 25 24 179
E-pošta / E-mail: ags@uni-mb.si

spletni naslov **web address**

<http://www.fg.uni-mb.si/journal-ags/>

Revija redno izhaja dvakrat letno. Članki v reviji so recenzirani s strani priznanih mednarodnih strokovnjakov. Baze podatkov v katerih je revija indeksirana: SCIE - Science Citation Index Expanded, JCR - Journal Citation Reports / Science Edition, ICONDA - The international Construction database, GeoRef. Izid publikacije je finančno podprla Javna agencija za raziskovalno dejavnost Republike Slovenije iz naslova razpisa za sofinanciranje domačih periodičnih publikacij.

The journal is published twice a year. Papers are peer reviewed by renowned international experts. Indexation data bases of the journal: SCIE - Science Citation Index Expanded, JCR - Journal Citation Reports / Science Edition, ICONDA - The international Construction database, GeoRef. The publication was financially supported by Slovenian Research Agency according to the Tender for co-financing of domestic periodicals.

VSEBINA

| | |
|----|---|
| 2 | bojana dolinar UVODNIK |
| 4 | mirko grošič in željko arbanas ČASOVNO ODVISNO OBNAŠANJE OJAČANIH ZASEKOV V PREPERELIH FLIŠNIH KAMNITIH MASA |
| 18 | osman sivrikaya in drugi UČINKI MLETE GRANULIRANE PLAVŽNE ŽLINDRE NA INDEKSNE IN ZBIJALNE PARAMETRE GLINENIH TAL |
| 28 | dipova nihar in drugi USEDANJE ŠIBKO CEMENTIRANEGA TUF |
| 40 | jože kortnik in drugi MONITORING STABILNOSTI VISOKIH VARNOSTNIH STEBROV Z EL PALIČNIMI MERILCI DEFORMACIJ V KAMNOLOMU LIPICA II |
| 50 | j.w. li in h.b. wang ANALITIČNE REŠITVE ENODIMENZIONALNE KONSOLIDACIJE NENASIČENIH ZEMLJIN OB UPOŠTEVANJU NE-DARCYJEVEGA ZAKONA VODNEGA TOKA |
| 62 | ghagwanjee jha in d. n. singh TVORJENJE MEZOPOR IN MIKROPOR V ELEKTROFILTRSKEM PEPELU ZEOLITA S TRI-STOPENJSKO AKTIVACIJO |
| 70 | NAVODILA AVTORJEM |

CONTENTS

| | |
|---|----|
| bojana dolinar EDITORIAL | 3 |
| mirko grošič and željko arbanas TIME-DEPENDENT BEHAVIOUR OF REINFORCED CUTS IN WEATHERED FLYSCH ROCK MASSES | 5 |
| osman sivrikaya et al. EFFECTS OF GROUND GRANULATED BLAST-FURNACE SLAG ON THE INDEX AND COMPACTION PARAMETERS OF CLAYEY SOILS | 19 |
| dipova nihar et al. SETTLEMENT OF WEAKLY CEMENTED TUFAS | 29 |
| jože kortnik et al. HIGH SAFETY PILLARS STABILITY CONTROL USING EL BEAM DISPLACEMENT SENSORS IN LIPICA II QUARRY | 41 |
| j.w. li and h.b. wang ANALYTICAL SOLUTIONS TO ONE-DIMENSIONAL CONSOLIDATION IN UNSATURATED SOILS CONSIDERING NON-DARCY LAW OF WATER FLOW | 51 |
| ghagwanjee jha and d. n. singh FORMATION OF MESO- AND MICRO- PORES IN FLY-ASH ZEOLITES BY THREE-STEP ACTIVATION | 63 |
| INSTRUCTIONS FOR AUTHORS | 71 |

UVODNIK

Ob deseti obletnici izhajanja revije Acta Geotechnica Slovenica, se je ob koncu leta 2013 z mesta glavnega urednika poslovil prof. dr. Ludvik Trauner. Bil je pobudnik ustanovitve revije, kot glavni urednik pa zaslužen tudi za njeno doseganje primerljive kvalitete s sorodnimi revijami, kar je v petem letu izhajanja omogočilo uvrstitev revije v Thomsonovo bazo Science Citation Index Expanded in Journal Citation Reports/Science Edition. Kljub številnim težavam je prof. dr. Ludviku Traunerju uspelo, tudi s pomočjo urednikov in članov uredniškega odbora ter ob finančni pomoči Javne agencije za raziskovalno dejavnost Republike Slovenije in soustanoviteljev revije, zagotoviti redno izhajanje revije. Ob tej priložnosti se mu zato vsi sodelujoči pri reviji najlepše zahvaljujemo, uvodnik pa namenjamo kratki predstavitvi njegovega dela.

Prof. dr. Ludvik Trauner se je posvečal tako znanstvenemu in strokovnemu delu na področju geotehnike kot prenašanju teh znanj na študente in sodelavce. V domačih in tujih revijah je objavil številne znanstvene in strokovne članke in sodeloval na pomembnih znanstvenih srečanjih. Je član več strokovnih združenj ter uredniških odborov znanstvenih revij. Na področjih reoloških odnosov za zemljine, interakcije objekt-tla, temeljenja in stabilnostnih problemov pobočij ter nasipov je vodil številne nacionalne in mednarodne projekte, podal je nekatere izvirne rešitve s področja zahtevnih temeljenj in opravljal pomembne naloge v praksi.

Na Fakulteti za gradbeništvo Univerze v Mariboru, kjer je bil prof. dr. Ludvik Trauner med leti 1995 in 2010 tudi dekan, je ustanovil *Laboratorij za mehaniko tal* in zasnoval *Zbirko mineralov in fosilov*, ki omogočata študentom spoznavanje fizikalnih lastnosti zemljin in kamnin kot osnovo geotehničnega inženirstva. Sodeloval je pri nastajanju novega, uspešnega in kakovostnega študijskega programa Arhitektura, ki se izvaja v okviru Fakultete za gradbeništvo. Prof. dr. Ludvik Trauner je tudi eden izmed pobudnikov in ustanoviteljev mednarodnega doktorskega študijskega programa (JPhD) z naslovom *Geo-inženirstvo in Upravljanje z vodami*.

Bil je mentor oz. somentor številnim dodiplomskim študentom, magistrrom in doktorjem tehniških znanosti, svoja znanja pa je preko številnih vabljenih predavanj posredoval tudi študentom v tujini.

Kot nova glavna urednica revije Acta Geotechnica Slovenica se prof. dr. Ludviku Traunerju še enkrat zahvaljujem za uspešno vodenje revije.

Bojana Dolinar
Glavna urednica

EDITORIAL

The 10th anniversary of the first release of the journal *Acta Geotechnica Slovenica* sees the farewell of Prof. Dr Ludvik Trauner, who resigned as the editor-in-chief at the end of 2013. He was the initiator of the journal, and it is to his credit as the editor-in-chief that the quality of the journal matched that of related journals, which enabled its placement in Thomson's database Science Citation Index Expanded and in Journal Citation Reports/Science Edition in the fifth year of the journal's publication. Despite many problems and with the assistance of the editors and the editorial board members, as well as the financial help of the Slovenian Research Agency and the founders of the journal, Prof. Dr Ludvik Trauner managed to ensure the regular publication of *Acta Geotechnica Slovenica*. On this occasion, we his colleagues, would like to express our gratitude and therefore we have decided to devote the Editorial to short overview of his work.

Prof. Dr Ludvik Trauner dedicated his work to science and the geotechnical discipline as well as to transmitting his knowledge to students and co-workers. He published numerous scientific and professional articles in Slovenian and foreign journals, and his work was reported at important scientific meetings. He is a member of many Slovenian and international associations and the editorial boards of recognised journals. He led various national and international projects in the fields of rheological relations for soils, object-ground interactions, foundations, the stability of slopes and dykes. Moreover, he introduced some original solutions to demanding foundation works and performed important practical work.

At the Faculty of Civil Engineering, University of Maribor, where Prof. Dr Ludvik Trauner acted as dean between 1995 and 2010, he founded the *Laboratory for Soil Mechanics* and designed *The Collection of Minerals and Fossils*, which enable students to obtain knowledge about the physical properties of soils and rocks as a basis for geotechnical engineering. He participated in designing a new, successful and high-quality study programme in Architecture at the Faculty of Civil Engineering. Prof Dr Ludvik Trauner is also one of the initiators and founders of the international Ph.D. study programme *Geoengineering and Water Management*. He was a mentor and co-mentor to many undergraduate students, Masters and Ph.Ds. of Engineering, and he passed his knowledge on to students abroad through numerous invited lectures.

As the new editor-in-chief I would like to give my thanks to Prof Dr Ludvik Trauner for his successful editing of the journal.

Bojana Dolinar
Editor-in-chief

ČASOVNO ODVISNO OBNAŠANJE OJAČANIH ZASEKOV V PREPERELIH FLIŠNIH KAMNITIH MASAH

MIRKO GROŠIĆ IŃ ŹELJKO ARBANAS

o avtorjih

Mirko Grošić
Geotech Ltd.
Moše Albaharija 10a, 51000 Reka, Hrvaška
E-mail: mirko.grosic@geotech.hr

Źeljko Arbanas
University of Rijeka,
Faculty of Civil Engineering
Radmile Matejčić 3, 51000 Reka, Hrvaška
E-mail: zeljko.arbanas@gradri.uniri.hr

izvleček

Poznavanje napetostno-deformacijskih odnosov kamnitih mas je ključnega pomena za mnoge inženirske probleme. Deformacije kamnitih mas in njihov vpliv na konstrukcijo opazujemo med gradnjo, redko pa med uporabo. Deformacije v fazi uporabe povzročajo časovno odvisno obnašanje kamnitih mas. Fliš je opredeljen kot heterogena krhka kamnina, ki je zelo podvržena preperevanju in lahko razpade v zemljino do globine nekaj metrov pod površino. Ojačane zaseke vzdolž Jadranske magistrale v bližini Reke na Hrvaškem smo opazovali sedem let, tako v obdobju gradnje kot uporabe. Izmerjene deformacije so v času uporabe ceste dosegle pomembne velikosti kot posledica časovno odvisnega obnašanja kamnitih mas. V prispevku so predstavljeni rezultati obnašanja preperele flišne mase in njene lastnosti, ki temeljijo na podrobnem geotehničnem raziskovanju in spremljanju rezultatov ter na povratni analizi. Ugotovljeno je, da je globino preperevanja posameznih slojev flišnih mas mogoče ugotoviti s podrobnim geotehničnim raziskovanjem. Podane so priporočene vrednosti parametrov trdnosti, deformabilnosti in polzenja za profil preperevanja flišne kamnite mase.

ključne besede

časovno odvisno obnašanje, preperevanje, krhke kamnite gmote, Burgerjev model, povratna analiza

TIME-DEPENDENT BEHAVIOUR OF REINFORCED CUTS IN WEATHERED FLYSCH ROCK MASSES

MIRKO GROŠIĆ and ŽELJKO ARBANAS

about the authors

Mirko Grošić
Geotech Ltd.
Moše Albaharija 10a, 51000 Rijeka, Croatia
E-mail: mirko.grosic@geotech.hr

Željko Arbanas
University of Rijeka,
Faculty of Civil Engineering
Radmile Matejčić 3, 51000 Rijeka, Croatia
E-mail: zeljko.arbanas@gradri.uniri.hr

abstract

Knowledge of stress-strain rock mass behaviour is crucial for many engineering purposes. Rock mass deformations and their influences on construction are observed during construction and even during exploitation phases. These deformations in the exploitation phase are caused by the time-dependent behaviour of the rock mass. A flysch rock mass is categorised as a heterogenic weak rock that has been intensely subjected to weathering processes. Due to weathering processes, the flysch rock mass degrades from fresh rock to residual soil within only a few meters of the geological profile below the surface. Observations of reinforced cuts along the Adriatic motorway near the City of Rijeka, Croatia, were conducted over a time period of seven years of spanning construction and exploitation. Measured displacements reached significant magnitudes during the exploitation period as a consequence of the time-dependent behaviour of the rock mass. The paper presents findings related to flysch rock mass weathering profile and its characteristics based on detailed geotechnical investigations and monitoring results coupled with back analyses. It was found possible to detect the thickness of the flysch rock mass weathering profile by performing detailed geotechnical investigations. Recommendations for the strength, deformation, and creep properties of the weathering profile of a flysch rock mass are given.

keywords

time-dependent behaviour, weathering, weak rock mass, Burger model, back analyses

1 INTRODUCTION

CREEP MECHANICS

According to Hackley and Ferraris [1], rheology is the science of the deformation and flow of matter. The term creep is used to describe the response of a material to the instantaneous application of a constant stress. The term creep refers to intact rock, whereas the term time-dependent behaviour refers to the much larger volume of a rock mass. A rock mass consisting of intact rock and discontinuities is extremely heterogeneous compared with intact rock; therefore, the term time-dependent behaviour consolidates all these factors.

In creep mechanics, there are three different phases—primary, secondary or stationary, and tertiary creep phases—which are presented in Fig. 1. These three phases correspond to decreasing, stationary, and increasing creep strain rates, respectively, and were introduced by Andrade [2]. Immediately after applying a load, an instantaneous elastic strain occurs, followed by the primary creep phase. It is a delayed process and is recoverable after unloading. After this primary phase,

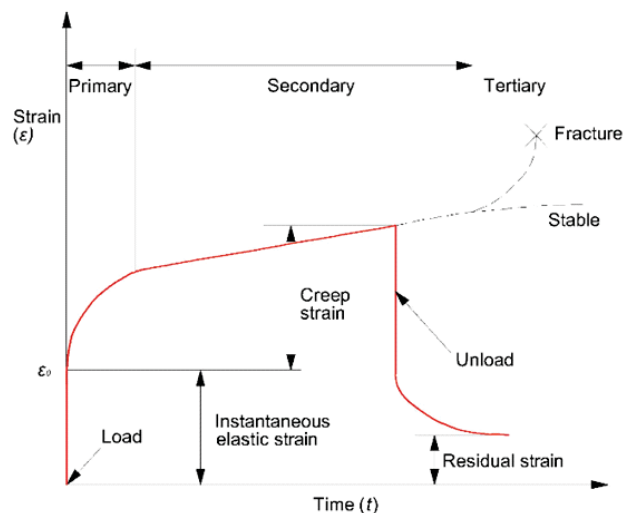


Figure 1. Time-strain curve and creep phases for specimen under constant load [33].

the secondary creep phase is characterised by a constant creep strain rate. The secondary creep phase is the longest of the entire creep processes and is usually observed as a linear strain rate. The final creep phase is tertiary creep, and it indicates a time-dependent deformation associated with crack growth and an increasing creep strain rate.

CREEP OF INTACT ROCK

The rheological parameters of different types of rocks have been comprehensively studied using numerous laboratory tests [3-6]. A few investigations have been performed on weak rocks, such as flysch rock masses [7-8] but the time-dependent behaviours of flysch rock cuts has never been thoroughly investigated.

Although the intact rock is generally part of a rock mass, it is very difficult to correlate the creep behaviour of intact rock and the time-dependent behaviour of a rock mass because of numerous associated variables such as the distribution, the frequency and creep characteristics of discontinuities, the scale effect, and the in situ stress distribution.

TIME-DEPENDENT BEHAVIOUR OF A ROCK MASS

Most of the studies conducted have been focused on the time-dependent behaviour of underground structures, whereas engineered slopes have been investigated in only a few studies. The behaviour of underground structures and slopes differs considerably because of many important factors, such as different stress fields, influence of weathering, pronounced inhomogeneity of layers and their parameters with depth, and increase in strength and deformability parameters with depth.

Panet [9] concluded that if very weak or heavily jointed or sheared rock is relatively homogeneous on a large scale, than it is reasonable to assume that the in situ rock mass

will follow trends similar to those obtained by laboratory tests. Several case studies have shown that there is no correlation between the creep parameters obtained from laboratory tests and the time-dependent behaviour of rock masses obtained from in situ measurements. To calibrate the equivalent rock mass creep parameters, Yu [10] used creep parameters obtained from laboratory tests (triaxial tests and a physical model of a tunnel) and concluded that even if there are significant differences between laboratory and in situ measured creep parameters, ratios between them and trends can be successfully determined.

The time-dependent behaviour of underground structures in rock masses has been detailed studied by many authors [9-18] while the time-dependent slope behaviour was less explored [19-23]. The time-dependent behaviour of reinforced cuts constructed in a weak rock mass, such as flysch, has never been investigated. In particular, the behaviour of the weathered profile as well as the variation in its strength, deformation, and creep properties has yet to be investigated.

2 WEATHERING OF A WEAK ROCK MASS

Weathering of a rock mass is a result of the destructive processes of atmospheric agents at or near the Earth's surface, whereas alteration is typically brought about by the action of hydrothermal processes. Both processes produce changes in the mineralogical composition of a rock, affecting colour, texture, composition, firmness, or form—features that result in a reduction of mechanical properties of a rock. Deterioration from weathering and alteration generally affects the walls of the discontinuities more than the interior of the rock [24]. During these processes, the fresh rock mass gradually transforms into residual soil – Fig. 2.

The description and classification of the state of weathering of a rock mass for engineering purposes has been

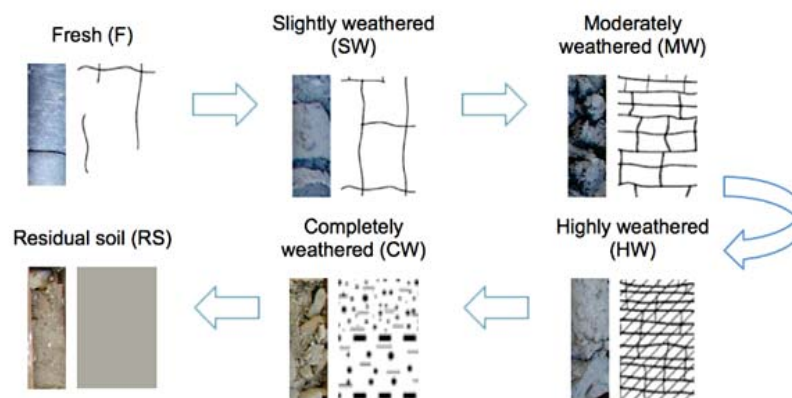


Figure 2. Process and grades of weathering in rock mass.

studied in detail by many authors [25-35]. Most of these classifications were established for a specific case, but the standard classification systems that have been recommended by several international committees are widely utilised and are most common in use: International Society for Rock Mechanics [36], British Standard Institution [37], the International Association of Engineering Geology [38].

Weak rock masses such as flysch have prominent weathering profiles below the surface that vary from residual soil (RS) and completely weathered (CW) rock mass near the surface, to highly weathered (HW) and moderately weathered (MW), to slightly weathered (SW) and fresh rock mass (F). A consequence of these different grades is a significant variation of the deformation and strength parameters with depth.

The deformation modulus for a rock mass weakened by weathering processes varies by several dozen times from low values for residual soils at the surface to very high values for a fresh rock mass in only a few meters of the weathering profile thickness. The strength reduction in slope layers due to the weathering of marl was investigated and numerically modelled by Eberhardt et al. [35] during the investigation of the Ruffi Landslide in Switzerland.

3 THE CASE STUDY OF DRAGA MOTORWAY

One of the most challenging sections of the Adriatic motorway along the Croatian Adriatic coast was constructed in the Draga Valley near the City of Rijeka during the period from 2004 to 2006. The Draga Motor-

way section is only 6.8 km long, but from geological, geotechnical, and construction points of view, it is a very complex transportation structure with 3 junctions, 2 tunnels, and several viaducts.

The major part of the motorway was constructed by cutting into the slopes made of a flysch rock mass. The stability of the cuts was established by reinforcing the rock mass with rockbolts and appropriate support systems such as multilayered shotcrete and reinforced concrete structures (Fig. 3).

GEOLOGICAL OVERVIEW

The geological fabric of the Draga Valley steep slopes is composed of limestone rock masses, and at the bottom of the valley, there are deposits of Paleogene flysch, which mainly consist of siltstone, with rare layers of sand, marl, and breccia. According to Arbanas et al. [39], the flysch rock mass is covered with slope formations, which tend to slide and denude the slope. The characteristic geological profile consists of clay cover originating from the disintegration of a flysch rock mass (RS) or brought gravitationally from hypsometrically higher parts of the slope, a layer of weathered flysch rock mass with variable characteristics that depend on the weathering stage (CW, HW, and MW), which significantly decreases with depth, and the fresh flysch zone as bedrock (SW and F).

WEATHERING PROFILE OF A FLYSCH ROCK MASS IN DRAGA VALLEY

The flysch rock mass in Draga Valley is mainly composed of a siltstone rock mass, which exhibits a visual transition from a completely weathered (CW) yellow coloured zone, through highly weathered (HW) and moderately

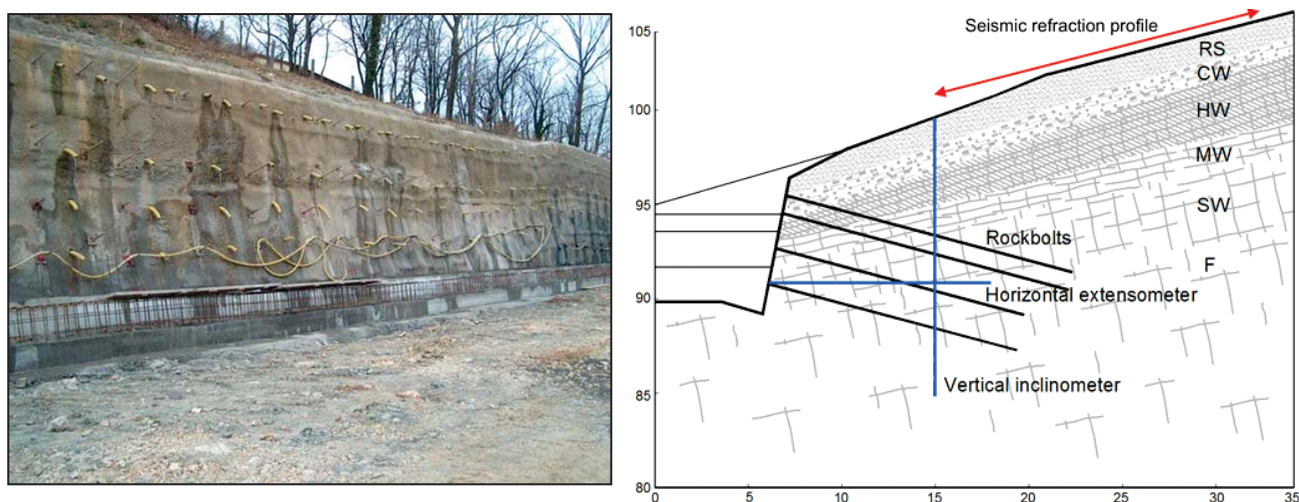


Figure 3. Reinforced cut in flysch rock mass at km 2+440.0: (left) during construction phase, and (right) cross section geometry.

weathered (MW), to the slightly weathered (SW) deposits and fresh rock mass (F) that are grey to blue (Fig. 2). In the zone of completely weathered siltstone, the rock mass is completely disintegrated, but the original structure of the rock mass is still intact. The layers of fresh siltstone have no visible weathering marks except for the colour change on the main discontinuity surfaces.

The weathering profile determination was based on geotechnical investigation, which consisted of drilling with core sampling, geophysical investigations, and laboratory tests. The depth of the weathering profile of the flysch rock mass with a complete transition from residual soil (RS) to fresh rock mass (F) was established as ranging from 5.0 to 8.0 m.

Determination of the geotechnical properties of the flysch rock mass during the geotechnical field investigations was difficult. During drilling, it was difficult to obtain undisturbed samples because of rock mass disintegration. Sudden degradation and disintegration of slightly weathered (SW) to fresh (F) siltstone occurred after removing geostatic loads and exposing the core to air and water. The consequence of these processes in the siltstone was that a very small number of undisturbed samples were taken for laboratory uniaxial strength tests.

There are other significant problems and unknowns when dealing with a heterogeneous flysch rock mass, which include vulnerability to weathering and sudden degradation and disintegration. These uncertainties include the following:

- The influence of weathering on reducing strength,
- Time dependence of weathering on reducing strength,
- Decrease in rock mass stiffness regarding the duration of the weathering process.

These unknowns are taken into account in geotechnical design by requiring higher safety factors and applying a conservative design approach based on limited experience.

GEOTECHNICAL INVESTIGATION RESULTS

Detailed geotechnical and geological studies of a flysch rock mass in Draga Valley were conducted and presented by Arbanas et al. [39-41].

The uniaxial strength of slightly weathered (SW) to fresh (F) siltstone obtained from uniaxial tests varied from 8 to 32 MPa. Obtaining undisturbed samples in completely (CW) to moderately weathered (MW) siltstone rock masses was not possible for the uniaxial test,

so point load tests (PLTs) were conducted immediately after drilling and sampling to avoid further weathering and strength reduction in the samples. A disadvantage of PLTs is the large dispersion of test results, which occurs especially in weak flysch rock masses. The use of this method is recommended when there is a lack of more reliable testing or a lack of appropriate representative samples and in combination with detailed descriptions of tested samples from the flysch rock mass. Test results of PLTs on fresh (F) siltstone samples showed that the representative uniaxial strength of these materials varies from 10 to 15 MPa, and in extreme cases, this value reached 20 MPa. The representative uniaxial strength of moderate (MW) to slightly weathered (SW) samples showed values <2 MPa. These values obtained from PLTs are uncertain and unacceptable for engineering analyses without adequate precautions.

The assessment of the strength parameters of the flysch rock mass was based on the Geological Strength Index (GSI) concept. Based on recommendations from Marinos and Hoek [42], a fresh (F) siltstone flysch rock mass from the Draga Valley slopes was placed in groups C to E, with GSI values from 10 to 30 [43], as shown in Fig. 4. The strength parameters are found to decrease as the weathering stage of the siltstone flysch rock mass increases, but the existing GSI estimate does not include the weathering grade as an influencing parameter that could affect the correction of the GSI value. This effect suggests the need for further evolution of the GSI concept in regard to different weathering categories of rock masses vulnerable to fast weathering processes.

Geophysical investigation involved seismic refraction and the downhole seismic survey method conducted during field investigations in the design phase. Additional geophysics investigations were performed at chainage 2+380.00 and 2+440.00 (Fig. 3) to obtain the thickness of the weathering profile of flysch and to investigate the distribution of shear wave's velocities through the weathering profile. Seismic refraction and a multichannel analysis of the surface wave method (MASW) were carried out at a length of 34.5 m with 24 channels and distances between geophones of 1.5 m. The results have shown that it is not possible to determine the disposition of the different grades of the weathering profile (from RS to F), but it is possible to determine the depth and the location of the fresh flysch rock mass – Fig. 5. Geophysics results were correlated with investigation drilling results and laboratory results, and it was observed that for longitudinal seismic wave velocities above 2,000.0 m/s, slightly weathered (SW) to fresh (F) flysch rock mass is present. Similar results were measured during field investigations at some other locations with similar geological profiles.

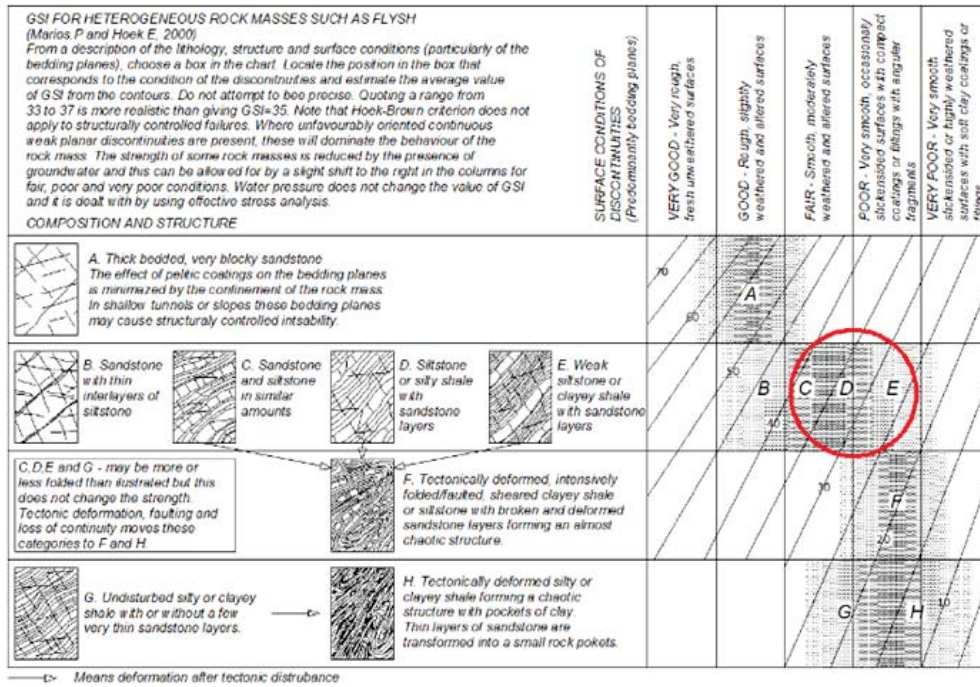


Figure 4. Properties of flysch rock mass in Draga Valley.

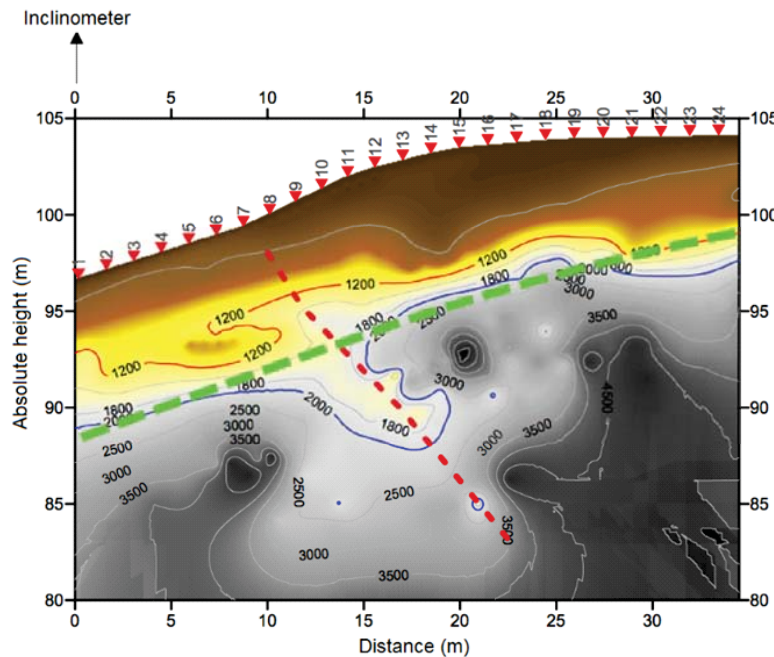


Figure 5. Longitudinal wave velocities obtained from seismic refraction measurement at chainage km 2+440.00 with marked border of SW to F flysch rock mass - green dashed line.

Geophysical investigations in correlation with other geotechnical investigations such as engineering geological core determination and classification and laboratory tests or in situ tests made it possible to determine the

borders of the slightly weathered (SW) and the fresh (F) flysch rock mass. This border also denotes the thickness of the weathering profile of the flysch rock mass, which is an important parameter for numerical analyses.

MONITORING DATA AND INTERPRETATION

The monitoring equipment were installed before construction included vertical inclinometers and horizontal extensometers installed in pairs, as shown in a cross section at chainage km 2+440.0, which was chosen as a representative cross section for the observation of the construction behaviour used in numerical analyses. Vertical inclinometer was installed in May 2004. and the reference measurement was carried out at 26th of May 2004., while the construction began at beginning of June 2004. The installed rockbolts were tested using pull-out tests, and the results of those tests made it possible to include the stiffness values of the installed anchors in numerical analyses.

The results of the horizontal displacement measurements at the vertical inclinometer at the chainage km 2+440.0 (Fig. 6) show that most of the displacement occurred in the upper part of the cut, i.e., in layers that

are characterised as residual soil (RS) to moderately weathered (MW) flysch rock mass. The maximum horizontal displacement occurred at the top of the inclinometer (6.0 mm), and the main part of these displacements occurred during the construction time period (3.9 mm) – marked in Fig. 6 as a dashed red line. The displacements that occurred during the exploitation period (2.1 mm) are significant and should not be neglected in the consideration of cut support stability analyses. Similar results were also obtained on other monitored profiles (0+560.0, 1+880.0, and 2+380.0), and it could be concluded that the delayed displacements reached up to 50% of the displacements that occurred during the construction time period – Table 2.

It is evident that most of the instantaneous displacements and time-dependent displacements occurred in the upper part of the cut and consisted of residual soil (RS) to moderately weathered (MW) flysch rock mass. A significant decrease of these displacements is observed as a function of the depth of the weathering profile of the flysch rock mass. Time-dependent displacements in the slightly weathered (SW) to fresh (F) flysch rock mass were not present and will not be considered and analysed in this research.

This transition between zones of different behaviour in the weathering profile of the flysch rock mass is evident and could be seen from monitoring results but also could be predicted from geotechnical investigation results.

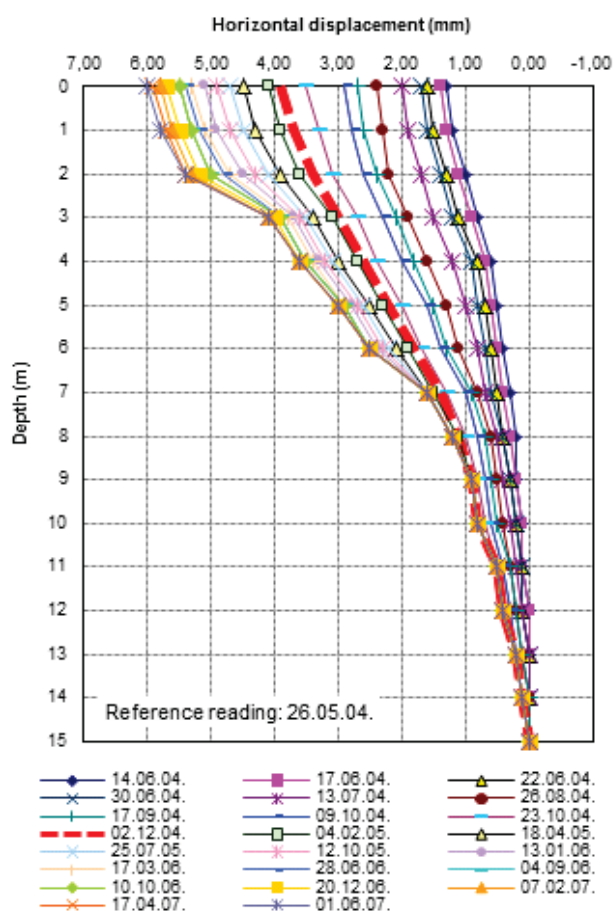


Figure 6. Measured horizontal displacements of vertical inclinometer installed at km 2+440.0 – end of construction phase is marked as dashed red line.

3 MODELLING OF THE TIME – DEPENDENT BEHAVIOUR OF THE FLYSCH ROCK MASS

BACK ANALYSIS

According to Cividini et al. [44], there are two different ways to conduct back analyses: the inverse approach and the direct approach. For the inverse approach, the formulation is the reverse of that in ordinary stress analyses, even though the governing equations are identical. According to this approach, the number of measured values should be greater than the number of unknown parameters, but it is unclear whether the method could be applied in geotechnical problems in which the measured values contain scattering. The direct approach to back analysis is based on an iterative procedure of correcting the trial values of unknown parameters by minimising the error function. Gioda and Maier [45] noted that a significant advantage of the direct approach method is that it may be applied to non-linear back analysis without reliance on a complex

Table 2. Review of measuring results at monitoring profiles through motorway in Draga valley.

| | Unit | 0+560 | 1+880 | 2+380 | 2+440 |
|---|------|-----------------|----------|----------|----------|
| Cut height | m | 4.2 | 4.6 | 7.20 | 7.40 |
| Inclinometer depth | m | 15.0 | 15.0 | 15.0 | 15.0 |
| Distance from the edge of the cut | m | 15.5 | 9.5 | 10.5 | 8.5 |
| End of construction date | - | 09/17/04 | 05/03/03 | 12/02/04 | 12/02/04 |
| Max. horizontal displacement (after construction phase) | mm | 1.80 | 1.00 | 3.60 | 3.90 |
| End of monitoring date | - | 06/01/07 | 02/22/12 | 06/01/07 | 06/01/07 |
| Max. horizontal displacement (after exploitation phase) | mm | 6.40 | 1.90 | 5.40 | 6.00 |
| Time period of monitoring in exploitation phase | days | 1,053 | 2,672 | 901 | 901 |
| Remark | - | Shallow sliding | - | - | - |

mathematical background. Cividini et al. [454] stated that standard algorithms of mathematical programming might be adopted for numerical solutions. Iterative solutions require quite time-consuming computations.

VISCOPLASTIC BURGER MODEL

There are many rheological models used to describe the creep behaviour of rock or the time-dependent behaviour of the rock mass. These models can generally be divided into two main categories: the classic viscoplastic models and the viscoplastic-damaged models. The constitutive laws in the classic viscoplastic models relate the current strain rate to the current stress directly, where the relationship between the deviatoric strain rate and the deviatoric stress are schematically represented

by a series of spring, dashpot, and plastic slider elements connected in parallel and/or in series. The constitutive laws in the viscoplastic-damaged models are based on the principle of strain and energy equivalence and are derived from a standard thermodynamic dissipation potential. In this study, the Burger viscoplastic model was used within the software package FLAC V7.0 [46]. The selection of a more complex creep model could lead to more complex numerical analyses with a significant number of input parameters as unknowns but also could make a questionable contribution to the final results.

The classical elastoplastic Burger model, or the Burger-Mohr Coulomb model, can be described by the constitutive law that includes elastic volumetric and viscoplastic deviatoric behaviour [46]. The model is schematically presented in Fig. 7 and consists of the Kelvin unit, the Maxwell unit, and the Mohr Coulomb unit, which are serially connected.

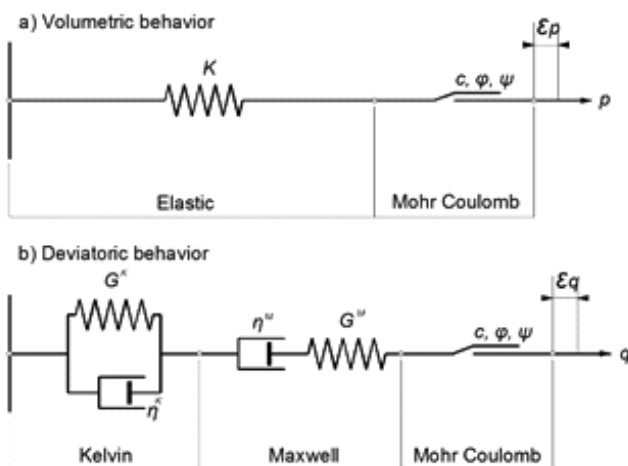


Figure 7. Sketch of Burger viscoplastic Mohr-Coulomb model: (a) volumetric behavior, and (b) deviatoric behavior [46].

The Kelvin unit is characterised by shear modulus G_K and viscosity η_K , the Maxwell unit by shear modulus G_M and viscosity η_M , and the Mohr-Coulomb unit by cohesion c , friction angle φ , and dilation angle ψ . The parameter G_K controls the total magnitude of the primary creep strain, or the so-called “delayed” elastic strain. A higher value of G_K denotes a lower amount of delayed strain, and the model tends to behave elastically in response to the applied stress. The viscosity parameter η_K controls the decaying rate of the primary creep strain of the material. A higher value of η_K denotes a longer time for the completion of the primary creep deformation phase. During the second creep phase, the parameter η_M controls the rate of increase of creep strain. A smaller value of this parameter denotes a more rapid increase of creep strain.

NUMERICAL ANALYSES

Numerical analyses and its results will be presented for the model established at the chainage 2+440; analyses conducted on other profiles (0+560.0, 1+880.0 and 2+380.0) showed similar results. Numerical analyses were performed in two phases: a construction phase (using elastoplastic Mohr-Coulomb model without taking into account time effects) and an exploitation phase (using Burger-Mohr-Coulomb model with taking into account time effects).

The numerical model used for the numerical analysis was divided into 7 different layers (geotechnical units) in reference to the geological weathering profile of the flysch rock mass. The disposition and thickness of these layers were defined based on geophysical measurements and longitudinal seismic wave velocities and divided into 7 groups: 0 – 400 – 800 – 1200 – 2000 – 3000 – 4000 m/s and higher, presented in Fig. 8. Those layers were described by different strength, deformability, and creep properties, which are summarised in Table 1. Similar determination of rock mass weathering grade in geological profile using seismic refraction method, MASW and electrical resistivity tomography method was presented in Olona et al. [47].

In the construction phase the slope was modelled using the linear elastoplastic Mohr-Coulomb model. Rockbolts in the model were defined as structural cables, with the stiffness obtained from in situ pull-out tests. Analyses were carried out in four stages, which represent excavation stages. After each stage, rockbolts and support construction installation were included in the model. The numerical model at the chainage 2+440 used for numerical analysis during the construction stage is presented in Fig. 8.

The back stress-strain analysis of the cut reinforced construction described above provided probable deformability parameter values: shear modulus, G , and bulk modulus, K , referring to the Mohr-Coulomb elastoplastic model. In the exploitation phase, the shear modulus, G , was used as the shear modulus of the Maxwell unit in the Burger model, G_M , whereas the shear modulus of the Kelvin unit, G_K , was taken as being ten times greater than G_M .

The exploitation phase analyses were carried out using the Burger-Mohr-Coulomb model for upper layers, denoted as RS, CW, HW, and MW, whereas the lower layers in the cut, denoted as SW and F, were modelled with the classic elastoplastic model and were not

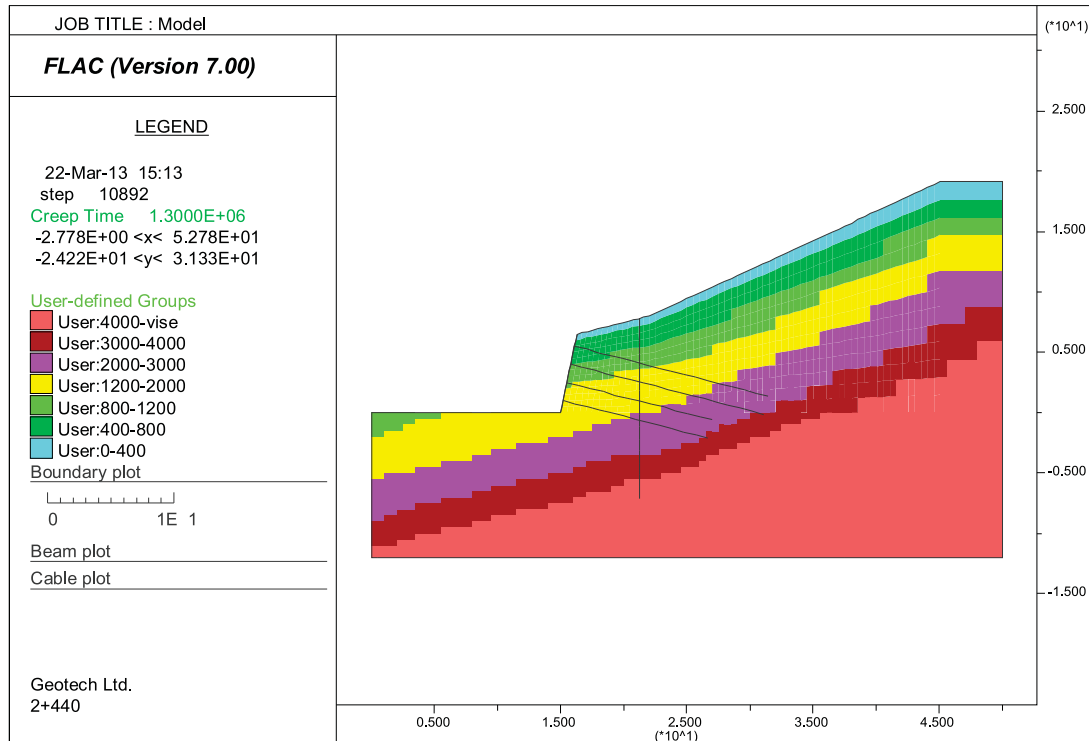


Figure 8. Numerical model at change km 2+440.0.

Table 1. Properties of different layers (geotechnical units) obtained from numerical back analysis of construction phase.

| | Symbol | Unit | GU 1 | GU 1 | GU 3 | GU 4 | GU 5 | GU 6 | GU 7 |
|----------------------------------|-----------|-------------------|--------|---------|----------|-----------|-----------|-----------|-------|
| Longitudinal wave velocity | v_p | m/s | 0-400 | 400-800 | 800-1200 | 1200-2000 | 2000-3000 | 3000-4000 | >4000 |
| Weathering grade | - | - | RS-CW | CW-HW | HW-MW | MW-SW | SW-F | F | F |
| Model | - | - | CVISC | CVISC | CVISC | CVISC | MC | MC | MC |
| Cohesion | c | kPa | 15 | 25 | 25 | 25 | 75 | 75 | 75 |
| Friction angle | φ | o | 25 | 32 | 32 | 32 | 32 | 32 | 32 |
| Poisson coefficient | ν | - | 0.25 | 0.25 | 0.25 | 0.25 | 0.25 | 0.25 | 0.25 |
| Mass density | γ | kg/m ³ | 2,200 | 2,200 | 2,200 | 2,200 | 2,200 | 2,200 | 2,200 |
| Shear modulus | G | kPa | 6.0e2 | 1.8e3 | 6.0e3 | 1.8e4 | 1.8e4 | 3.0e4 | 4.8e4 |
| Shear modulus of the Kelvin unit | G_K | kPa | 3.0e3 | 9.0e3 | 3.0e4 | 9.0e4 | - | - | - |
| Kelvin viscosity | η_K | kPamin | 3.0e10 | 5.0e10 | 5.0e10 | 1.0e11 | - | - | - |
| Maxwell viscosity | η_M | kPamin | 3.0e12 | 5.0e12 | 5.0e12 | 1.0e13 | - | - | - |

processed as time dependent. The initial stress and strain states in the model were obtained from construction phase modelling.

The determination of the Burger model parameters for each geotechnical unit was the most challenging part of numerical analyses. Because of numerous uncertainties, a simplified method for parameter estimation in the first iteration was used: the shear modulus of the Maxwell unit, G_M , in the Burger model was referred to as a shear modulus, G , in the elastoplastic model obtained from a back analysis carried out from the construction phase. The shear modulus of the Kelvin unit, G_K , that controls primary creep is set to be five times higher than the shear modulus of the Maxwell unit, G_M (i.e., $G_K=5G_M$). The creep parameters of the viscosity of the Kelvin unit, η_K , and the Maxwell unit, η_M , were assumed to satisfy $\eta_M/\eta_K=100$. The values of the creep parameters of the viscosity of the Kelvin unit η_K were varied from 3e13 for GU 1, 5e13 for GU 2 and GU 3 and 10e13 kPa min for GU 4. The viscosity of the Maxwell unit η_M varied from 3e15 for GU 1, 5e15 for GU 2 and GU 3 and 10e15 kPa min for GU 4. Similar relationships were obtained from other studies [10, 15, 17, 18, 21, 23].

Using those relationships in the parameter selection, the number of parameters determined in the creep back analyses was considerably reduced.

Back analyses of the time-dependent behaviour of engineered slopes in the flysch rock mass were performed using a trial and error method to obtain the creep parameters of materials in the numerical model.

RESULTS OF NUMERICAL ANALYSES AND INTERPRETATION

Analyses were iterated until the values obtained from the inclinometer monitoring and the numerical model agreed. Using the technique described above, the deformation parameters were identified for 7 different layers of the cut weathering profile throughout the depth of the cut. Back analyses of the time-dependent behaviour of the reinforced cut enabled an estimation of creep parameters for 4 upper layers of the weathering profile. Those parameters ensured satisfactory adjustment of the numerical simulation results to field measurements for the different time periods presented in Fig. 9. The deformability and creep parameters obtained for the flysch rock mass in the analysed cuts were used for further simulations of time-dependent reinforced cut behaviour in the 50-year time period of the exploitation period – Fig. 10. Displacements gradually developed from the lower region to the top of the cut, with the tendency of displacement diminishing over the time.

Analyses have shown that the time-dependent behaviour of reinforced rock mass cuts resulted in stress-strain redistributions during the time period of exploitation and it has a significant influence on the rock cut reinforcing system. It is well known that the forces on rockbolts strictly depend on realised deformation in the cut, which consequently affect the cut stability expressed by the factor of safety.

Rockbolts in the rock cut support were activated during the construction phase as a consequence of initial rock bolt prestressing and the actual realised deformation

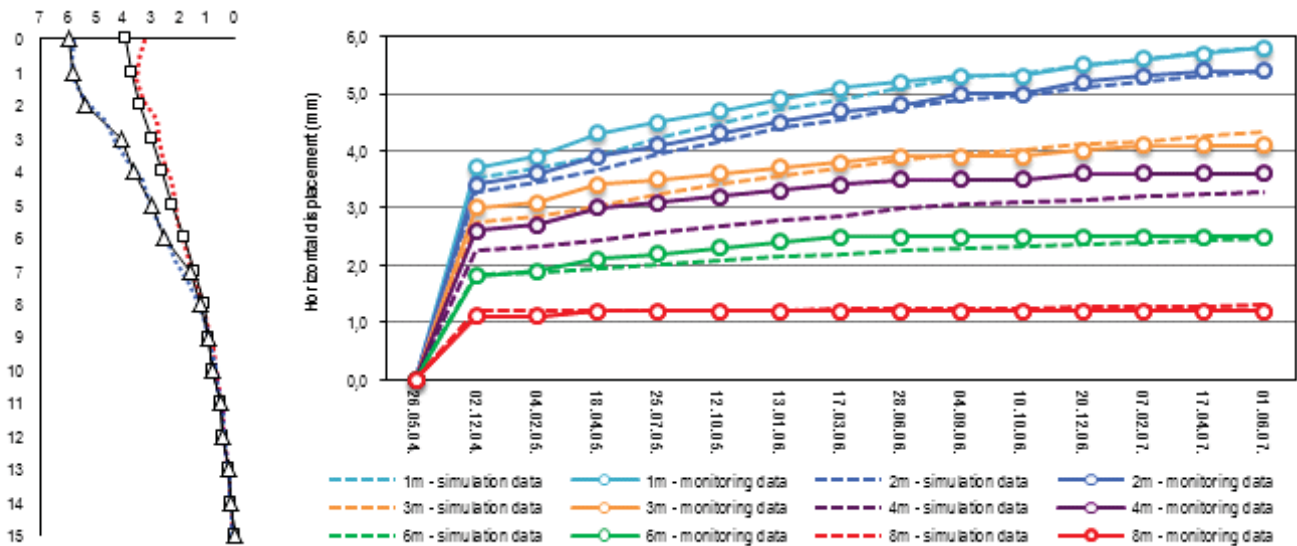


Figure 9. Results of numerical simulation and monitoring data at inclinometer at change km 2+440.0 (left) and displacements over time vs. depth of 1, 2, 3, 4, 6 and 8 m (right).

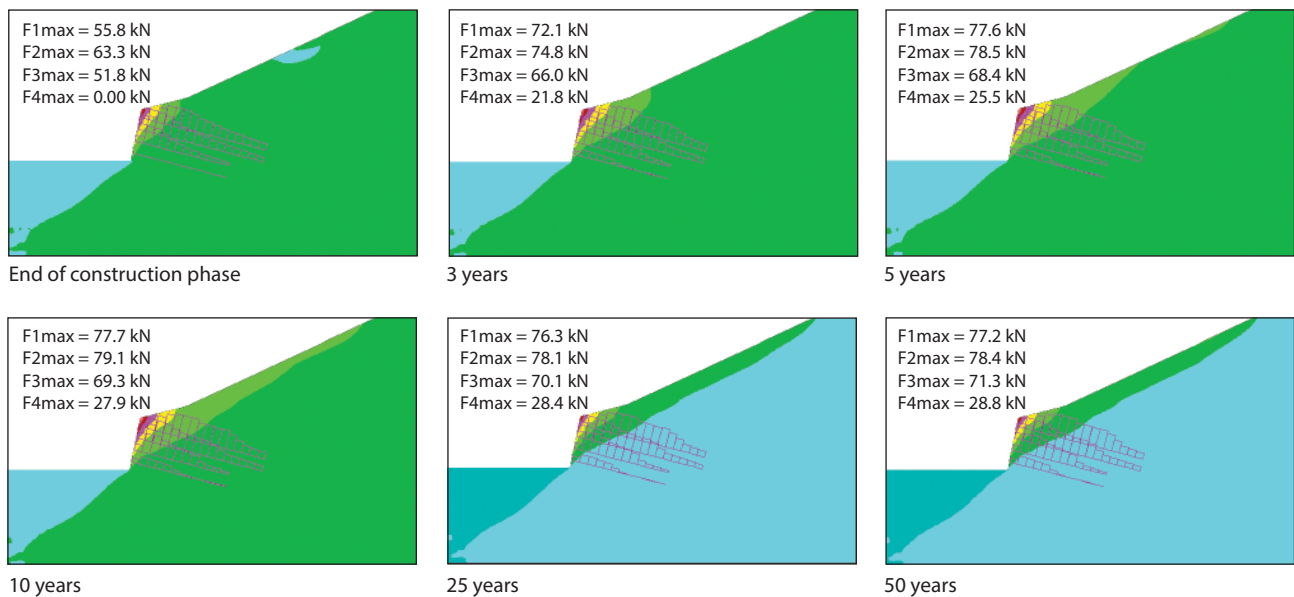


Figure 10. Propagation of horizontal displacements and axial forces distribution in rockbolts with maximal activated force in rockbolt during time period of 1, 3, 5, 10, 25 and 50 years.

in the cut due to excavation of consequent phases. In the case of no prestressing force in the fully grouted rockbolt, the lowest row of rockbolts, which was installed after the excavation was completed, was not activated, and the forces in the rockbolts were equal to

zero. The development of horizontal displacement over time consequently causes an increase in the forces on the rockbolts. The time-dependent behaviour of the reinforced cuts indicates that during the time period of exploitation, the stress and strain distribution affected

the activation of the bottom row of rockbolts and caused a significant redistribution of forces in all rockbolts and in the support construction – Fig. 10. It is noted that the axial forces in rockbolts increase during time. During time period of 5 years axial forces increase as follows: in the first (upper) row from 55.8 to 77.5 kN, in the second row from 63.3 to 78.4 kN, in the third row from 51.9 to 68.3 kN and in the fourth (bottom) row from 0.0 to 25.4 kN.

4 CONCLUSIONS

Flysch is categorised as a weak rock mass intensely subjected to weathering. Due to weathering processes, a flysch rock mass degrades from fresh rock to residual soil in only a few meters of the geological profile below the surface. This transition between different behaviours of the weathering profile of the flysch rock mass is evident and can be defined from geotechnical investigation results.

Displacements that occurred during the exploitation time period are significant and should not be neglected. It is evident that most parts of the instantaneous displacements and time-dependent displacements occurred in the upper part of the cut and consisted of residual soil (RS) to moderately weathered (MW) flysch rock mass layers. A significant decrease in these displacements is observed as a function of the depth of the flysch rock mass weathering profile. Parameters obtained from back analyses ensured satisfactory adjustment with numerical simulation results and field measurements for the different time periods.

In numerical analyses for geotechnical units from RS to MW, the shear modulus of the Kelvin unit, G_K that controls primary creep is set to be ten time higher than the shear modulus of the Maxwell unit, G_M . The creep parameters of the viscosity of the Kelvin unit, η_K , and the Maxwell unit, η_M , are taken as the ratio $\eta_M/\eta_K=100$. Using those relationships in parameter selection, the number of parameters determined in the creep back analyses was considerably reduced.

The development of displacement over time consequently causes an increase in the forces in the supporting systems such as rockbolts. The time-dependent behaviour of the reinforced cuts indicates that during the time period of exploitation, the stress and strain distribution affected the activation of the lowest row of rockbolts and caused a significant redistribution of forces in all other rockbolt rows and in the support construction.

REFERENCES

- [1] Hackley, A.V. and Ferraris, F.C. (2001). Guide to Rheological Nomenclature: Measurements in Ceramic Particulate Systems. NIST Special Publication 946, National Institute of Standards and Technology, Technology Administration, U. S. Department of Commerce
- [2] Andrade, E. (1910). The viscous flows in metals and allied phenomena. Proceedings of the Royal Society of London, Series A, Containing Papers of a Mathematical and Physical Character, Volume 84, Issue 567: 1-12
- [3] Maranini, E. and Brignoli, M. (1999). Creep behavior of a weak rock: experimental characterization. Int. J. of Rock Mechanics and Mining Sciences, Vol. 36, pp. 127-138.
- [4] Li, Y.S. and Xia, C.C. (2000). Time-dependent tests on intact rocks in uniaxial compression. Int. J. of Rock Mechanics and Mining Sciences, Vol. 37, pp. 467-475.
- [5] Fabre, G. and Pellet, F. (2006). Creep and time-dependent damage in argillaceous rocks. Int. J. of Rock Mechanics and Mining Sciences, Vol. 43, pp. 950-960.
- [6] Yang, S. and Jiang, Y. (2010). Triaxial mechanical creep behavior of sandstone. Mining Science and Technology, Vol. 20, pp. 339-349.
- [7] Tomanović, Z. (2006). Rheological model of soft rock creep based on the tests on marl. Mechanics of Time-dependent Materials, Vol. 10, pp. 135-154.
- [8] Fortsakis, P. and Kavvadas, M. (2009). Estimation of time dependent ground parameters in tunneling using back analyses of convergence data. Proc. Int. Conf. on Computational Methods in Tunneling, Ruhr University Bochum, Bochum
- [9] Panet, M. (1993). Understanding deformations in tunnels. Comprehensive Rock Engineering, Vol. 1, Pergamon Press.
- [10] Yu, C.W. (1998). Creep characteristics of soft rock and modelling of creep in tunnel. PhD Thesis, Department of Civil and Environmental Engineering University of Bradford, U.K
- [11] Gnirk, P.F. and Johnson, R.E. (1964). The deformational behavior of a circular mine shaft situated in a viscoelastic medium under hydrostatic stress. Proc. of 6th Symposium of Rock Mechanics, University of Missouri Roll.
- [12] Sakurai, S. (1978). Approximate time-dependent analysis of tunnel supports structure considering progress of tunnel face. Int. J. for Numerical Analytical Methods in Geomechanics, Vol. 2, pp. 159-175.

- [13] Gioda, G. (1981). A finite element solution of non-linear creep problems in rock. *Int. J. of Rock Mechanics and Mining Sciences & Geomechanics Abstracts*, Vol. 8, pp. 35–46.
- [14] Ladanyi, B. and Gill, D. (1984). Tunnel lining design in creeping rocks. *Proc. of Symposium on Design and Performance of Underground Excavations*, ISRM, Cambridge.
- [15] Goodman, R. E. (1989). *Introduction to Rock Mechanics*, Wiley, New York.
- [16] Likar, J. (2004). Back analyses of time-dependent displacement at the Trojane tunnel construction. *Acta Geotechnica Slovenica*, Vol. 1, pp. 21–36.
- [17] Likar, J., Vesel, G., Dervarič, E. and Jeromel, G. (2006). Time-Dependent Processes in Rocks. *RMZ – Materials and Geoenvironment*, Vol. 53, No. 3, pp. 285–301.
- [18] Guan, Z., Jiang, Y., Tanabashi, Y. and Huang, H. (2008). A new rheological model and its application in mountain tunneling. *Tunnelling and Underground Space Technology*, Vol. 23, pp. 292–299.
- [19] Martin, C.D. (1993). Time dependent behavior of rock slopes. PhD Thesis, University of London.
- [20] Feng, J., Chuhan, Z., Gang, W. and Guanglun, W. (2003). Creep Modeling in Excavation Analysis of a High Rock Slope. *J. of Geotechnical and Geoenvironmental Engineering*, Vol. 129, pp. 849–857.
- [21] Apuani, T., Masetti, M. and Rossi, M. (2007). Stress–strain–time numerical modelling of a deep-seated gravitational slope deformation: Preliminary results. *Quaternary International*, Vol. 171–172, pp. 80–89.
- [22] Kodama, J., Nishiyama, E. and Kaneko, K. (2009). Measurement and interpretation of long-term deformation of a rock slope at the Ikura limestone quarry, Japan. *Int. J. Of Rock Mechanics and Mining Sciences & Geomechanics Abstracts*, Vol. 46, pp. 148–158.
- [23] Bozzano, F., Martino, S., Montagna, A. and Prestinzi, A. (2011). Back analysis of a rock landslide to infer rheological parameters. *Engineering Geology*, Vol. 131–132, pp. 45–56.
- [24] Piteau, D.R. (1970). Geological factors significant to the stability of slopes cut in rock. *Proc. Symp. on Planning Open Pit Mines*, Johannesburg, South Africa.
- [25] Vargas, M. (1953). Some engineering properties of residual clay soils occurring in southern Brazil. *Proc. of the 3rd International Conference on Soil Mechanics and Foundation Engineering*, Zurich, Vol. 1, pp. 259–268.
- [26] Ruxton, B.P. and Berry, L. (1957). Weathering of granite and associated erosional features in Hong Kong. *Bulletin of Geological Society of America*, Vol. 68, pp. 1263–1292.
- [27] Ward, W.H., Burland, V.B. and Gallois, R.W. (1968). Geotechnical assessment of a site at Mundford, Norfolk for a large proton accelerator. *Géotechnique*, Vol. 18, pp. 399–431.
- [28] Chandler, R.J. (1969). The effect of weathering on the shear strength properties of Keuper marl. *Géotechnique*, Vol. 19, pp. 321–334.
- [29] Saunders, M.K. and Fookes, P.G. (1970). A review of the relationship of rock weathering and climate and its significance to foundation engineering. *Engineering Geology*, Vol. 4, pp. 289–325.
- [30] Fookes, P.G. and Horswill, P. (1970). Discussion on engineering grade zones. *Proc. of the In Situ Investigations in Soils and Rocks*, London, pp. 53–57.
- [31] Knill, J.L., Cratchley, C.R., Early, K.R., Gallois, R.W., Humphreys, J.D., Newbery, J., Price D.G. and Thurrell, R.G. (1970). The logging of rock cores for engineering purposes. *Geological Society Engineering Group Working Party Report, Quarterly Journal Engineering Geology*, Vol. 3, pp. 1–24.
- [32] Geological Society of London (1972). The preparation of maps and plans in terms of engineering geology. *Geological Society Engineering Group Working Party Report, Quarterly Journal Engineering Geology*, Vol. 5, pp. 293–382.
- [33] Lama, R.D. and Vutukuri, V.S. (1978). *Handbook on mechanical properties of rocks*. Trans Tech Publications, Clausthal, Germany.
- [34] Sancio, R.T. and Brown, I. (1980). A classification of weathered foliated rocks for use in slope stability problems. *Proc. of the 3rd Australia – New Zealand Conference on Geomechanics*, Wellington, Vol. 2, pp. 81–86.
- [35] Eberhardt, E., Thuro, K. and Luginbuehl, M. (2005). Slope instability mechanisms in dipping interbedded conglomerates and weathered marls – the 1999 Ruffi landslide, Switzerland. *Engineering geology*, Vol. 77, pp. 35–56.
- [36] ISRM (1978). Suggested methods for the quantitative description of discontinuities in rock masses. *Int. J. of Rock Mechanics Mining Sciences and Geomechanics Abstracts*, Vol. 15, pp. 319–368.
- [37] BSI (1981). *Code of Practice for site investigations*, BS 5930. British Standards Institution, London, p. 147.
- [38] IAEG (1981). Rock and soil description and classification for engineering geological mapping. *Bulletin of International Association of Engineering Geology*, Vol. 24, pp. 253–274.
- [39] Arbanas, Ž., Benac, Č., Andrić, M and Jardas, B. (1994). Geotechnical Properties of Flysch on the Adriatic Motorway from Orehovica to St. Kuzam.

- Proc. of the Symposium of Geotechnical Engineering in Transportation Projects, Croatian Geotechnical Society, Vol. 1, pp. 181-190.
- [40] Arbanas, Ž., Grošić, M. and Jurić-Kaćunić, D. (2007). Experiences on flysch rock mass reinforcing in engineered slopes, The Second Half Century of Rock Mechanics. Proc. of the 11th Congress International Society for Rock Mechanics, Lisbon, Portugal, pp. 597-600.
- [41] Arbanas Ž, Grošić M, Dugonjić S (2008). Behaviour of the reinforced cuts in flysch rock mass, Proc. of 1st Int. Conf. On Transportaion Geotechnics, Nottigham, UK, pp. 283-291.
- [42] Marinos, P. and Hoek, E. (2001). Estimating the Geotechnical Properties of Heterogeneous Rock Masses such as Flysch. Bulletin of Engineering Geology and the Environment, Vol. 60, pp. 85-92.
- [43] Brunčić, A., Arbanas, Ž. and Kovačević, M.-S. (2009). Design of engineered slopes in flysch rock mass, Proc. Int. Conf. on Soil Mechanics and Geotechnical Engineering.
- [44] Cividini, A., Jurina, L. and Gioda, G. (1981). Some Aspects of Characterization Problems in Geomechanics. Int. J. Of Rock Mechanics and Mining Sciences & Geomechanics Abstracts, Vol. 18, pp. 487-503.
- [45] Gioda, G. and Maier, G. (1980). Direct Search Solution of an Inverse Problem in Elastoplasticity: Identification of Cohesion, Friction Angle and In-situ Stress by Pressure Tunnel Tests. Int. J. For Numerical Methods in Engineering, Vol. 15, pp. 1823-1848.
- [46] Itasca Consulting Group Inc. (2011). FLAC, Fast Lagrange Analysis of Continua, Version 7.0, User Manual, Minneapolis.
- [47] Olona, J., Pulgar, A. J., Fernández-Viejo, G., López-Fernández, C. and González-Cortina, J. M. (2009) Weathering variations in a granitic massif and related geotechnical properties through seismic and electrical resistivity methods. Near Surface Geophysics, Vol. 8, pp. 585-599

UČINKI MLETE GRANULIRANE PLAVŽNE ŽLINDRE NA INDEKSNE IN ZBIJALNE PARAMETRE GLINENIH TAL

OSMAN SIVRIKAYA, SELMAN YAVASCAN İN EMRE CECEN

o avtorjih

vodilni avtor

Osman Sivrikaya
Niğde University,
Civil Engineering Department
51240 Niğde, Turčija
E-pošta: osivrikaya@nigde.edu.tr

Selman Yavascan
Civil Engineering Company
51100, Niğde, Turčija
E-pošta: s_yavascan@hotmail.com

Emre Cecen
Fatih University,
Civil Engineering Department
Istanbul, Turčija
E-pošta: emrececen@fatih.edu.tr

izvleček

Uporaba industrijskih odpadkov pri stabilizaciji tal ne zagotavlja samo ponovne uporabe odpadkov, ki lahko povzročajo onesnaževanje okolja, ampak tudi finančne koristi. Zaradi tega je postala uporaba industrijskih odpadkov pri stabilizaciji drobozrnatih tal predmet raziskav zadnjih let. Namen te študije je oceniti potencialno uporabo mlete granulirane plavžne žlindre (MGPŽ) za stabilizacijo glinenih tal. V študiji je bil MGPŽ, pridobljen kot industrijski odpadek železarne in jeklarne Iskendurun, zmlet v dve različni velikosti. Raziskovali smo učinke mešanja te žlindre v slabo gnetljivo Kolsuz glino in dobro gnetljivo bentonitno glino v različnih razmerjih (5%, 10%, 20%, 30%, in 50%) na prostorninsko težo, konsistenčne meje in zbijalne parametre. Eksperimentalni rezultati so pokazali, da ima MGPŽ pozitiven učinek na stabilizacijo obeh vrst glinenih tal. Prav tako lahko zaključimo, da je izboljšanje v bentonitni glini večje kot v Kolsuz glini. Zaradi tega je MGPŽ obetaven material za stabilizacijo glinenih tal.

ključne besede

glinena tla, indeksne lastnosti, mleta granulirana plavžna žlindra, stabilizacija

EFFECTS OF GROUND GRANULATED BLAST-FURNACE SLAG ON THE INDEX AND COMPACTION PARAMETERS OF CLAYEY SOILS

OSMAN SIVRIKAYA, SELMAN YAVASCAN and EMRE CECEN

about the authors

corresponding author

Osman Sivrikaya
Niğde University,
Civil Engineering Department
51240 Niğde, Turkey
E-mail: osivrikaya@nigde.edu.tr

Selman Yavascan
Civil Engineering Company
51100, Niğde, Turkey
E-mail: s_yavascan@hotmail.com

Emre Cecen
Fatih University,
Civil Engineering Department
Istanbul, Turkey
E-mail: emrececen@fatih.edu.tr

abstract

The use of industrial wastes in soil stabilization not only provides for the re-use of waste materials, which may cause environmental pollution, but also leads to cost benefits. In this context, the use of industrial wastes in the stabilization of fine-grained soils has become a research topic in recent years. The aim of this study is to evaluate the potential use of granulated blast-furnace slag (GBFS) in clayey soil stabilization. In this study, the GBFS obtained from the Iskenderun iron-steel plant as an industrial waste was ground into two different fineness levels, and the effects of their incorporation into low-plasticity Kolsuz clay and high-plasticity bentonite clay in various rates (5%, 10%, 20%, 30%, and 50%) on the particle weight of unit volume, the consistency limits, and the compaction parameters are investigated. Based on the experimental results, it is clear that the GBFS has a positive effect on the stabilization of both clayey soils. It was also concluded that the improvement in bentonite clay is greater than that in Kolsuz clay. Thus, GBFS seems to be a promising material for the stabilization of clayey soils.

keywords

clayey soils, index properties, granulated blast-furnace slag, stabilization

1 INTRODUCTION

One of the main environmental problems in this century is the storage of solid waste materials such as municipal waste, industrial waste, hazardous waste and low-level radioactive waste [1]. While countries are being industrialized, enormous amounts of solid waste are being generated. These waste materials are generally placed in landfills. As a result of the extensive recovery and usage of natural resources there exists a shortage of high-quality natural materials all over the world. In addition, the disposal of industrial waste or by-products has become a more difficult and expensive process as a result of the increasing strictness of environmental regulations and a shortage of suitable disposal sites.

Waste utilization is an attractive alternative to disposal in that disposal costs and potential pollution problems are reduced or even eliminated along with the goal of resource conservation. Nevertheless, the utilization strategy must be coupled with environmental and energy considerations to use the available materials most efficiently. The increasing global awareness of environmental pollution as well as increasing waste-material disposal legislation provides the impetus for material upgrading by the stabilization of in-situ soil as an alternative to its export to land-fill and replacement by imported granular fill [2, 3].

In this context, significant quantities of slag are being generated as a solid waste material or as a by-product of the iron-steel industry every day. Furthermore, from an energy-conservation point of view, slag can be considered as an environment-friendly material in terms of resource saving, and CO₂ reduction in the 21st century. However, these products pose a great threat to the environment unless they are stored or exploited for use in various sectors [4].

Iron and steel slag is broadly divided into blast-furnace slag (BFS) and steel slag. BFS may be either granulated blast-furnace slag (GBFS), a glass form that is quenched, or air-cooled slag, which is cooled in the atmosphere. During the production of iron, GBFS and steel slag are

formed as by-products. BFS is a non-metallic by-product during the manufacture of pig iron in a blast furnace. BFS consists primarily of silicates, alumina-silicates, and calcium-alumina-silicates. The color of GBFS is whitish. Slag has some unique pozzolanic properties that are difficult to obtain from natural materials. GBFS is used as a cement additive, a concrete admixture, an earthwork material such as in backfilling, covering, embankments and sub-grade improvement, a fine aggregate for concrete, an aggregate for asphalt mixtures and a fertilizer, etc. Air-cooled blast-furnace slag (ACBFS) is primarily used as a road-building material. Most of the steel slag is used in such civil-engineering works as weak ground improvement [4, 5, 6, 7].

Based on typical ratios of slag to crude iron and steel output, it is estimated that the annual amount of world iron furnace slag was about 200 to 250 million tons, and steel slag was about 110 to 160 million tons, [8]. A total of 50 million tons of steel slag is produced per year as a residue throughout the world. In Europe, nearly 12 million tons of steel slag is produced each year [9, 10]. GGBS has been widely used in Europe, and its usage is expanding in the United States and Asia because of its superiority [8, 5, 11]. It is estimated that approximately 15.5 million tons of BFS is produced annually in the United States [12]. Just a single plant in Turkey has 4 million tons of granulated blast-furnace slag (GBFS) and 3 million tons of steel slag storage in 2006 [13]. According to the Nippon slag Association, in Japan the cumulative field sales of ferrous slag products from 1978 to 2004 amounts to 790 million tons, of which 610 million tons are blast-furnace slag and 180 million tons are steel slag products. While the consumption of ACBFS was about 6 million tons (27 %), that of GBFS was about 19 million tons, with 1 % used in-house, 59 % in the cement industry, and, of the remainder, 9 % as concrete aggregate and 4 % for civil-engineering purposes [4]. Research shows that the production of GBFS reached approximately 20 million tons, where 4 % was used as soil-improvement material in Japan in 2010 [14].

In the literature, studies have been performed on the possible utilization of ground granulated blast-furnace slag (GGBFS) as a binder in the stabilization of clayey soils and its effect on the volume change of expansive soils [3, 6, 7, 15]. The authors noticed that there is limited work on the usage of GBFS in comparison with other industrial by-products, such as fly ash and silica fume on the stabilization of soils. The published literature has given little attention to the use of GGBFS for the stabilization of soils. The aim of the current research work is to investigate the possibility of the use of GBFS obtained from the Iskenderun Iron Steel Factory, Turkey, as an active material for the stabilization of fine-grained soils.

2 MATERIALS AND METHOD

In this study, the variations in the particle unit weights, consistency and compaction parameters of the clay samples of low and very high plasticity that are mixed with different ratios of GGBFS are examined. A series of laboratory experiments on a variety of samples by blending GGBFS have been conducted in the soil mechanics laboratory of the Civil Engineering Department, Niğde University, Turkey.

All the soil tests were conducted in accordance with ASTM standards. The unit weight of the particle (γ_s) value was obtained in accordance with [16]. The liquid limit (w_L), plastic limit (w_P) and plasticity index (I_P) of the natural and stabilized clayey soil samples were determined by Atterberg tests in accordance with [17]. The plasticity index was calculated as the difference in the liquid limit and plastic limit values. The compaction parameters (optimum water content w_{opt} and maximum dry unit weight γ_{dmax}) were obtained using the Standard Proctor (SP) test in accordance with [18].

2.1 FINE-GRAINED SOILS

Two types of clayey soils were used in this study. The clayey soil with low plasticity was collected from clay deposits of the Kolsuz area in Niğde, Central Anatolia, Turkey. The Kolsuz deposit is characterized by successions of red siliciclastic deposits that are more than 60 m thick and contain massive amounts of conglomerate, sandstone, and silt-mudstone. The bulk mineralogy is characterized by small amounts and variable proportions of clay minerals, quartz, feldspar, and calcite. Most clayey sediments are made up of relatively homogeneous clay assemblages with dominant detrital chlorite, illite and smectite in terms of clay mineralogy [19]. The other clay type of bentonite with a very high plasticity was supplied by Bensen Ltd. Co., Turkey, for this study. It is produced from raw bentonite in Edirne, Turkey. The material is used in drilling mud, and includes large amounts of montmorillonite.

The clayey soils are classified in accordance with the Unified Soil Classification System (USCS) [20]. The Kolsuz clay can be described as an inorganic clay of low plasticity (CL) and Bensen Bentonite clay can be classified as inorganic clay of high plasticity (CH), (Fig. 1). The sieve analysis and hydrometer tests [20, 21, 22] were performed to determine the grain size distributions, which are given in Fig. 2. Furthermore, their chemical, index and compaction properties are summarized in Table 1 and Table 2, respectively.

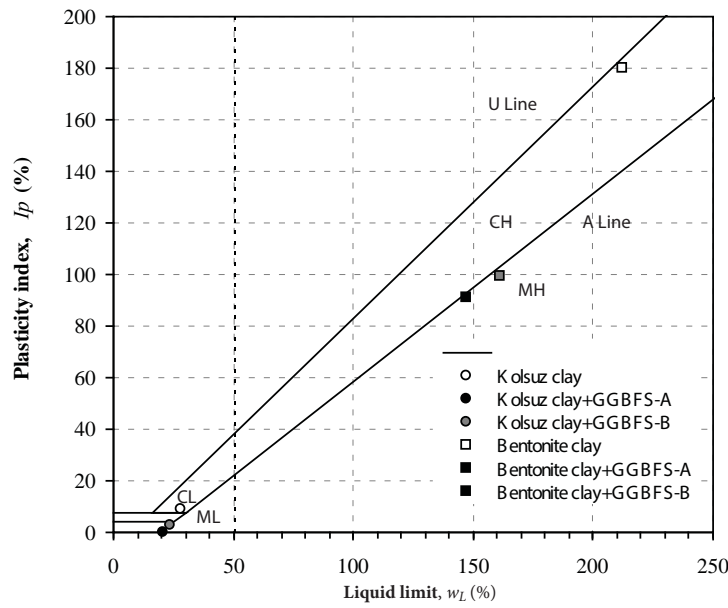


Figure 1. The plasticity chart for clays and stabilized clay samples with 50% GGBFS.

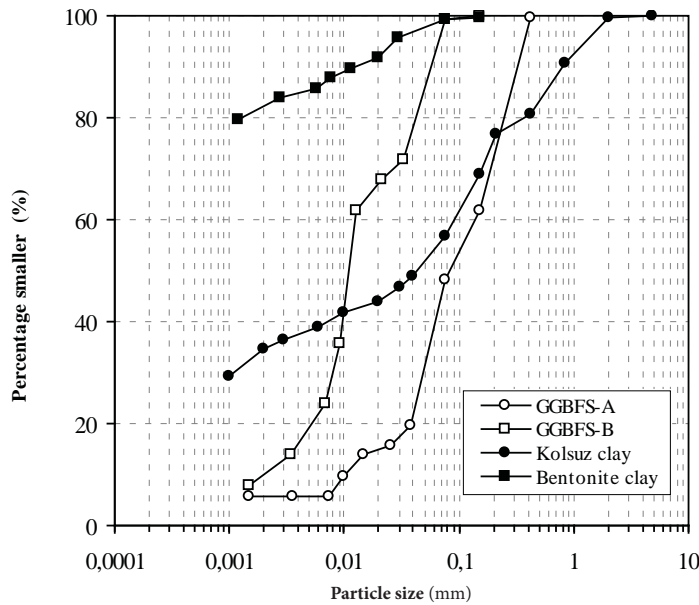


Figure 2. The grain size distributions of the clays and GGBFS used in the tests.

Table 1. Chemical composition of clayey soils and GGBFS.

| Property | Kolsuz clay | Bentonite clay | GGBFS |
|------------------------------------|--------------|----------------|-------|
| SiO ₂ (%) | 49.12 -48.57 | 64.0 | 37.60 |
| Al ₂ O ₃ (%) | 9.46-13.97 | 21.0 | 14.21 |
| Fe ₂ O ₃ (%) | 4.24-8.10 | 3.5 | 0.98 |
| MgO (%) | 2.90-5.09 | 2.3 | 10.12 |
| CaO (%) | 15.04-6.94 | 0.5 | 32.61 |
| Na ₂ O (%) | 1.72-1.10 | 2.6 | 0.42 |
| K ₂ O (%) | 1.65-2.64 | 0.4 | 0.76 |
| SO ₃ (%) | - | - | 0.99 |

Table 2. Engineering properties of clayey soils and GGBFS.

| Property | Kolsuz clay | Bentonite clay | GGBFS-A | GGBFS-B |
|--------------------------------------|-------------|----------------|---------|---------|
| γ_s (gr/cm ³) | 2.55 | 2.62 | 2.81 | 2.79 |
| Grain size | | | | |
| Gravel (%) | 0 | 0 | 0 | 0 |
| Sand (%) | 43 | 0.8 | 52 | 1 |
| Silt % | 22 | 7.2 | 42 | 88 |
| Clay (%) | 35 | 92 | 6 | 11 |
| Atterberg limits | | | | |
| w_L (%) | 28 | 212 | | |
| w_P (%) | 19 | 32 | | |
| I_P (%) | 9 | 180 | | |
| Compaction parameters | | | | |
| SP w_{opt} (%) | 14.20 | 16.97 | | |
| γ_{dmax} (kN/m ³) | 17.61 | 15.65 | | |
| Soil classification | | | | |
| USCS | CL | CH | | |

2.2 BLAST-FURNACE SLAG

The granulated blast-furnace slag (GBFS) samples were collected from the Iskenderun Iron-Steel Factory as an industrial by-product in Hatay, Turkey. In this study, the GBFS was ground into two different fineness levels (GGBFS-A and GGBFS-B) and used in the tests (Fig. 3). The particle unit weight of the ground granulated blast-furnace slag (GGBFS) was on average 2.80 g/cm³. The grain size distributions of the ground granulated



Figure 3. Samples of GBFS and GGBFS.

blast-furnace slags are shown in Fig. 2. The chemical and index properties are summarized in Table 1 and 2, respectively.

2.3 PREPARATION OF SAMPLES FOR THE TESTS

The clayey soil was first dried in an oven at approximately 105°C before being used in the mixture. The required amounts of clayey soil and GGBFS were weighed and mixed together in their dry state. The dry clayey soil and GGBFS were then mixed with the required amount of water for the preparation of test samples. All the mixing procedures were performed manually, and great care was taken to prepare homogeneous mixtures at each stage of the mixing. The stabilized clayey soil samples were obtained at various GGBFS contents (5%, 10%, 15%, 20%, 30% and 50% of dry weight of soil).

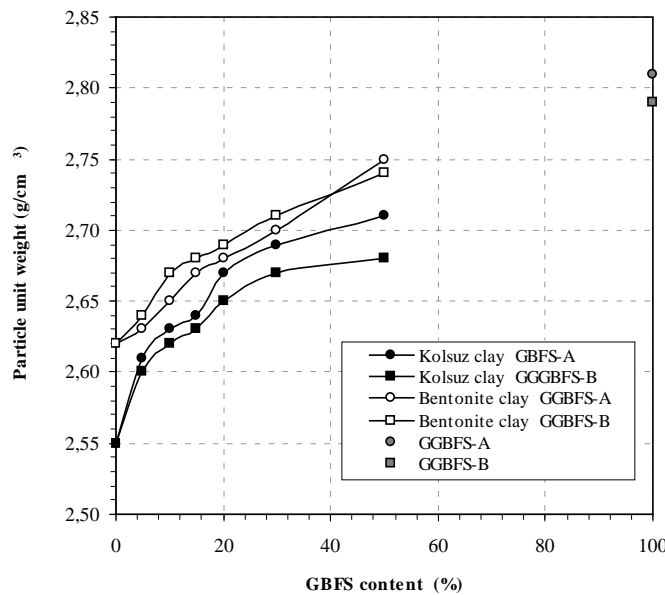


Figure 4. Effect of GGBFS on the unit weight of a particle of the clayey soils.

3 RESULTS AND DISCUSSION

3.1 EFFECT OF BLAST-FURNACE SLAG ON THE UNIT WEIGHT OF A PARTICLE

The unit weights of a particle (γ_s) for the destabilized (raw) and stabilized clayey soil samples prepared at a desired percentage of GGBFS were determined and the results are plotted for the low and high plastic clays in Fig. 4. It is clear from Fig. 4 that the unit weights of a particle for the stabilized clayey soil sample increases with an increase of the content of GGBFS. This indicates that the stabilized clayey soil sample is heavier than that of its natural conditions.

3.2 EFFECT OF BLAST-FURNACE SLAG ON THE CONSISTENCY LIMITS

The effects of GGBFS on the consistency limits are presented for low-plasticity Kolsuz clay (CL) and high-plasticity Bentonite clay (CH) in Figs. 5 and 6, respectively. The liquid limit and plasticity index values decrease and the plastic limit values increase with increasing GGBFS content up to 50% for all the stabilized samples of both the low-plasticity and high-plasticity clays (Figs. 5 and 6). These may be due to the soil type, the associated exchangeable cations and the relative amount of silicate clay mineral in the samples.

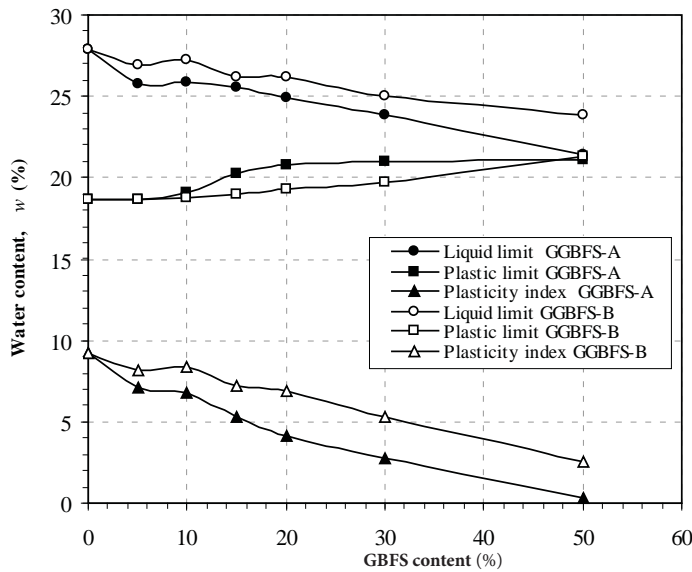


Figure 5. Effect of GGBFS on the consistency parameters of the Kolsuz clay.

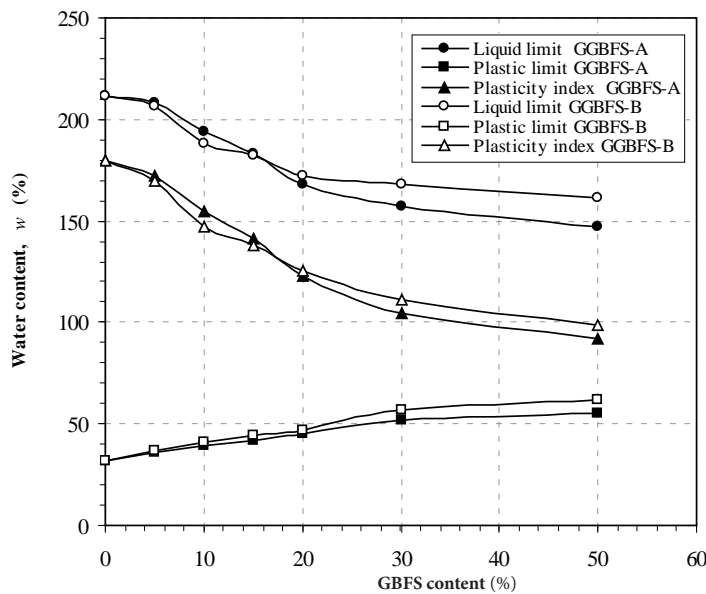


Figure 6. Effect of GGBFS on the consistency parameters of Bentonite clay.

In the Kolsuz clay of low plasticity, the plastic limit of the stabilized clay samples slightly increased from 19% to 21% for both GGBFS-A and GGBFS-B. However, the liquid limit of the stabilized clay samples decreased from approximately 28% to 21% and from 28% to 24% for the GGBFS-A and GGBFS-B, respectively. The plasticity index of the stabilized clay samples decreased from approximately 9% to 0% and from 9% to 3% for GGBFS-A and GGBFS-B, respectively. Thus, the stabilization at 50% GGBFS content for the low-plasticity Kolsuz clay converted it almost into a non-plastic soil, irrespective of the GGBFS level (Fig. 5).

In the Bentonite clay with high plasticity, the plastic limit of the stabilized clay samples increased slightly from 32% to 55% and from 32% to 62% for the GGBFS-A and GGBFS-B, respectively. The increase in the plastic limit is approximately 100%. However, the liquid limit of the stabilized clay samples decreased approximately from 212% to 147% and from 212% to 161% for the GGBFS-A and GGBFS-B, respectively. Therefore, the plasticity index of the stabilized clay samples decreased from approximately 180% to 92% and from 180% to 99%, respectively (Fig. 6).

In addition, it is clear from Fig. 5 and Fig. 6 that there is no major influence of the fineness of the GGBFS (grain size distribution) on the stabilization in both the low and highly plasticity clays.

3.3 EFFECT OF BLAST-FURNACE SLAG ON THE COMPACTION PARAMETERS

The Standard Proctor test was performed on both the clayey and stabilized clayey soil samples to determine their compaction curves. The compaction curves for the Kolsuz clay stabilized with GGBFS-A and GGBFS-B are presented in Figs. 7 and 8, respectively. Fig. 9 also shows the variation of the water content and the dry unit weight values of the Bentonite clay samples stabilized with GGBFS-A.

The optimum water content and maximum dry unit are determined from these compaction curves, shown in Figs. 7, 8 and 9. The optimum water contents of the stabilized soil samples belonging to the Kolsuz clay range from 14.2% to 14.9% and from 14.2% to 14.7% for GGBFS-A and GGBFS-B, respectively. In addition, the maximum dry unit weights of the stabilized soil samples belonging to the Kolsuz clay range from 17.6 to 18.2 kN/m³ and from 17.6 to 18.1 kN/m³ for GGBFS-A and GGBFS-B, respectively. The grain size distribution effect (GGBFS-A, GGBFS-B) was not observed to any significant extent on the stabilized soil samples. In the same way, the optimum water contents of the stabilized soil samples belonging to the Bentonite clay range from 16.8% to 17.5% for GGBFS-A, and the maximum dry unit weights of the stabilized soil samples belonging to the Bentonite clay range from 15.65 to 16.41 kN/m³ for GGBFS-A.

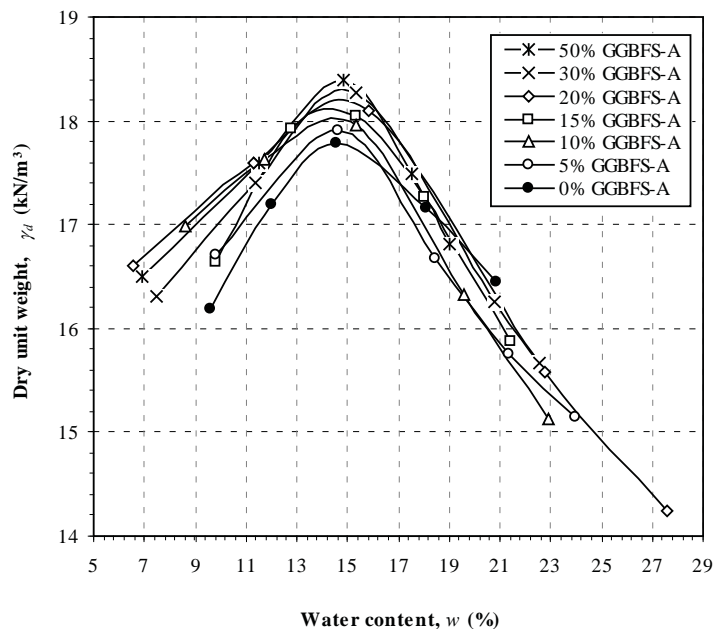


Figure 7. Effect of GGBFS-A on the compaction curves of the Kolsuz clay.

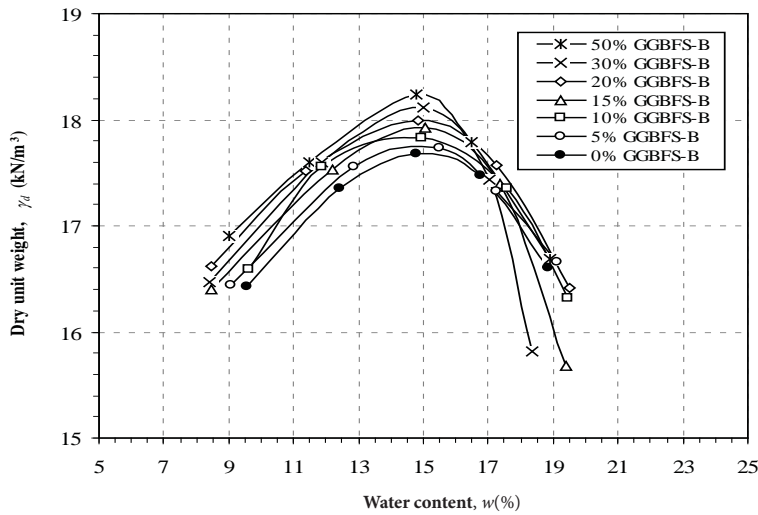


Figure 8. Effect of GGBFS-B on the compaction curves of the Kolsuz clay.

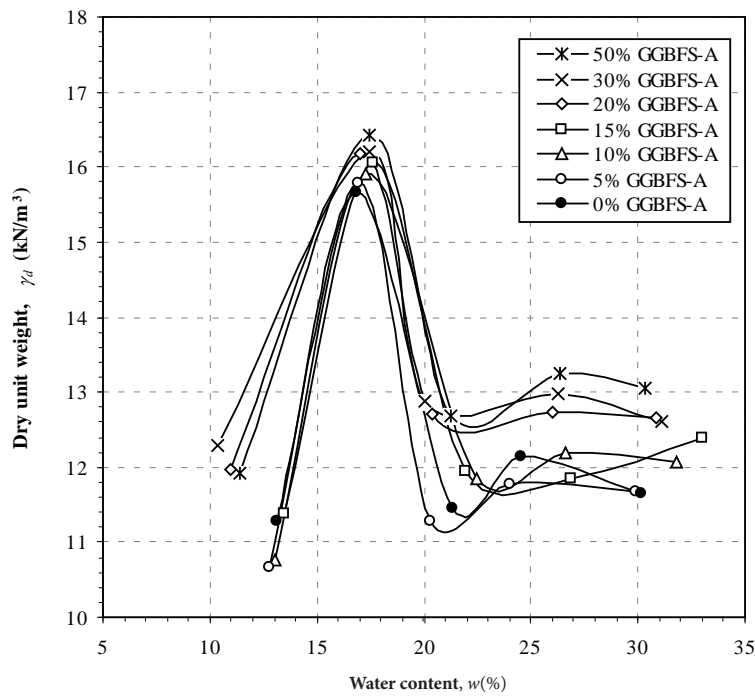


Figure 9. Effect of GGBFS-A on the compaction curves of the Bentonite clay.

The low optimum water contents and dry unit weights occur in the destabilized soil (raw) samples, while the high optimum water contents and dry unit weights occur in the 50% GGBFS - clay stabilized soil samples. There is an increase in the optimum water content and the maximum dry unit weight due to the addition of GGBFS to the clay samples for the same compaction effort (Figs. 10 and 11). The cause of the increase in the water content is due

to the change in surface area of the stabilized soil samples. In the same way, the cause of the increase in the maximum dry unit weight is thought to be due to the addition of higher GGBFS with high density, which fills the voids in the stabilized soil samples. The amount of increase in the optimum water content and the maximum dry unit weight for the Bentonite clay is higher than for the Kolsuz clay in a manner that is proportional to their plasticity.

4 CONCLUSIONS

In this study, the effect of ground granulated blast-furnace slag (GGBFS) on the index and compaction parameters of two clayey soils with different plasticities has been examined and the following conclusions have been derived:

- The unit weights of a particle of the stabilized clayey soils increase with increasing GGBFS in the clays of low and high plasticity.
- The GGBFS decreases the liquid limits and plasticity index and increases the plastic limits in all the stabilized clay samples. Thus, the soil types of the stabilized clay samples with 50% GGBFS changed from low plasticity clay (CL) to low plasticity silt (ML) and from high plasticity clay (CH) to high plasticity silt (MH) for Kolsuz and Bentonite clays, respectively.
- The GGBFS changes the compaction parameters. The addition of GGBFS increases both the optimum water content and maximum dry unit weight.

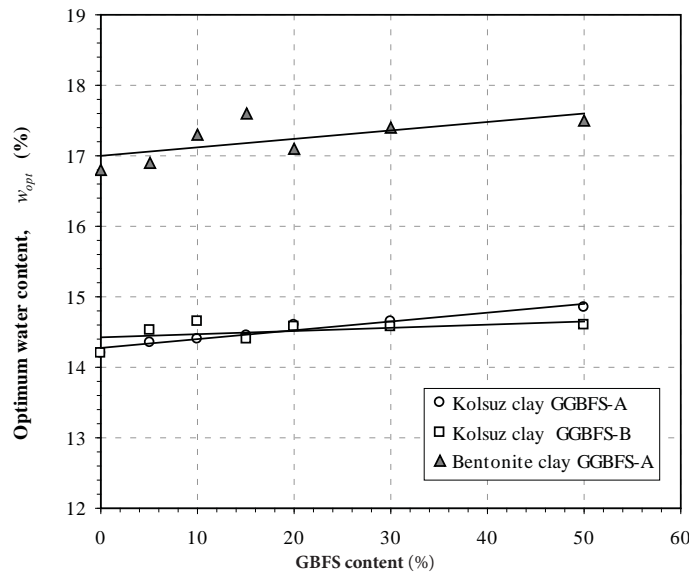


Figure 10. Effect of GGBFS on the water content of clayey soils.

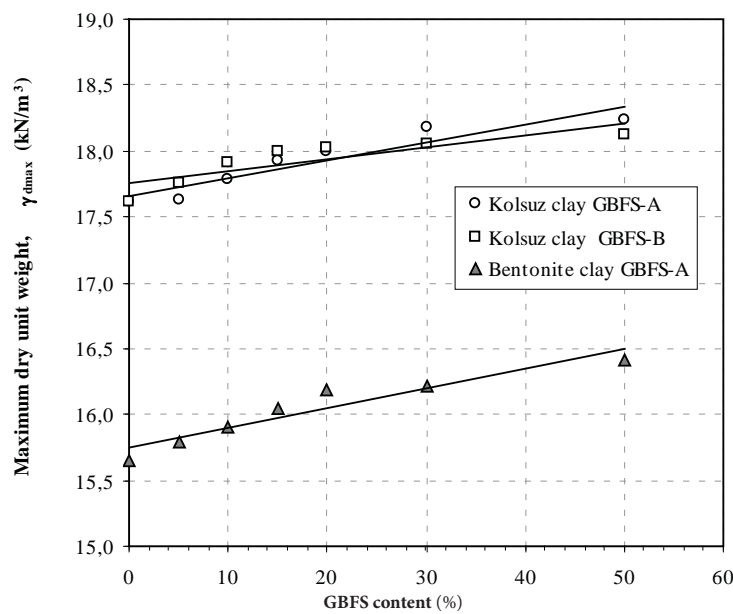


Figure 11. Effect of GGBFS on the maximum dry unit weight of clayey soils.

- The stabilization performance of the high plastic clay is higher than that of the low plastic clay for each of the GGBFS contents. However, the grain size distribution of the GGBFS on the stabilization performance was not observed to any great extent.
- This study has revealed that the use of GGBFS waste material has the potential to modify the properties of clays in order to decrease their swelling potential, and therefore positively affect the stabilized soil samples.

ACKNOWLEDGEMENTS

The authors would like to express their sincere thanks to Asst. Prof. Dr. Burak UZAL, the Division of Material Science, Civil Engineering Department, Nigde University, for his precious comments and help in the preparation of the paper.

REFERENCES

- [1] Hanson, D.J. (1989). Hazardous waste management: planning to avoid future problems. *Chemical and Engineering News* 21(7), 6–32.
- [2] Tsakiridis, P.E., Papadimitriou, G.D., Tsvivilis, S., Koroneos, C. (2008). Utilization of steel slag for Portland cement clinker production. *Journal of Hazardous Materials* 152, 805–811.
- [3] Wild, S., Kinuthia, J.M., Jones, G.I., Higgins, D.D. (1998). Effects of partial substitution of lime with ground granulated blast furnace slag (GGBS) on the strength properties of lime-stabilised sulphate-bearing clay soils. *Engineering Geology* 51, 37–53.
- [4] JISF (2006). *The Slag Sector in the Steel Industry*, The Japan Iron and Steel Federation, Nippon Slag Association, p. 40.
- [5] Das, B., Prakash, S., Reddy, P.S.R., Misra, V.N. (2007). An overview of utilization of slag and sludge from steel industries. *Resources, Conservation and Recycling* 50, 40–57.
- [6] Al-Rawas, A.A. (2002). Microfabric and mineralogical studies on the stabilization of an expansive soil using cement by-pass dust and some types of slags. *Canadian Geotechnical Journal* 39, 1150–1167.
- [7] Cokca, E., Yazici, V., Ozaydin, V. (2009). Stabilization of expansive clays using Granulated Blast Furnace Slag (GBFS) and GBFS-Cement. *Geotechnical and Geological Engineering* 27, 489–499.
- [8] Van Oss, H.G. (2010). Iron and steel slag, U.S. Geological Survey, Mineral Commodity Summaries, January 2010, p. 2.
- [9] Motz, H., Geiseler, J. (2001). Products of steel slags an opportunity to save natural resources. *Waste Management* 21 (3), 285–293.
- [10] Altun, A., Yilmaz, I. (2002). Study on steel furnace slags with high MgO as additive in Portland cement. *Cement and Concrete Research* 32(8), 1247–1249.
- [11] Cheng, T.W., Chiu, J.P. (2003). Fire-resistant geopolymer produced by granulated blast furnace slag. *Minerals Engineering* 16, 205–210.
- [12] MCS (1993). *Mineral Commodity Summaries*, Bureau of mines, U.S. Department of the interior, Washington, DC.
- [13] Ozkan, O., 2006. Properties of portland cement with steel and furnace slag. *İMO Teknik Dergi*, 3893-3902 (in Turkish with English abstract).
- [14] NSA (2010). Nippon Slag Association. <http://www.slg.jp/e/statistics/index.html>. January 2012.
- [15] Veith, G. (2000). Essay competition Green, ground and great: soil stabilization with slag. *Building Research and Information* 28(1), 70–72.
- [16] ASTM D-7263 (2000). Standard Test Methods for Laboratory Determination of Density (Unit Weight) of Soil Specimens. ASTM International 100 Barr Harbor Drive, PO Box C700, West Conshohocken, United States.
- [17] ASTM D-4318 (2000). Standard Test Methods for Liquid Limit, Plastic Limit, and Plasticity Index of Soils. ASTM International 100 Barr Harbor Drive, PO Box C700, West Conshohocken, United States.
- [18] ASTM D-1557 (2003). Standard Test Methods for Laboratory Compaction Characteristics of Soil Using Modified Effort. ASTM International 100 Barr Harbor Drive, PO Box C700, West Conshohocken, United States.
- [19] Gurel, A. (2008). Geology, mineralogy and origin of clay minerals of the Pliocene fluvial-lacustrine deposits in the Cappadocian volcanic province, Central Anatolia, Turkey. *Clays and Clay minerals* 56(6), 660-676.
- [20] ASTM D-2487 (2000). Standard Practice for Classification of Soils for Engineering Purposes (Unified Soil Classification System). ASTM International 100 Barr Harbor Drive, PO Box C700, West Conshohocken, United States.
- [21] ASTM D-221 (2003). Standard Practice for Dry Preparation of Soil Samples for Particle-Size Analysis and Determination of Soil Constants. ASTM International 100 Barr Harbor Drive, PO Box C700, West Conshohocken, United States.
- [22] ASTM D-422 (2003). Standard Test Method for Particle-Size Analysis of Soils. ASTM International 100 Barr Harbor Drive, PO Box C700, West Conshohocken, United States.

USEDANJE ŠIBKO CEMENTIRANEGA TUFA

NIHAT DIPOVA, M. UFUK ERGUN İN VEDAT DOYURAN

o avtorjih

Dipova Nihat
Akdeniz University,
Department of Civil Engineering,
Antalya, Turčija
E-pošta: ndipova@akdeniz.edu.tr

Ergun M. Ufuk
Middle East Technical University,
Department of Civil Engineering,
Ankara, Turčija
E-pošta: eruf@metu.edu.tr

Doyuran Vedat
Middle East Technical University,
Department of Geol. Engineering,
Ankara, Turčija
E-pošta: vedat@metu.edu.tr

izvleček

Šibko cementiran tuf je zemljina z velikostjo zrn peska in melja, ki so šibko povezana s tankimi plastmi karbonatnega cementa. Količnik por je dokaj velik, okoli 1,2. Zrušitev teh zemljin se pojavi kot rezultat popuščanja rahlih vezi zaradi obtežitve ali namočenosti. Njihove indeksne lastnosti in zrušitveni potencial smo določili v laboratoriju. Pri določanju vrednosti zrušitvenega potenciala smo uporabili edometriško metodo, s tem da smo pri risanju rezultatov testov privzeli naravno skalo in ne logaritemske, tako da je razmerje med količnikom por in tlakom polinomsko. Pri obremenitvi se naravno vlažna zemljina posede, poveča se zasičenost in s tem obseg zrušitve. Pritisk je pomemben parameter pri obsegu zrušitve in s tem tudi pri celotnem posedku. Posedanje temeljev zaradi zrušenja zemljinske strukture lahko neposredno ocenimo iz rezultatov edometriških testov in empirično z uporabo indeksnih lastnosti kot so začetni količnik por, razlika v fini sestavi med suho in mokro sejalno metodo in prostorninska teža. Primerjava med direktnimi in empiričnimi pristopi je pokazala precejšnje ujemanje.

ključne besede

Antalya, zrušitveni potencial, zrušljive zemljine, usedlina, tuf

SETTLEMENT OF WEAKLY CEMENTED TUFAS

NIHAT DIPOVA, M. UFUK ERGUN and VEDAT DOYURAN

about the authors

Nihat Dipova
Akdeniz University,
Department of Civil Engineering,
Antalya, Turkey
E-mail: ndipova@akdeniz.edu.tr

M. Ufuk Ergun
Middle East Technical University,
Department of Civil Engineering,
Ankara, Turkey
E-mail: eruf@metu.edu.tr

Vedat Doyuran
Middle East Technical University,
Department of Geol. Engineering,
Ankara, Turkey
E-mail: vedat@metu.edu.tr

abstract

Weakly cemented tufas are sand and silt size soils that are weakly bonded with thin films of carbonate cement. The void ratio is rather high and equal to approximately 1.2. Collapse occurs as a result of the destruction of the weak bonds upon loading and/or wetting. The index properties and the collapse potential (C_p) of tufa were determined in the laboratory. In the determination of the collapse-potential values the single-ring oedometer method was considered to be a suitable and simpler tool. In plotting the oedometer test results the use of a natural scale was preferred over a logarithmic scale so that the void ratio-pressure relationship is polynomial. Under loading the soil settles with the natural water content; however, saturation increases the collapse that is initially triggered by the pressure increase. The pressure level is a significant parameter in the magnitude of the collapse and therefore in the total settlement. The settlement of foundations due to a collapse of the soil structure can be estimated directly using the oedometer test results and empirically using the index properties, like the initial void ratio (e_0), the difference in the fine content between the dry and the wet sieve analyses (PFAW) and the natural unit weight. A comparison of the direct and empirical approaches yielded a good agreement.

keywords

Antalya, collapse potential, collapsible soils, settlement, tufa

1 INTRODUCTION

Antalya, the study area, is a well-known tourist destination that is famous for its tufa coastal cliffs and wide beaches. These appealing features increased the population of Antalya and also the value of the land extending behind the cliffs, leading to high-rise constructions. However, some of these luxurious, high-rise buildings suffered from foundation instabilities. Cracking of the walls and a general tilting were typical indications of the foundation problems that the buildings suffered. The maximum tilting was observed on an 11-story building (Figure 1). The tilt amount was 1.6 degrees and the deflection at the top of the building was 85 cm. During construction the loading for every floor resulted in a



Figure 1. Leaning apartment building in Antalya (Turkey).

partial settlement at the natural water content of the soil. The pressure distribution under the foundation was non-uniform, which led to the differential settlement. To solve this, leveling concrete was applied. This resulted in an increased eccentricity and a large differential settlement. The water pipes broke due to the high shear force on the pipe. Leakage from the pipe through the foundation soil caused the saturation of the soil. After the saturation, maximum settlement occurs instantaneously. The foundation soils are composed of varieties of tufa, which can be classified as weakly cemented silt-sand [1]. The grains of the Antalya tufa deposits are bonded to each other by a meniscus cementation of thin calcium carbonate films. The cementation in these deposits is due to the deposition of calcium carbonate, carried downward by percolating water under unsaturated flow conditions. Later, rainwater or water leakage from pipes dissolves this thin film and destroys the interparticle bonding. As a consequence, the voids are closed and, finally, collapse occurs [2].

The geo-mechanical behavior of cemented materials is characterized by a high initial stiffness, which decreases after the yield due to the degradation of the bonding, and the progressive transformation of the cemented soil into a granular material [3]. Cemented sands, as well as the other structured soils, are considered as intermediate materials: they are stronger than soils but do not perform as rocks [4]. Cementation makes the soil stronger; however, the natural cementation tends to be highly irregular, causing significant spatial variations in strength over relatively short distances within a soil deposit, so making characterization difficult [5]. As a result of the cementation, carbonate sands exhibit true cohesion, which makes cemented sands stronger than uncemented sands. However, this apparent stiffness can suddenly be lost under loading when flooded. When soils show this behavior, they are called "collapsible soils".

Collapsible soils have a highly porous soil structure that sustains large stresses in the unsaturated state but collapses in a short time upon wetting, under constant total vertical stresses, leading to diverse consequences that affect the serviceability and stability of the structures supported by these soils. It is known that the collapsibility of soils depends on the soil porosity and moisture content [6, 7, 8]. A procedure was suggested in ASTM (2005) [9] to describe the collapse potential of a soil. According to this method, step loading is applied to the specimen up to a pressure level of 200 kN/m², using a conventional oedometer cell. At this pressure, the specimens are flooded. This test provides the natural void ratio (e_0), and the void ratios before (e_1) and after (e_2) the flooding. The collapse potential, C_p , can be calculated as:

$$C_p = \frac{e_1 - e_2}{1 + e} \quad (100) \quad (1)$$

where ($e_1 - e_2$) represents the decrease in the void ratio on saturation and "e" is the initial void ratio of the soil specimen. Abelev (1948) [10] used "e" as the void ratio of the soil specimen before water was added at that particular pressure.

The mechanisms of collapse have been examined and reported for different types of soils, such as soft sensitive clays, loose unsaturated sands, silty sands and loess, residual soils and cemented alluvium [11, 12, 13, 14, 15, 16, 17]. The low interparticle bond strength, which is common for all cases, comes from clay bridges or weak meniscus cementation. Similar to other collapsible soils, collapsible tufas exhibit common properties. In collapsible tufas grains and cement are both calcium carbonate and the soil structure is more heterogeneous than for other types of collapsible soils.

The main purpose of this investigation is to clarify the settlement behavior of weakly cemented tufas upon loading and wetting. In this study, predictive models were developed to determine the collapse potential values through multiple regression analysis, stress-collapse-time relationships were investigated and finally analytical and empirical procedures have been developed for the prediction of the settlement of the foundations resting on collapsible tufas.

2 GEOLOGICAL BACKGROUND

The tufas are terrestrial carbonate units that precipitate by both physico-chemical and biogenic processes. The rate of precipitation affects the physical properties of the tufas. Lithoclast, intraclast and microdetrital tufas, which are deposited rapidly in the fluvial environments, form weakly cemented clastics and soft tufas. In contrast, in stagnant water in large-scale lacustrine environments, fine carbonates are deposited as hard micrite rock. The final appearance of the tufa is also dependent on post-depositional modifications (diagenesis). In the biogenic precipitation process, precipitation is the cause of the decreasing partial pressure of CO₂ by the photosynthesis of algae or bacteria. The daylight photosynthesis of blue-green algae results in the removal of CO₂ from the water in the day. Calcite crystals can be observed as hanging on the algae (Figure 2a). In very recent (<1 year) precipitates, on one fiber of algae, several crystals were hanging over, while in rather aged precipitates (e.g., at a depth of 2 m in a completely filled pool) the number of crystals increases, and in diagenetic rocks

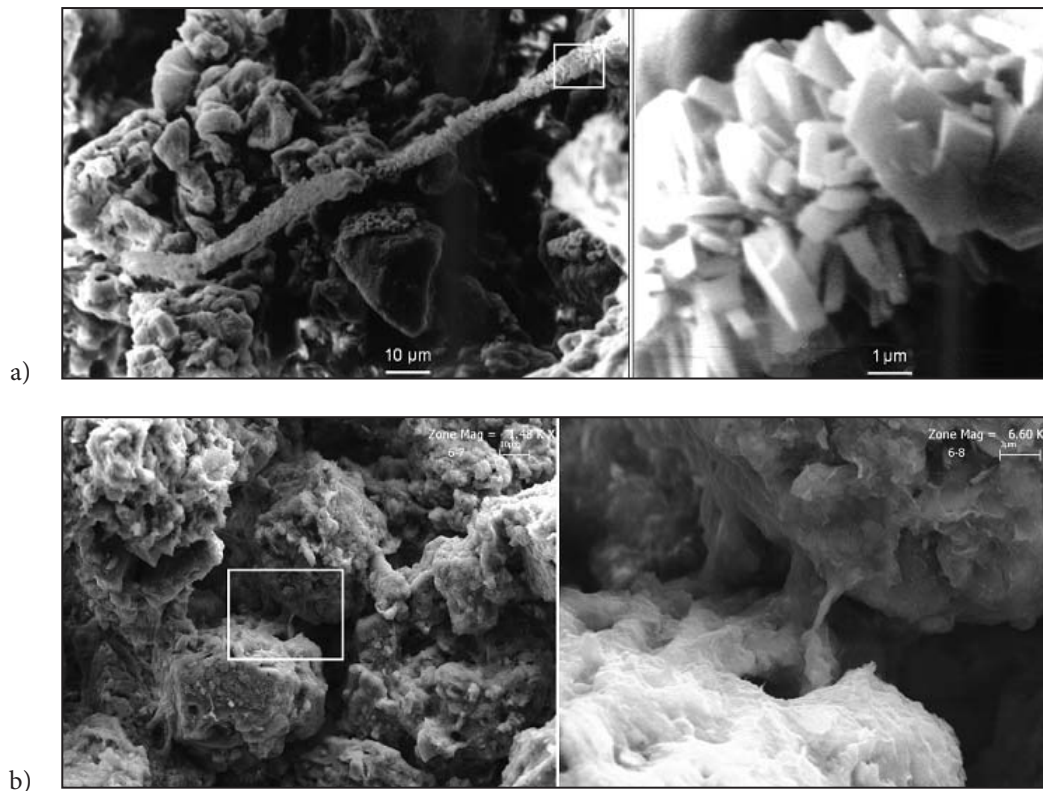


Figure 2. a) Scanning Electron Microscope (SEM) view of calcite cover around a fibrous algae (right), close up views of white rectangle (left), b) SEM view of meniscus cementation between tufa grains (left), close-up view (right).

spar micritization causes a completely covered calcite tube. After the precipitation or deposition of grains, diagenesis starts with meteoric cementation in the phreatic and vadose zones. Carbonate sediments in the vadose zone have often suffered less diagenetic modification. Recent sediments sampled from a depth of 4–6 m show only thin meniscus cements, concentrated at the grain contacts. However, this is only detectable in SEM analyses (Figure 2b). Where phreatic zone sediments or sediments through which water flows as seepage are available, spary-calcite cement development at the grain contacts and as void fill is possible.

Among tufa deposits, clastics (lithoclast, intraclast, phytoclast, oncoliths, pisoliths) and micro-clastics (micrite and peloidal tufa) may show soil-like behavior. These tufas are made of grain-supported sand and silt size grains. A weak meniscus cementation makes these deposits bonded, but with a highly porous soil structure. If these deposits do not contain secondary cavity fill cementation or re-crystallization, they can be classified as “weakly cemented soil” having the potential to be collapsible soils.

3 GEOTECHNICAL TESTING

For geotechnical testing purposes, 36 undisturbed soil samples were obtained from 2-m-deep test pits and excavation pits that were opened for various civil-engineering works. Due to the highly porous and brittle nature of the tufa, the preparation of laboratory specimens from the block samples was very difficult. To solve this problem, in this research, sampling from the walls of the excavation was preferred to the base. In this way the disturbance of the excavation machine is more effectively controlled and the soil type is properly observed. The pressure to push the sampler into the ground was applied hydraulically instead of manual pushing or hammering (Figure 3). High-quality, thin-walled, hard steel samplers with an area ratio of 8.5 % and a sharp cutting shoe were used. The inside of the sampler was covered with oil before the sampling. A series of laboratory tests was performed on the samples to determine the index and compressibility properties of weakly cemented tufas. Table 1 provides a summary of the test results.

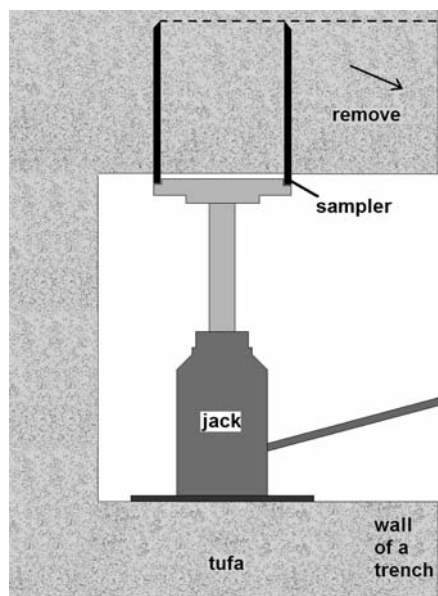


Figure 3. Method for field sampling of collapsible tufa from the wall of a trench.

Table 1. Mean and marginal values of the geotechnical properties.

| Soil Property | Minimum | Mean | Maximum |
|--|----------|----------|---------|
| Specific Gravity (G_s) | 1.98 | 2.29 | 2.47 |
| Dry Unit Weight (kN/m^3) | 10.37 | 11.90 | 13.92 |
| Initial Void Ratio (e_0) | 0.703 | 1.254 | 1.666 |
| Total Fines ($D < 63 \text{ mic}$) (%) | 20 | 49.76 | 91 |
| PFAW (%) | 12 | 36 | 83 |
| m_v (m^2/kN) | 0.000054 | 0.000101 | 0.00018 |
| C_p (%) | 0.81 | 5.20 | 14.5 |

3.1 SPECIFIC GRAVITY, UNIT WEIGHT AND POROSITY

The specific gravity of the soils was determined according to ASTM D854-00e1 [18]. The maximum specific gravity value of five samples is $G_s = 2.47$, which is much less than the characteristic value for calcium carbonate minerals. This results from the determination technique and the material characteristics. The specific-gravity values were determined by applying a vacuum into the pycnometer. There must have been unreachable and closed micro-voids, and such voids can be seen on the SEM images. Taking into account the closed voids, for the void ratio calculations a theoretical value of $G_s = 2.7$ was used.

The unit weight of soils was determined for the oedometer test samples as the ratio of the soil weight to the internal volume of the ring. The void ratio of the soil specimens found in the oedometer tests ranged between 0.71 and 1.67, which classifies them as medium to highly porous in the IAEG classification system [19].

3.2 GRAIN SIZE DISTRIBUTION

The grains in the tufa samples are sand-silt-sized non-plastics. As the collapsible behavior is related to the weak cementation between the grains, the fine-material content gives an important clue regarding the degree of cementation of the grains. The performed grain size distribution tests were applied in accordance with the procedure suggested by ASTM D422-63 [20]. In dry conditions, due to the cementation between the grains, the dominant grain size is the sand size tufa lumps. In wet sieving, however, the cementation is destroyed and the fraction of the fines is increased (Figure 4). In wet sieving the soil is sieved by applying a tap-water flow through the 63-micron sieve without any dispersing agent. In this way only weak bonds, which dissolve in water without any frictional force or acidic agent, are disrupted. Saturation results in the dissolution of the carbonate bonds between the grains of lumps, and thus the solid grains become free, and finally the grain size decreases. A new parameter given in Dipova and Doyuran (2006b) [2] "Percent Fines After Wetting (PFAW)", which is in fact the difference in the fine fraction between the dry and wet sieving loosened after the dissolution of the soil lumps as a result of the saturation. This parameter is also used in the predictive models in this paper.

3.3 COMPRESSIBILITY AND COLLAPSIBILITY

To observe the compressibility and collapsibility of the soil specimens, standard oedometer tests were applied. Due to the highly porous and brittle nature of the tufa, special care was required during the preparation of the oedometer test samples from the 100-mm Shelby tube samples. A specially manufactured hydraulic sample extruder with two adapter plates was used (Figure 5). A little wetting of the soil around the ring was helpful when pushing the ring without any break up of the sample edge. A constant specimen diameter of 75 mm and a height of $H = 20$ mm were used. All the specimens were allowed to air-dry before testing.

Due to the sample heterogeneity and the difficulties encountered in the preparation of two samples that have

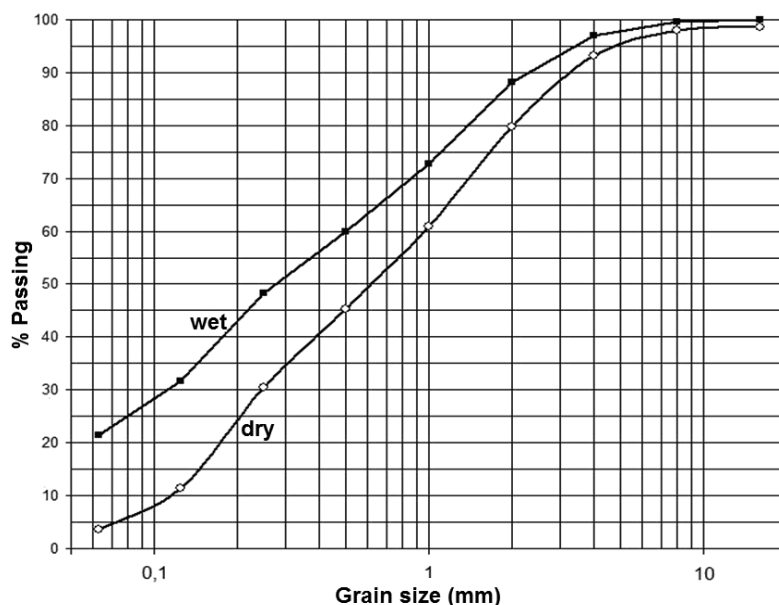


Figure 4. Grain size distribution after dry and wet sieving.

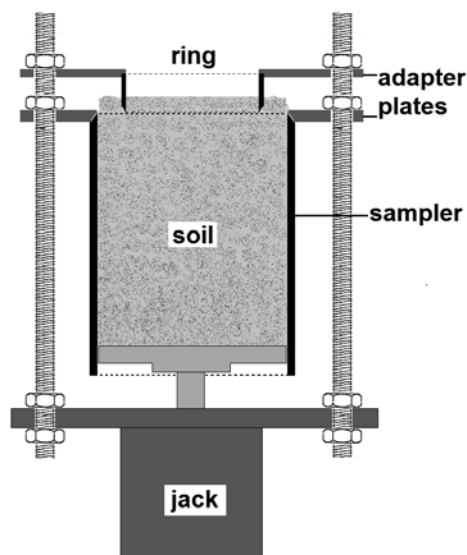


Figure 5. Sample extruder having two adapters set, which were used in the oedometer sample preparation.

In the oedometer test, a freshly undisturbed unsaturated specimen is incrementally loaded (the load increment ratio is unity) to a desired vertical stress (200 kPa in this study) without wetting the specimen. The samples were saturated at a stress of 200 kPa and the collapse potentials were determined at this stress level. The time-settlement readings during unsaturated loading, during the collapse process and after the collapse, were continuously recorded with the aid of sensitive electronic deformation sensors and an analog-to-digital converter (ADC) interface. By step loading before and after the 200 kPa, the behavior of the soil under dry (at the natural water content) and fully saturated conditions was determined. In particular for the prediction of the settlement under dry conditions before wetting, a determination of the volume compressibility (m_v) is possible in this way. The collapse potential of an unsaturated specimen was calculated from equation (1) taking “ e ” as the void ratio of the soil specimen before the water saturation.

the same initial void ratio for a double oedometer test, the tests were carried out by applying the “single-ring method” on a single specimen. The double-ring oedometer method is suitable for observing the differences in the deformation characteristics between the partially and fully saturated specimens at different stress levels. However, if the purpose of the test is to obtain a measure of the amount of volume change that occurs when a partially saturated soil becomes submerged under constant stress, it would be more practical and simpler to use the single-ring oedometer test.

4 GEOTECHNICAL EVALUATIONS

The mechanism for collapse includes an increase in the loading and/or an increase in the water content. In this section the collapse will be discussed for weakly cemented tufa for the air-dry condition (dry) and for the fully saturated state (wet). Similar to the investigated foundation settlement of buildings on weakly cemented tufa, a total collapse that results from loading and saturation should be considered.

4.1 STRESS LEVEL-COLLAPSE POTENTIAL RELATIONSHIP

To investigate the stress level-collapse potential relationship, a group of samples was tested in the laboratory and the collapse deformations were measured at different stress levels. To create a hydro-collapse, the samples were saturated at different stress levels, ranging between 25 kPa and 400 kPa. Typical compression curves are shown for dry and saturated samples in Figure 6. From this figure it is concluded that for both curves the trend is polynomial within the testing limits. The vertical distance between these two polynomial lines at any pressure level gives the void ratio difference ($e_1 - e_2$) upon saturation. In the figure it is also clear that the void ratio difference ($e_1 - e_2$) changes almost linearly up to 200 kPa. Thus, for small foundation pressures, the collapse potential changes almost linearly with pressure.

4.2 TIME-SETTLEMENT RELATIONSHIP

To assess the rate of settlement, the one-dimensional deformation during the oedometer tests was measured using an electronic deformation sensor and stored on a computer. The recorded data were plotted on time-settlement graphs (Figures 7 and 8). In both the dry and wet loading the rate of settlement is rather high. In the dry-loading phase, just after the load application, 80 % of the collapse settlement occurred in less than an hour. The remaining settlement occurred as a creep-like deformation throughout the day (Figure 7). For the same sample, after 24 hours in the dry condition, saturation results in a collapse, which causes a large displacement with respect to the dry loading (Figure 8). The rate of settlement was higher than that of the dry phase. Almost 95 % of the total settlement was completed in an hour, and 5 % of the deformation was creep. This behavior implies that the

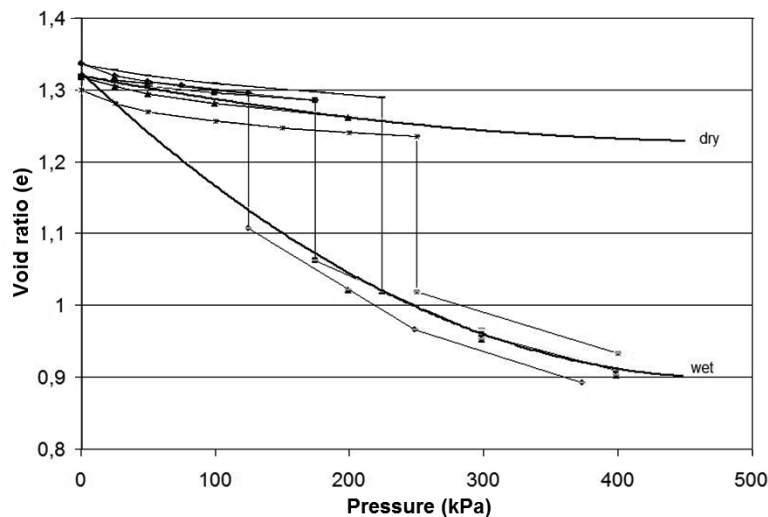


Figure 6. Stress level-collapse potential relationship of a group of tufa samples.

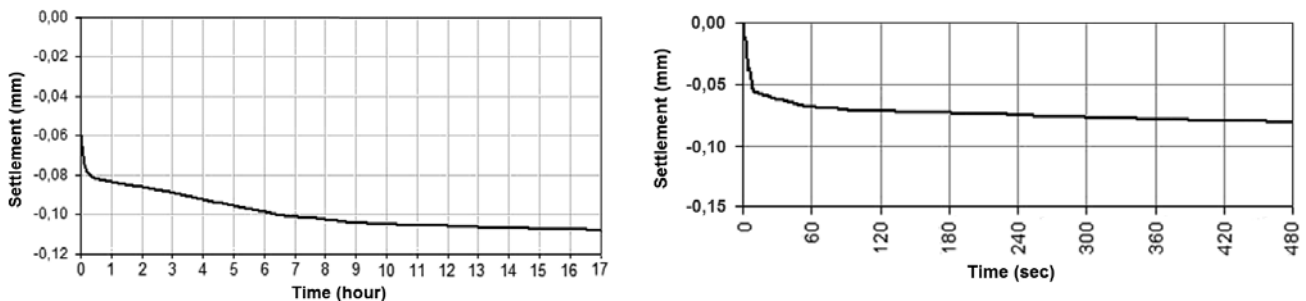


Figure 7. left - Time-settlement curve of tufa under 100 kPa pressure (dry), right - Time-settlement curve of tufa under 100 kPa pressure (dry) (close up view).

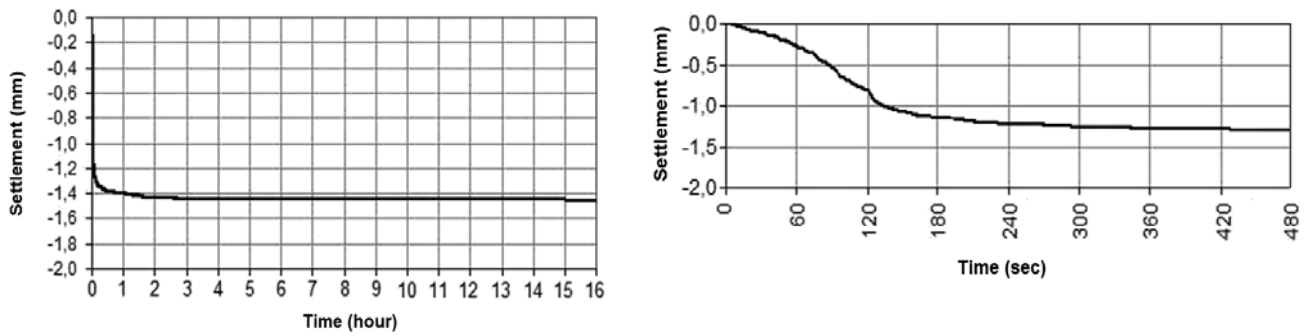


Figure 8. left - Time-settlement curve of tufa under 100 kPa pressure (wet), right - Time-settlement curve of tufa under 100 kPa pressure (wet) (close up view).

destruction of the inter-particle bonding occurs relatively quickly. The time for the completion of the settlement, even if it is relatively short, should have been spent for the re-arrangement of the particles and the stress re-distribution cycles, up to the final arrangement.

4.3 STATISTICAL EVALUATIONS AND PREDICTIVE MODELS

In the face of the complicated behavior of the collapsible tufa deposits and the various parameters that affect it, an alternative route would be the development of prediction models that can, to some extent, substitute expensive and time-consuming laboratory techniques. Although the laboratory techniques are quite reliable, for a quick appraisal of the collapse potential, an empirical method based on simple index tests for the prediction of foundation settlement will be helpful.

The values of the collapse potential (C_p) change over a wide range. However, statistical analyses showed that C_p is in a relatively close relationship with the initial void ratio (e_0) and the difference in the fine content between dry and wet sieving (PFAW) and also with the natural unit weight (γ_n). Similarly, another statistical analysis was performed to search for relationships between the coefficient of volume compressibility (m_v), e_0 and PFAW. Utilizing the results of multiple regression analyses the following best-fit equations were found to obtain the C_p and m_v parameters (Equations 2 and 3). This approach will be used in the settlement predictions in the following section.

$$C_p = 1.06 * e_0 + 115.61 * \left(\frac{1}{PFAW}\right) - 0.45, (R^2=0,63) \quad (2A)$$

$$C_p = 12 * \gamma_n^{-4}, (R^2=0,56) \quad (2B)$$

$$m_v = 0.0001 * (1.55 * e_0^2 - 2.98 * e_0 + 3.58 * \left(\frac{1}{PFAW}\right) + 2.05), (R^2=0,71) \quad (3)$$

5 PREDICTION OF THE SETTLEMENT OF FOUNDATIONS

5.1. DIRECT LABORATORY METHOD

A simple oedometer method can be used for settlement predictions at a particular pressure level. The collapse potential may be estimated for an applied stress less than this particular level by calculating the difference in the strain between the inundated and un-inundated curves in an e -log vs P plot, as suggested in ASTM D5333 – 03 [9]. The inundated curve is obtained by drawing a line between the starting point of the dry loading and the end of the collapse. This procedure can be applied in an e - P graph, in which the trend shows polynomial behavior (Figure 9a).

On the test curve the void ratio reductions for loading at the natural water content and collapse (Δe_1 and Δe_2 respectively) corresponding to the incremental pressure (Δp) are determined. The settlement of soil without any change in the natural moisture content (S_1) and the settlement caused by the collapse in the soil structure (S_2) are given by the following expressions:

$$S_1 = \frac{\Delta e_1}{1 + e_0}(H) \quad (4)$$

$$S_2 = \frac{\Delta e_2}{1 + e_1}(H) \quad (5)$$

where H is the thickness of the soil susceptible to collapse, and e_0 , e_1 and e_2 are the void ratios shown in figure 9a.

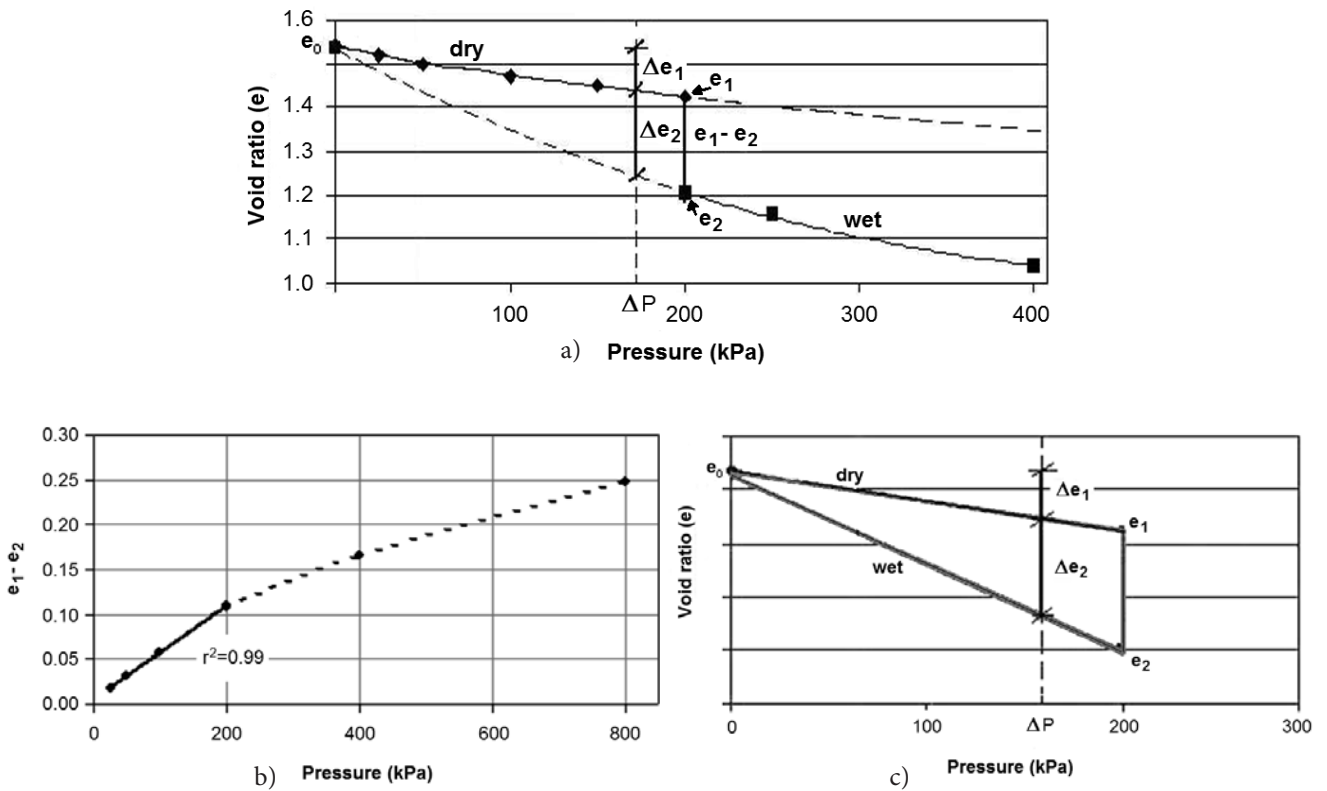


Figure 9. a) Settlement calculation from single oedometer test for a foundation pressures less than 200 kPa (Modified from ASTM 5333),
 b) For pressures below 200 kPa, Δe_2 changes almost linearly,
 c) Assumed triangle model used in empirical settlement calculation for foundation pressures less than 200 kPa.

5.2 EMPIRICAL METHOD

Settlements that result from the pore collapse of tufa occur very rapidly. When a stability problem arises, engineers have to make a reliable decision quickly. The technique for determining the collapse potential and to estimate settlement, which is given in the previous sections, is based on undisturbed sampling, careful sample preparation and laboratory testing. However, to have an idea about the soil, the collapse potential calculations and the settlement predictions can be made empirically, in a short time and with less effort. Using the empirical procedure, the collapse potential calculations and the settlement predictions can be made in hours and without the need for complicated laboratory equipment.

The laboratory test results reveal that for small pressures less than 200 kPa, Δe_2 changes almost linearly (Figure 9b). This allows us to assume a triangular shape for the behavior of the collapse for the changing stress levels, as shown in Figure 9c. In this way, Δe_2 for any pressure level less than 200 kPa can be calculated by making a linear interpolation.

The empirical method that is proposed in this study starts with a determination of the dry density. For this purpose, a soil specimen of known volume (V) should be obtained. A sample taken in a steel tube or a cube sample can be used. After determining the mass of the dry soil sample (M), the dry density (ρ_{dry} , Mg/m^3) and the initial void ratio (e_0) can be obtained ($G_s = 2.7$).

$$\rho_{dry} = \frac{M}{V} \quad (6)$$

$$e_0 = \frac{G_s}{\rho_{dry}} - 1 \quad (7)$$

Using a sieve analysis the PFAW can be calculated. Using equations 2 and 3, C_p , (at 200 kPa), m_v (for 100-200 kPa) can be estimated and $e_1 - e_2$ (at 200 kPa), can be calculated.

$$e_1 = e_0 - (m_v \cdot \Delta p \cdot (1 + e_0)) \quad (8)$$

$$e_1 - e_2 = \frac{C_p(1 + e_1)}{100} \quad (9)$$

Using a linear interpolation Δe_2 can be calculated (Equation 10), and using m_v , Δe_1 can be calculated for the pressure level at which the settlement calculations are being carried out (Equation 11).

$$\Delta e_2 = \frac{(e_1 - e_2) \cdot (\Delta P)}{200} \quad (10)$$

$$\Delta e_1 = m_v \cdot \Delta P \cdot (1 + e_0) \quad (11)$$

The settlement of soil without a change in the moisture content and the settlement caused by any further collapse in the soil structure due to saturation can be calculated using equations 4 and 5, respectively.

To make a comparison between the direct (single ring oedometer) method and the empirical method, the settlement of a 4-m-thick collapsible soil layer is calculated at 100 kPa base pressure making use of the laboratory data from 36 samples. Figure 10 shows the comparison between settlement values calculated with the direct oedometer technique and the empirical method mentioned above. The results of the direct oedometer technique are in close agreement with the empirical method.

6 CONCLUSIONS

- (1) The grains in the Antalya tufa deposits are bound together by meniscus cementation, comprising thin calcium carbonate films. Most of the paludal and fluvial environment tufas are made of grain-supported sand and silt size grains. A weak meniscus cementation makes these deposits bonded but with a highly porous soil structure. An increase in the water content can easily dissolve these thin films and destroy the interspatial bonding.
- (2) The collapse potential (C_p) values determined from the oedometer tests fall between 0.8% and 14.5%. Most of the studied tufa samples fall into the collapsible class. The collapse potential (C_p) is in a close relation with the initial void ratio (e_0) and the percentage fines after wetting (PFAW). Similarly, a relationship between the coefficient of volume compressibility (m_v), the initial void ratio (e_0) and the percentage fines after wetting (PFAW) was obtained.
- (3) The collapsibility of tufas depends on the stress level. The void ratio difference between the dry and wet testing ($e_1 - e_2$) changes almost linearly

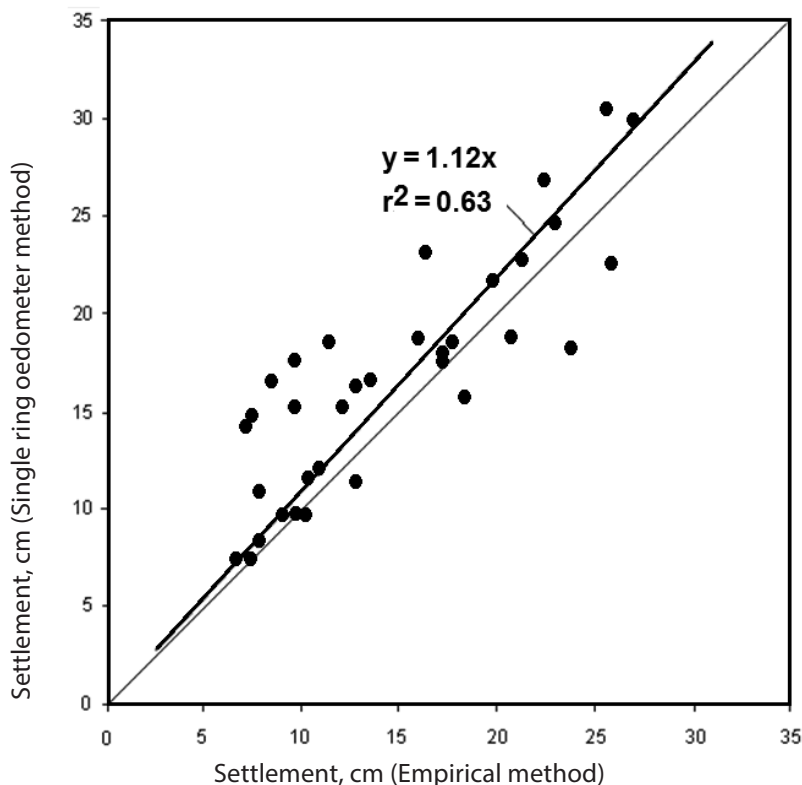


Figure 10. Comparison between settlement calculations using single-ring oedometer and empirical settlement methods.

up to 200 kPa. Thus, for foundation pressures less than 200 kPa, which is common for most low-rise and middle-rise buildings, the collapse potential changes almost linearly with pressure.

- (4) The settlement of foundations due to the collapse of a soil structure can be estimated directly and empirically. The direct method is based on undisturbed sampling and an evaluation of the oedometer test results. The indirect method was improved based on the relationship between the collapse potential – index parameters and the coefficient of volume compressibility. The comparison of the direct and empirical approaches yielded good agreement.

ACKNOWLEDGEMENTS

This study was supported by the Research Fund of Akdeniz University (Antalya, Turkey).

REFERENCES

- [1] Dipova, N. and Doyuran, V. (2006a). Characterization of the Antalya (Turkey) tufa deposits. *Carbonates and Evaporites*, 21(2), 144-160.
- [2] Dipova, N. and Doyuran, V. (2006b). Assessment of the collapse mechanism of tufa deposits. *Engineering Geology*, 83, 332-342.
- [3] Cuccovillo, T. and Coop, M. R. (1997). Yielding and pre-failure deformation of structured sands. *Geotechnique*, 47, 3, 491-508.
- [4] Leroueil, M. (2000). Contribution to the round table: Peculiar aspects of structured soils. In A. Evangelista and L. Picarelli (Eds.), *The geotechnics of hard soils – soft rocks: Proceedings of the second International Symposium on Hard Soils – Soft Rocks*, Naples, Italy, 12-14 October 1998 (v.3, pp. 1669-1677). Rotterdam, the Netherlands: A. A. Balkema.
- [5] Airey, D. W. (1993). Triaxial testing of naturally cemented carbonate soil. *Journal of Geotechnical Engineering*, 119,9, 1379-1398.
- [6] Denisov, N. Y. (1953). *Stroitel'nye Svoystva Loessov I Lessovidnykh Suglinkov (Construction Properties of Loesses and Loessial Soils)*, Gosstrojizdat, Moscow, CIS.
- [7] Dudley, J. G. (1970). Review of collapsing soils. *The Journal of Soil Mechanics and Foundation Division ASCE*, 96, 925-947.
- [8] Reznik, Y. M. (1994). Evaluation of collapse potentials using single oedometer test results. *Bulletin of the Association of Engineering Geologists XXXI* 2, 255-261
- [9] ASTM. (2005). ASTM, D5333-03, Standard test method for measurement of collapse potential of soils, ASTM Standards, Philadelphia, Pennsylvania.
- [10] Abelev, Y. M. (1948). *The essentials of designing and building on micro-porous soils*. Stroital Naya Promyshlemast, No.10.
- [11] Derbyshire, E., Meng, X., Wang, J., Zhou, Z. and Li, B. (1995). Collapsible loess on the loess plateau of China. In: E. Derbyshire, T.A. Dijkstra and I.J. Smalley, Ed. *Genesis and Properties of Collapsible Soils*. NATO ASI Series C: Mathematical and Physical Sciences vol. 468, Kluwer Academic Publishers, Dordrecht, The Netherlands, 267-293.
- [12] Jefferson, I. and Smalley, I. (1995). Six definable particle types in engineering soils and their participation in collapse events: proposals and discussions. In E. Derbyshire, T. Dijkstra and I. J. Smalley, ed. *Genesis and properties of collapsible soils*, NATO ASI Series C: Mathematical and Physical Sciences vol. 468, Kluwer Academic Publishers, Dordrecht, The Netherlands, 19-32.
- [13] Lefebvre, G. (1995). Collapse mechanisms and designs for partly saturated soils. In E. Derbyshire, T. Dijkstra and I. J. Smalley, ed. *Genesis and properties of collapsible soils*, NATO ASI Series C: Mathematical and Physical Sciences vol. 468, Kluwer Academic Publishers, Dordrecht, The Netherlands, 361-374.
- [14] Rogers, C. F. D. (1995). Types and distribution of collapsible soils. In E. Derbyshire, T. Dijkstra and I. J. Smalley, ed. *Genesis and properties of collapsible soils*, NATO ASI Series C: Mathematical and Physical Sciences vol. 468, Kluwer Academic Publishers, Dordrecht, The Netherlands, 1-18.
- [15] Torrance, J. K. (1995). Post-depositional processes in high sensitivity, fine grained, collapsible sediments. In E. Derbyshire, T. Dijkstra and I. J. Smalley, ed. *Genesis and properties of collapsible soils*, NATO ASI Series C: Mathematical and Physical Sciences vol. 468, Kluwer Academic Publishers, Dordrecht, The Netherlands, 295-312.
- [16] Rao, S. M. and Revanasiddappa, K. (2002). Collapse behaviour of a residual soil, *Geotechnique* 52(4), 259-268
- [17] Rollins K. M., Rollins R. L., Smith T. D. and Beckwith G. H. (1994). Identification and characterization of collapsible gravels, *Journal of geotechnical engineering*, 120(3), 528-542.
- [18] ASTM. (2000). ASTM D854-00e1, Standard test methods for specific gravity of soil solids by water pycnometer, ASTM Standards, Philadelphia, Pennsylvania.
- [19] IAEG. (1981). *Rock and soil descriptions for engineering geological mapping*. Report by the IAEG

Commission on Engineering Geological Mapping.
Bull. Int. Assoc. Eng. Geol. 24, 235–274.

- [20] ASTM. (1998). ASTM D422-63, Standard test method for particle-size analysis of soils, ASTM Standards, Philadelphia, Pennsylvania.

MONITORING STABILNOSTI VISOKIH VARNOSTNIH STEBROV Z EL PALIČNIMI MERILCI DEFORMACIJ V KAMNOLOMU LIPICA II

JOŽE KORTNIK, SUNNY O. NWAUBANI IN ANDREJ KOS

o avtorjih

vodilni avtor

Jože Kortnik
University of Ljubljana,
Faculty of Natural Sciences and Engineering,
Department of Geotechnology and Mining
Ljubljana, Slovenija
E-pošta: joze.kortnik@guest.arnes.si

Sunny O. Nwaubani
Anglia Ruskin University,
Faculty of Sciences and Engineering
Cambridge&Chelmsford, Velika Britanija
E-pošta: sunny.nwaubani@anglia.ac.uk

Andrej Kos
Marmor Sežana
Sežana, Slovenija
E-pošta: kos@marmorsezana.com

izvleček

Podzemno pridobivanje blokov naravnega kamna v kamnolomu Lipica II. poteka po nahajališču prilagojeni komorno – stebrni odkopni metodi. Za podpiranje in zagotavljanje stabilnosti podzemnih prostorov se uporablja samonosilna kamnina v obliki visokih varnostnih stebrov. Visoke varnostne stebre sekajo številne diskontinuitete, ki lahko predstavljajo različna tveganja pri zagotavljanju stabilnosti podzemnih prostorov in izvajanju del na podzemnih deloviščih. Za zagotavljanje varnosti se izvaja monitoring napetostnih in deformacijskih parametrov visokih varnostnih stebrov z uporabo (WV) nape-tostnih merilnih celic, vgrajenih v notranjosti in EL paličnimi merilci deformacij, vgrajenimi na površini varnostnih stebrov. V članku so podrobneje predstavljeni postopki in rezultati izvajanja monitoringa potencialnih klinov v visokih varnostnih stebrih z EL paličnimi merilci pri podzemnem pridobivanju blokov naravnega kamna v kamnolomu Lipica II.

ključne besede

EL (elektronski) palični merilec, naravni kamen, visoki varnostni steber, komorno stebrna odkopna metoda

HIGH SAFETY PILLARS STABILITY CONTROL USING EL BEAM DISPLACEMENT SENSORS IN LIPICA II QUARRY

JOŽE KORTNIK, SUNNY O. NWAUBANI and ANDREJ KOS

about the authors

corresponding author

Jože Kortnik
University of Ljubljana,
Faculty of Natural Sciences and Engineering,
Department of Geotechnology and Mining
Ljubljana, Slovenia
E-mail: joze.kortnik@guest.arnes.si

Sunny O. Nwaubani
Anglia Ruskin University,
Faculty of Sciences and Engineering
Cambridge&Chelmsford, United Kingdom
E-mail: sunny.nwaubani@anglia.ac.uk

Andrej Kos
Marmor Sežana
Sežana, Slovenia
E-mail: kos@marmorsezana.com

abstract

In underground Lipica II. quarry for the excavation of natural stone, a modified room-and-pillar mining method is used, that is adjusted to the conditions of the site. In order to support and ensure the stability of underground chambers high safety pillars (HSP) are used. These pillars are made of surrounding stone and therefore intersected by discontinuities. The discontinuities represent high risk to the stability of underground facilities and workmen below/itself. To ensure their safety the stress and strain parameters in high safety pillars are continuously monitored using two vibrating wire (WV) stressmeters inside the high safety pillars and two EL (Electronic level) beam sensors on the surface of the high safety pillar VS3. In the time period October 2010/June 2012 absolute max. measured deviation with EL beam sensors were $D_1=0.9$ mm and $D_2=1.1$ mm, which does not compromise the stability of the high safety pillar VS3. This paper presents the procedures of wedges deformation monitoring in safety pillars with EL beam sensors in the Lipica II underground natural stone quarry.

keywords

beam sensor, high safety pillar, monitoring, natural stone, room and pillar mining method

1 INTRODUCTION

Mining engineers have to work with the limitations of available technology. The strength and deformation characteristics of the rock and the discontinuities play a major role in determining the suitability as well as the reinforcement and support requirements in underground excavation of natural stone. Proper monitoring of safety pillars and rock masses can help a mining engineer recognize when the probability of a failure is higher than usual. This pre-failure warning can help the mining engineer in many ways. Not only do safety pillar failures wreak havoc on current production, they are able to seriously damage machine equipment, and in the worst case injure workers too close to the point of failure [2]. The objective of safety pillars monitoring is to detect, before failure, possible instabilities to allow the mining engineer to take appropriate remedial measures. The main concern and main purpose of monitoring is the protection of workers and equipment [10].

In analysis of special phenomena such as failure of structures, pillar wedge stability, etc. requires deformation measurement with specific high precision instruments. In various scientific papers demonstrates mostly two types of measuring instruments, EL beam or tiltmeter and 3 screw open fissures displacement meter. Several types of sensitive tiltmeters have been developed to measure and observe ground deformations. A tiltmeter gives the rotation of a line segment fixed in the rock about a chosen horizontal axis perpendicular to the local gravity vector [3, 15]. A 3 screw dyke-displacement meter measures the change in distance between three points(screws) on the rock which are a finite triangle distance apart [8, 9]. Both instruments enables the detection of small deformations that cannot be detected and measured by ordinary surveying instruments to be determined. These instruments were used to study the movement of ceiling/roof and walls in underground structures of the Lipica II. quarry.

In the Lipica II. quarry near city Sežana, the underground excavation blocks of natural stone runs for



Figure 1. 3 screw open fissures displacement meter (left) and glass fissures displacement meter/seal (right) for visual monitoring of underground structures stability in Lipica II. quarry.

more than 12 years. One of the important advantages of the underground mining operations is that they do not affect the surface above. For the purposes of safe and stable excavation of natural stone in underground structures a good knowledge of rock properties in high safety pillars, primary geomechanical conditions in the overburden and discontinuity orientations in the deposition is required. In addition, during the excavation careful monitoring of stress conditions in the safety pillars and ceiling is required. In the context of in-situ measurements and control of the room-and-pillar mining method use is made of stress measurements (2D WV stressmeter device) and deformation measurements (EL beam gauge and 3 screw open fissures displacement meters) in the safety pillars, such as on the ceiling of large open underground spaces. Use of two vertical EL beam gauges, with the task of monitoring the wedges movements or the major discontinuities (open cracks) displacement at the surface area of high safety pillar VS3 (Figure 6.) the Lipica II. quarry was started in 2010.

Purpose of the study presented in this article is to observe the movement of the rock wedges and the impact on the stability of high safety pillars. Additional several 3 screws open fissure displacement meters, cement and glass seals (Figure 1.) were used for visual monitoring the rock deformations in the Lipica II. quarry.

2 PILLARS WITH JOINTS THEORY

Geological discontinuities such as faults, bedding plane contacts, fractures - "joints" for brevity - that transect pillars may fail even though the pillar proper does not. Joint failure mechanisms as well as strength failure of a pillar therefore need to be examined for pillar design. An appropriate safety factor for joints is [11]

$$FS_j = \frac{\tau_j(strength)}{|\tau_j(stress)|} \quad (1)$$

where

$\tau_j(strength)$... shear strength relate to joint
 $\tau_j(stress)$... sheara stress relate to joint.

A Mohr-Coulomb criterion for joint strength is reasonable, so shear strength is given by

$$\tau_j = \sigma_j \tan(\varphi_j) + c_j \quad (2)$$

where the subscript j refers to the joint.

Joint properties are considered known, but stress analysis is necessary to determine the normal stress acting across the joint and the shear stress acting along the joint.

Flat seam pillars with joints [11]; A simple force equilibrium analysis suffices for the determination of joint stresses that, in fact, are average stresses. With reference to Figure 2, equilibrium in the flat seam case requires

$$\begin{aligned} \sigma_j \cdot A_j &= S_p \cdot A_p \cos(\alpha) \\ \tau_j \cdot A_j &= -S_p \cdot A_p \sin(\alpha) \end{aligned} \quad (3)$$

where the stresses are indeed averages over the respective areas acted upon. In view of the relationships $A_p = A_j \cdot \cos(\alpha)$,

$$\begin{aligned} \sigma_j &= S_p \cdot \cos^2(\alpha) = S_p \cdot \left(\frac{1 + \cos(2\alpha)}{2} \right) \\ \tau_j &= -S_p \cdot \sin(\alpha) \cdot \cos(\alpha) = - \left(\frac{S_p}{2} \right) \cdot \sin(2\alpha) \end{aligned} \quad (4)$$

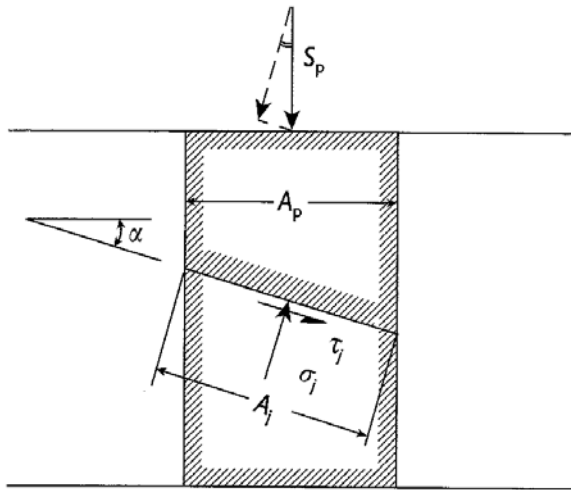


Figure 2. Pillar in a flat seam with a joint [11].

where the negative sign on the shear stress relates to the directions shown in Figure 2. The absolute value is used in the safety factor calculation.

A variation on the question of pillar safety when a joint is present is a question concerning dangerous joint dips. Is there a range of joint dips that are safe? If slip is impending, then

$$\tau_j(stress) = \left(\frac{S_p}{2}\right) \cdot \sin(2\alpha) > \tau_j(strength) = \left(\frac{S_p}{2}\right) \cdot [1 + \cos(2\alpha)] \cdot \tan(\varphi_j) + c_j \quad (5)$$

where absolute shear stress value is used. After rearrangement, this criterion is

$$\left(\frac{S_p}{2}\right) \cdot \sin(2\alpha - \varphi_j) > \left(\frac{S_p}{2}\right) \cdot \sin(\varphi_j) + c_j \cdot \cos(\varphi_j) \quad (6)$$

A graphical interpretation of this criterion is shown in Figure 3 that contains Mohr-Coulomb failure criteria for pillar and joint and the Mohr circle that represents the stress state in the pillar. Figure 3 shows that in the range \$(\alpha_A, \alpha_B)\$ joint slip is possible. This range increases with pillar stress and is maximum when the pillar stress equals pillar unconfined compressive strength, as shown in Figure 3 where the Mohr circle just touches the pillar strength line. Formal solution requires finding the inverse sine of the function containing \$\alpha\$ in the slip condition. There are actually four solutions because there is symmetry to the problem. This symmetry is graphically represented in the lower half of Mohr's circle where shear stresses and (strengths) are negative. Physi-

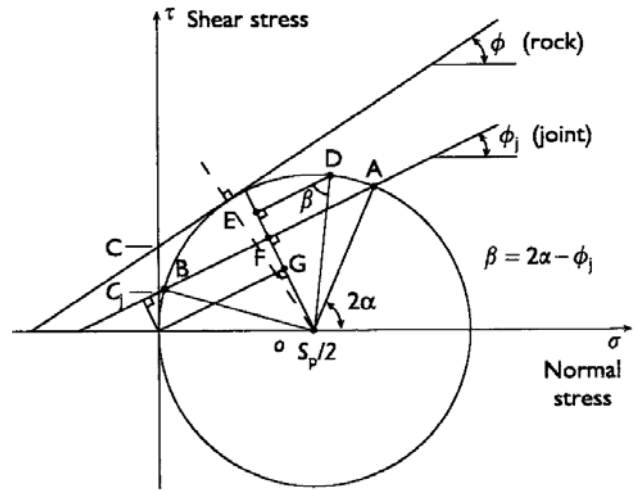


Figure 3. Pillar in a flat seam with a joint [11].

cally, there is symmetry of dangerous and safe dips about the vertical load axis. Near vertical and near horizontal joints will be safe as one would intuitively suppose [11].

3 DISCONTINUITIES IN LIPICA II. QUARRY

Discontinuities (open cracks) appearing in the Lipica II. quarry have rough walls and in space variable dip, which is a favorable property regarding the stability of randomly generated wedges. Cracks are mostly empty or filled with heavy mouldable reddish-brown clay (Figure 4.). The thickness of clay fillers varies from thin clay trash to few inches thick clay layer. Cracks walls are mostly lined with red calcite incrustation, which is also advantageous feature of the stability of cracks. In cases where cracks have no incrustation, they are wavy and rough, which means that the unevenness of the cracks surface increases the shear strength of the cracks. Spacing between the cracks is 1 ÷ 5 m. This means that the choice of GSI index less than 50 is not appropriate, since this is applicable in the case of smooth cracks filled with clay. Geomechanical parameters of Lipica limestone are reduced by Hoek analysis [1,6].

The index GSI (Geological Strength Index) was determined on the basis of engineering-geological mapping of cracks and is \$55 \pm 5\$ [5]. For \$GSI = 55 \pm 5\$ is characterized by a block structure with three rock fracture systems and with good merged blocks, whereas the walls of the crack to the flat smooth, with a moist surface. Cracks are closed or open. Open cracks are filled with a compact infill or coarser primary rock particles.



Figure 4. Samples of falling rock wedges in underground structures of Lipica II. quarry.

Geotechnical properties of cracks were accurately determined by reverse analysis of the quarry Lipica II. underground structures. Robertson's test of the samples with a crack-free clay showed values of the angle of internal friction $\varphi = 26^\circ$, cohesion $c = 21$ kPa at 100 kPa load and angle of internal friction $\varphi = 16^\circ$, cohesion $c = 50$ kPa at 160 kPa load [5].

Deposit of natural stone in Lipica II. quarry is a strong tectonic disrupted with at least seven leading towards discontinuity (casting) [12], which cause the danger of underground mining. The cracks link together and form in the ceiling and the side of the underground spaces of the dangerous rock wedges (Figure 4.). Precisely because of this, in order to ensure stability and safe working conditions in-situ monitoring and controlling devices were implemented. In addition to the stress gauges use were also made of EL beams gauges for rock wedge movement and deformation monitoring.

4 EL BEAM GAUGES

The use of the EL beam gauges (also tiltmeter) is an extremely versatile, since they may be used to measure vertical movements, declination or movements on dams, observation of the stability and convergences of banks areas, observation of the tunnels stability, observe of the structures around exploitations areas, etc. EL beam sensors monitor differential movement and rotation in structures. In table 1. is introduced two types of

Table 1. Technical characteristics of EL beam gauge manufacturer Slope Indicator [14].

| | Horizontal | Vertical |
|-----------------------|------------------------------------|----------|
| Measurement range | ± 40 arc min, (± 11 mm/m) | |
| Accuracy | ± 0.1 mm/m | |
| Operating temperature | -20 to +50°C | |
| Weight | 210 g | 890 g |

sensors – horizontal and vertical type. Horizontal beam sensors monitor settlement and heave (Figure 5.) and vertical beam sensors monitor lateral displacement and deformation.

The beam sensor consists of an electrolytic tilt sensor attached to a rigid metal beam. The tilt sensor is a precision bubble-level that is sensed electrically as a resistance bridge. The bridge circuit outputs a voltage proportional to the tilt of the sensor. The beam, which is typically one to two meters long, is mounted on anchor bolts that are set into the structure. Movement of the structure changes the tilt of the beam and the output of the sensor. The voltage reading from the sensor is converted to a tilt reading in mm per meter. Displacements are then calculated by subtracting the initial tilt reading from the current reading and multiplying by the gauge length of the sensor (the distance between anchors). When sensors are linked end to end, displacement values can be accumulated from anchor to anchor to provide a profile of differential movements or settlement.



Figure 5. Horizontal EL beam gauge [14].

The metal rods, on which the meters are installed, are very sensitive to temperature changes, which may be quite great (in the underground mining of natural stone) in winter/summer period quite great. Heating and cooling of the air in the underground spaces result in the expansion and contraction of metal rods. It is therefore necessary to take this into account by introducing a correction factor in data processing of metal rod expansion.

The following polynomial equations is used to calculate the metal beam deflection [4]:

$$\frac{mm}{m} = C5 \cdot EL^5 + C4 \cdot EL^4 + C3 \cdot EL^3 + C2 \cdot EL^2 + C1 \cdot EL + C0 \quad (7)$$

where

EL ... measured voltage value
 C5...C0 ... polynomial coefficients.

Table 1. Example of deviation calculation considering calibration test coefficients - EL beam sensor [4].

| | Polynomial coefficient | EL reading | Value |
|----|------------------------|------------------|---------------|
| C5 | 1.6426E ⁻¹ | -0.585715 | -0.1132257000 |
| C4 | -1.5836E ⁻² | -0.585714 | -0.0018637002 |
| C3 | -2.6881E ⁻¹ | -0.585713 | 0.0510123829 |
| C2 | -7.9904E ⁻² | -0.585712 | -0.0274115629 |
| C1 | 3.5098 | -0.585711 | -2.0557249580 |
| C0 | 8.1185E ⁻² | -0.585710 | 0.0811850000 |
| | | mm/m deviation = | -1.961154082 |

Reading in mm/m it is necessary to multiply with the length of the metal beam (in our case, 2 m), which comes out (2 x -1.961) -3.922 mm.. Due to temperature variations during the period of summer/winter it is necessary to take into account the temperature resistance equation [4]:

$$T = \frac{1}{\left[A + B \cdot (\ln R) + C \cdot (\ln R)^3 \right]} - 273.2^\circ C \quad (8)$$

where

T ... temperature in °C
 ln R ... natural log of termistor resistance
 A ... 1.4051 · 10⁻³
 B ... 2.369 · 10⁻⁴
 C ... 1.019 · 10⁻⁷

5 APPLICATION OF EL BEAMS IN LIPICA II. QUARRY

Two vertical EL beams were have built in safety pillar (VS3) at level 359 on the open discontinuities, both located on the corners of the high safety pillar. Discontinuities with the direction 120°/60° and 110°/75° are open and filled with clay. Both discontinuities cross-cut the safety pillar. In the case of additional compressive load of safety pillar, there could appear a deformation which may cause the slippage of stone wedges from the safety pillars. For a visual check on the safety pillars, cement and glass seals were also installed (Figure 1.). Dangerous rock wedges on the security pillar are stabilized with anchors (Figure 7.).

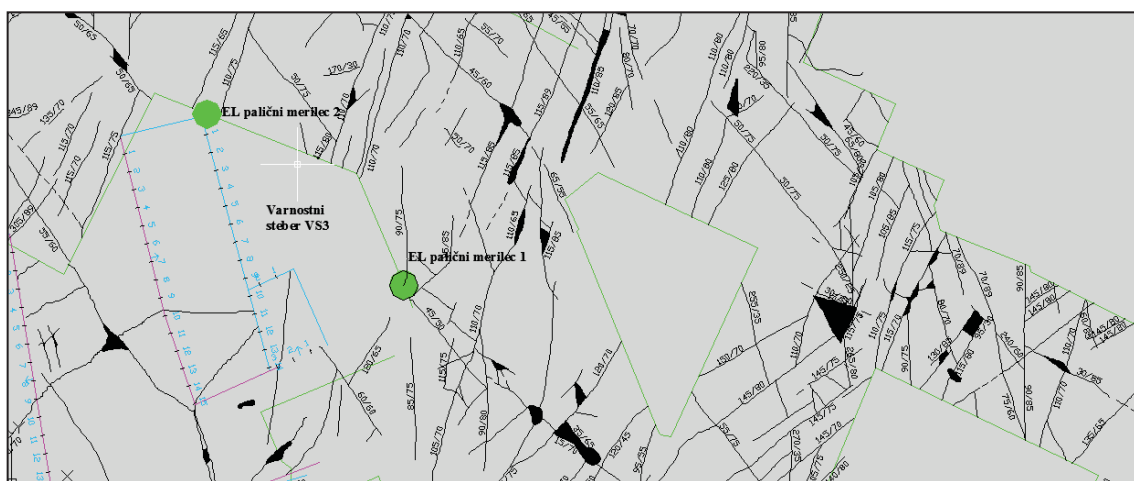


Figure 5. Map of the rock discontinuity orientations and locations (green circle) of two vertical EL beams gauges instalations (safety pillar VS3) in Lipica II. quarry [7, 12].



Figure 7. Datalogger (left) with vertical EL beam gauge (right) installation on the high safety pillar VS3 stabilized with anchors (middle) in Lipica II. quarry.

Figure 6. shows a map of the rock discontinuities appearing on the sealing of underground structures and locations (green circle) of EL beam gauges instalations in Lipica II. quarry.

In Lipica II. quarry EL beam meter manufacturer Slope Indicator is used to measure supervisory convergences in one vertical plane in high safety pillar VS03 (Figure 7). A bar gauge is installed through the cracks, so that there is one screw on the part of the anchor windlass for anchor, such as flexible wedge screw for stable work. From practical experience, the best indicators of developments are movements in pillar corners. Consequently, it was decided to monitor the developments on the safety pillar corner, where the sliding surfaces of the main crack are driving out.

6 DISCUSSION

In the time period October 2010/June 2012 absolute max. measured deviation was $D_1=0.9$ mm and $D_2=1.1$

mm (see Table 3. and Figure 8.), which does not threaten the stability of the heigh safety pillar VS3. EL beam gauges have so far proved to be a reliable tool for high safety pillar stability monitoring.

As already mentioned the heating and cooling of air in underground structures leads to expansion and contraction of metal rods. Therefore, the data processing involves use of correction factor for metal rods. From Figure 8, we can see that in the summer times, the EL beam rod stretches but in the winter time the EL beam rod shrinks. The metal rod, on which there is displacement meter was observed to be sensitive to changes in temperature, which occurs in the underground extraction during the winter/summer and may be relatively large (ΔT of air in period from 2010/2011 winter -6.4°C / summer 22.3°C).

Problems with rock wedge spalling and pillar stability have been studied to a great extent in the mining industry, but they take a different approach to the safety factor for their underground openings. Localized yield-

Table 3. Data of deviation measurement with EL beam 1 and EL beam 2 [7].

| Date | EL beam 1 – deviation [mm] | | Date | EL beam 2 – deviation [mm] | |
|-------------------------|----------------------------|-----------|-------------------------|----------------------------|-----------|
| 15.11.2010 | - 0.09336 | | 03.11.2010 | - 0.11903 | |
| 19.12.2010 | | + 0.31603 | 19.12.2010 | | + 0.53867 |
| 27.08.2011 | - 0.48343 | | 09.03.2011 | | + 0.39831 |
| 21.12.2011 | | + 0.30086 | 27.08.2011 | - 0.34415 | |
| 05.02.2012 | | + 0.41547 | 06.02.2012 | | + 0.35279 |
| 18.06.2012 | - 0.42992 | | 18.06.2012 | - 0.57776 | |
| $D_{1\text{max, min.}}$ | - 0.48343 | + 0.41547 | $D_{2\text{max, min.}}$ | - 0.57776 | + 0.53867 |
| D_1 | 0.89890 mm | | D_2 | 1.11643 mm | |

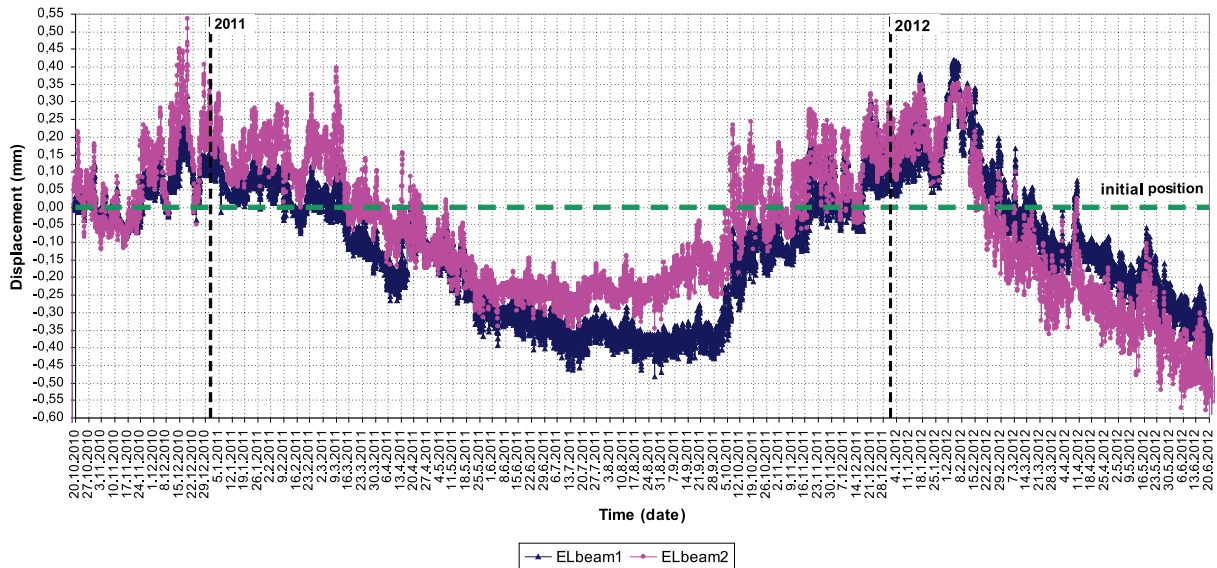


Figure 8. Diagram of the measured EL beam1 and EL beam 2 true deflections/movements in mm in the time period October 2010/June 2012.

ing or failure is a natural part of the process, since the extraction ratio has to be as large as possible. Different empirical methods have been developed, but very few people have taken a more theoretical look at the problem and verified the theories with controlled field experiments. From a high safety pillar stability point of view, these empirical results are just first step to the solution and the problem has to be further studied on a more both empirical and theoretical basis.

7 CONCLUSION

In the underground excavation of natural stone blocks using the room-and-pillar excavation method, special attention needs to be paid to the determination of the appropriate dimensions (width and height) of large open underground spaces (rooms) and high safety pillars, as well as the installation of appropriate systems for continual monitoring and identification of instability phenomena in their ceilings.

Due to large heights (even in excess of 20 m) of such open underground spaces, deepening of the plane renders access to the ceiling for any repair work or the installation of additional supports more difficult or even impossible. In order to maintain a stable underground structure and the provision of safety and health at work, high safety pillars in Lipica II. quarry are constantly monitored. Even small changes in strain-stress state in the vicinity of underground structures can mean a

potential risk of the wedge failure, if it is not stabilized properly with anchors. EL beam gauges have so far proved to be a reliable tool for high safety pillar stability monitoring. The advantage of these meters is that in case of gauge failure, we can easily check the operation of the instrument, supply power cable, etc. and in case of any failure also easily replace or repair (in comparison with VW stressmeter gauge, it is cemented in the borehole and replacement is not possible). An important role is played also by the relatively lower price of the EL beam instrument. Efforts to overcome these limitations have resulted in use of the EL beam gauges in Lipica II quarry.

EL beam gauges when compared with other continuously operating strain gauges, for example, vibrating wire (WV) stressmeters significantly cheaper, simpler to install, the installation of surface rock are readily available to eliminate potential errors / repair and the possibility of multiple use by relocating to the current location of the new measurements of displacements / deformations.

Constant monitoring of instability wedges in the pillars hips or in the ceiling of the underground spaces with EL beam gauges will provide more information for the planning of the final dimensions of the new high safety pillars. The experience and results of measurements that are currently gained can be useful in development and/or modifications of existing monitoring systems and to ensure even greater safety in the underground excavation of natural stone.

ACKNOWLEDGEMENT

Special thanks go to Marmor Sežana they enabled not formally funded study with unselfish understanding, attention, a lot of voluntary work and engagement of their human resources, as well as their hardware and software.

REFERENCES

- [1] Brown, E.T. and Hoek, E. (1978): Trends in relationships between measured rock in situ stresses and depth. *Int. J. Rock Mech. Min. Sci. & Geomech. Abstr.* 15, pp.211-215.
- [2.] Dal Moro, G., Zadro, M. (1998): Subsurface deformations induced by rainfall and atmospheric pressure: tilt/strain measurements in the NE Italy seismic area. *Earth and Planetary Science Letters*, vol. 164, no. 1., pp. 193-203.
- [3.] D'Oreye, L.N. (1998): Qualification test of a dual-axis bubble type resistive tiltmeter (AGI-700 series): earth tides recorded and analyzed in the underground laboratory of Walferdange. *Marees Terrestres Bulletin d'Information*, 129, pp. 9953-9961.
- [4.] EL beam Sensor Manual (2003): Slope Indicator Company 2009/10/12, Standard &SC Versions 56801399, 24 p.
- [5.] Fifer-Bizjak, K. (2003): Geotechnical research of Lipica II. quarry underground structures / Geotehnične raziskave za podzemne prostore kamnolom Lipica II.; Nr. P 73/03-750, ZAG, 32 p.
- [6.] Hoek, E., Brown, E.T. (1997): Practical estimates or rock mass strength. *Int. J. Rock Mech. & Mining Sci. & Geomechanics Abstracts*. 34 (8), pp. 1165-1186.
- [7.] Kos, Andrej, Kortnik, J. (2013): Monitoring of high safety pillars stability in quarry Lipica II - EL beam displacement sensors = Merilni nadzor stabilnosti visokih varnostnih stebrov v kamnolomu Lipica II - palični merilniki deformacij EL. *RMZ - Materials and geoenvironment*, vol. 60, no. 2, pp. 111-119.
- [8.] Kortnik, J. (2007): Monitoring and optimization of safety pillars at underground excavation of natural stone / Spremljava in optimiranje varnostnih stebrov pri podzemnem pridobivanju blokov naravnega kamna, 8th conference od mining and geotechnology experts at »40. jump over the leather«, Faculty of Natural Sciences and Engineering, pp. 46-54.
- [9.] Kortnik, J. (2009): Optimization of the high safety pillars for the underground excavation of natural stone blocks, *Acta geotechnica Slovenica*, vol. 2009/1, pp. 34-48.
- [10.] Likar, J. (2012). Geomechanical effects of operation and closing the Idrija mercury mine on the environment. *Acta geodynamica et geomaterialia*, vol. 9, no. 1, str. 43-55.
- [11.] Pariseau, W.G. (2012). Design analysis in rock mechanics, 2nd edition. CRC Press Taylor & Francis Group, pp. 356-360.
- [12.] Rijavec, J. (2011): Report about geological research of natural stone Marmor Sežana -2011 / Porocilo o geoloskih raziskavah naravnega kamna na območjih kamnolomov družbe Marmor, Sežana d.d. - leto 2011, archives of Marmor, Sežana d.d., 36 p.
- [13.] Sheory, P.R. (1994): A theory for in situ stresses in isotropic and transversely isotropic rock. *Int. J. Rock Mech. Min. Sci. & Geomech. Abstr.* 31(1), pp. 23-34.
- [14.] Slope Indicator [cited 20/9/2013] Available on: <<http://www.slopeindicator.com/.../tilt-elbeam.html>>.
- [15.] Teskey, W.F. (1988): Special survey instrumentation for deformation measurements. *Journal of Surveying Engineering*, ASCE, 114(1), pp. 2-12.

ANALITIČNE REŠITVE ENODIMENZIONALNE KONSOLIDACIJE NENASIČENIH ZEMLJIN OB UPOŠTEVANJU NE-DARCYJEVEGA ZAKONA VODNEGA TOKA

J. W. LI IN H. B. WANG

o avtorjih

Jiwei Li
Huazhong University of Science & Technology,
School of Civil Engineering and Mechanics,
Wuhan 430074, Kitajska
E-pošta: iamliji_007@126.com

Huabin Wang
Huazhong University of Science & Technology,
School of Civil Engineering and Mechanics,
Wuhan 430074, Kitajska
E-pošta: huabin@mail.hust.edu.cn

izvleček

Analitične rešitve smo izpeljali za nelinearne enodimenzionalne konsolidacijske enačbe nenasičenih zemljin. Predstavili smo vodilne enačbe z nehomogenim mešanim mejnim stanjem, v katerih je privzeto, da vodni tok sledi ne-Darcyjevemu zakonu, medtem ko sledi zračni tok Darcyjevemu zakonu. Ne-Darcyjev zakon je pravzaprav nelinearno razmerje med tokom in višino. Enačbe za konsolidacijo so torej v nelinearnem načinu. Da bi rešili enačbo analitično, smo v tej študiji uvedli metodo homotopijske analize (HAM), ki je analitična tehnika za nelinearne probleme. Najprej je bila izpeljana vodilna enačba v brezdimenzionalni obliki, za enodimenzionalno konsolidacijo nezasičenih zemljin. Metodo smo potem uporabili za tehniko preslikave za prenos nelinearnih diferencialnih enačb v številne linearne diferencialne enačbe. Te diferencialne enačbe niso bile odvisne od manjših parametrov in so bile primerne za nadzor območja konvergence. Po tem prenosu smo dobili niz rešitev enačb s HAM s selekcijo linearnih operatorjev in dodatnih parametrov. Primerjava med analitičnimi rešitvami in rezultati končne diferencialne metode je pokazala, da je analitična rešitev bolj učinkovita. Naše rešitve so pokazale, da je disipacija zračnega pritiska veliko hitrejša od vodnega pritiska in da imajo vrednosti gradienta I očitno učinek na disipacijske vrednosti presežnega pritiska porne vode, nimajo pa pomembnega učinka na presežni pritisk pornega zraka.

ključne besede

nenasičena zemljina, metoda homotopijske analize, analitične rešitve, ne-Darcyjev zakon, začetni in mejni pogoji

ANALYTICAL SOLUTIONS FOR ONE-DIMENSIONAL CONSOLIDATION IN UNSATURATED SOILS CONSIDERING THE NON-DARCY LAW OF WATER FLOW

J. W. LI and H. B. WANG

about the authors

Jiwei Li
Huazhong University of Science & Technology,
School of Civil Engineering and Mechanics,
Wuhan 430074, P. R. China
E-mail: iamliji_007@126.com

Huabin Wang
Huazhong University of Science & Technology,
School of Civil Engineering and Mechanics,
Wuhan 430074, P. R. China
E-mail: huabin@mail.hust.edu.cn

abstract

Analytical solutions were derived for the non-linear, one-dimensional consolidation equations for unsaturated soils. The governing equations with a non-homogeneous mixed-boundary condition were presented, in which the water flow was assumed to be governed by a non-Darcy law, whereas the air flow followed the Darcy law. The non-Darcy law was actually the non-linear, flux-gradients relationship. The consolidation equations were thus present in a strong, non-linear way. In order to analytically solve the equation, a homotopy analysis method (HAM) was introduced in the study, which is an analytical technique for nonlinear problems. Firstly, a governing equation in a dimensionless form was derived for a one-dimensional consolidation under unsaturated soils. The method was then used for a mapping technique to transfer the original nonlinear differential equations to a number of linear differential equations. These differential equations were independent with respect to any small parameters, and were convenient for controlling the convergence region. After this transferring, a series solution to the equations was then obtained using the HAM by selecting the linear operator and the auxiliary parameters. Meanwhile, comparisons between the analytical solutions and the results of the finite-difference method indicate that the analytical solution is more efficient. Furthermore, our solutions indicate that the dissipation of air pressure is much faster than that of water pressure, and the values for the threshold gradient I have obvious effects on the dissipation values of the excess pore-water pressure, but no significant effect on that of the excess pore-air pressure.

keywords

unsaturated soil, homotopy analysis method, analytical solutions, non-Darcy law, initial and boundary conditions

INTRODUCTION

The consolidation of unsaturated soils is a subject of great interest in geotechnical engineering practice [1-3]. In fact, the excess pore pressures dissipate with time and eventually return to their initial values in unsaturated soils, generated by external loading. The dissipation processes of excess pore pressures are called consolidation and result in a volume decrease [1]. Indeed, it is important to describe the dissipation of the excess pore pressures in understanding the consolidation of unsaturated soils, and the identification of the influencing internal mechanisms also plays an important role.

Several consolidation theories in unsaturated soils have been proposed over the past few years. The notable contributions have included the work of Blight [4], Scott [5], Barden [6] and Fredlund [7]. Fredlund and Hasan [7] proposed a one-dimensional consolidation theory, the most popular in the geotechnical engineering community, in which two partial differential equations were employed to describe the dissipation processes of excess pore pressures in unsaturated soils. Meanwhile, Qin et al. [2] gave an analytical solution for Fredlund's one-dimensional consolidation equation by applying the Laplace transform and Cayley-Hamilton mathematical methods in unsaturated soil with a finite thickness. Their boundary conditions were the top surface being permeable and the bottom surface being impermeable to air and water. Subjecting to the load exponentially varying with time, and using the same method and employing the same boundary conditions, Qin et al. [8] presented an analytical solution to the one-dimensional consolidation in unsaturated soils. Subjected to an arbitrary load, Shan et al. [9] employed a segregation variable method to obtain some exact solutions with three basic boundary conditions for unsaturated single-layer soils.

However, the assumption focuses in the above contributions were based on Darcy’s law, which is valid regardless of the magnitude of the hydraulic gradients. Indeed, some evidence shows that the flow of pore water in unsaturated soil may not obey Darcy’s law. There are currently very few models of unsaturated soils that take into account the non-linear flux-gradient relationship. The non-Darcy law is actually a non-linear flux-gradients relationship. In particular, there are no analytical solutions of the consolidation in unsaturated soils that take into account the non-Darcy law. Cui et al. [10] reported non-Darcy behavior for a range of observed hydraulic gradients under unsaturated conditions. Considering water as a non-Newtonian fluid, Liu [11] deduced a constitutive model for unsaturated soils. Liu and Birkholzer [12] proposed a relationship by generalizing the existing non-Darcy law and Darcy law.

This paper aims to present a mathematical model of one-dimensional consolidation in unsaturated soils by considering the non-linear flux-gradient relationship, and derive its exact solution by a homotopy analysis method.

A homotopy analysis method (HAM) [13] was adapted to solve the non-linear model of one-dimensional consolidation under unsaturated conditions. The method was independent of any small or large parameters and was valid for most non-linear problems in science and engineering. The homotopy analysis method has been successfully applied to many non-linear problems [14-16]. Finally, in order to verify the analytical solution, a comparison was carried out between the analytical solutions and the results of the finite-difference method in some cases. The results indicated that the analytical solution in the present study was reasonable. Moreover, the analytical solutions given here were valuable for understanding consolidation in unsaturated soil.

2 GOVERNING EQUATIONS

2.1 ASSUMPTIONS

The main assumptions for the one-dimensional consolidation governing equations are listed as follows:

- (1) the solid particles and water phase are incompressible.
- (2) the water flow is governed by a non-Darcy-type law, but air flow is governed by a Darcy-type law.
- (3) the effects of temperature change, air dissolved in water, air diffusion, and the generation and diffusion of vapor are ignored.

2.2 NON-DARCY LAW

A general relationship between water flux and hydraulic gradients under unsaturated conditions was proposed by Liu [12] based on Swartzendruber’s work [13]. The relationship can be written as

$$v = -k(i - \int_0^i \exp\{-\frac{x}{I}\} dx) \tag{1}$$

where v is the water velocity, k is the water permeability coefficient, i is the hydraulic gradient, I is the threshold gradient, and α is a constant parameter.

The one-dimensional differential form of Eq. (1) can be written as

$$v = -k(\frac{\partial u_w}{\gamma_w \partial z} + 1 - \int_0^{\frac{\partial u_w}{\gamma_w \partial z} + 1} \exp\{-\frac{x}{I}\} dx) \tag{2}$$

where u_w is the pore-water pressure, $\gamma_w = \rho g$, ρ is the water density, and g is the acceleration due to gravity.

The integrand of the third item in equation (2) can be expanded as a Taylor series

$$\exp\{-\frac{x}{I}\} = \sum_{n=0}^{\infty} (-1)^n \frac{x^{n\alpha}}{n! I^{n\alpha}} \tag{3}$$

Taking the first two of the Taylor series, integral terms with the condition of $v = 0$ at $\frac{\partial u_w}{\gamma_w \partial z} + 1 = 0$ are simplified as

$$\int_0^{\frac{\partial u_w}{\gamma_w \partial z} + 1} (1 - \frac{x}{I})^\alpha dx = \frac{\partial u_w}{\gamma_w \partial z} + 1 - \frac{1}{(\alpha + 1) I^\alpha} (\frac{\partial u_w}{\gamma_w \partial z} + 1)^{\alpha + 1} \tag{4}$$

Substituting Eq. (4) into Eq. (2), the following equation can be obtained as

$$v = -k \frac{1}{(\alpha + 1) I^\alpha} (\frac{\partial u_w}{\gamma_w \partial z} + 1)^{\alpha + 1} \tag{5}$$

The equation reduces to Darcy’s law when α becomes zero ($I \neq 0$), i.e.,

$$v = -k(\frac{\partial u_w}{\partial z} + 1) \tag{6}$$

2.3 CONSOLIDATION OF UNSATURATED SOILS

Following Fredlund and Morgenstern [18], the constitutive relation for the water and air phases are

$$\frac{\partial(V_w / V)}{\partial t} = m_{1k}^w \frac{\partial(\sigma - u_a)}{\partial t} + m_2^w \frac{\partial(u_a - u_w)}{\partial t} \quad (7)$$

$$\frac{\partial(V_a / V)}{\partial t} = m_{1k}^a \frac{\partial(\sigma - u_a)}{\partial t} + m_2^a \frac{\partial(u_a - u_w)}{\partial t} \quad (8)$$

where, $\frac{\partial(V_w / V)}{\partial t}$ is the volume change of water in the soil, m_{1k}^w is the coefficient of water volume change with respect to the change in the net normal stress $\sigma - u_a$, m_2^w is the coefficient of water volume change with respect to the change in the matrix suction $u_a - u_w$, $\frac{\partial(V_a / V)}{\partial t}$ is the volume change of the air in the soil, m_{1k}^a is the coefficient of air volume change with respect to the change in the net normal stress $\sigma - u_a$, and m_2^a is the coefficient of air volume change with respect to the change in the matrix suction $u_a - u_w$. The subscript k stands for the K_0 -loading condition without lateral deformation.

The continuity requirement leads to the following relations [3,18]:

$$m_{1k}^s = m_{1k}^w + m_{1k}^a \quad (9)$$

$$m_2^s = m_2^w + m_2^a \quad (10)$$

where m_{1k}^s and m_2^s are the coefficients of volume change of the soil with respect to a change in the net normal stress $\frac{\sigma_z}{2} - u_a$, and the matrix suction $u_a - u_w$, respectively. σ_z is the total normal stress in the z direction.

According to the law of mass conservation for water, the change in water volume can be written as follows:

$$\frac{\partial(V_w / V_0)}{\partial t} = \frac{\partial v_w}{\partial z} \quad (11)$$

Substituting Eq.(5) and Eq.(7) into Eq.(11), the following equation can be obtained as

$$\frac{\partial u_w}{\partial t} + C_w \frac{\partial u_a}{\partial t} = -C_V^w \frac{\partial^2 u_w}{\partial z^2} \left(\frac{\partial u_w}{\gamma_w \partial z} + 1 \right)^\alpha \quad (12)$$

where, $C_w = \frac{1 - m_2^w / m_{1k}^w}{m_2^w / m_{1k}^w}$, $C_V^w = \frac{k_w}{\gamma_w m_2^w I^\alpha}$.

The air is considered to behave as ideal air, and based on Boyle's law and Darcy's law. The governing equation for the air phase yields

$$\frac{\partial u_a}{\partial t} + C_a \frac{\partial u_w}{\partial t} = -C_V^a \frac{\partial^2 u_a}{\partial z^2} \quad (13)$$

where $C_a = \frac{m_2^a}{m_{1k}^a - m_2^a - (1 - S)nu_{atm} / (\bar{u}_a^0)^2}$,

$$C_V^a = k_a \frac{RT}{g\bar{u}_a^0 M(m_{1k}^a - m_2^a - (1 - S)nu_{atm} / (\bar{u}_a^0)^2)}$$

$\bar{u}_a^0 = u_a^0 + u_{atm}$, k_a is the air conductivity, R is the universal air constant, T is the absolute temperature, M is the average molecular mass of the air phase, u_a^0 is the initial excess air pressure, and u_{atm} is the atmospheric pressure.

2.4 BOUNDARY AND INITIAL CONDITIONS

In the present study, an unsaturated soil layer was considered as an infinite horizontal extent and thickness H (as shown in Fig.1). The top surface is permeable to water and air, whereas the bottom is impermeable to water and air.

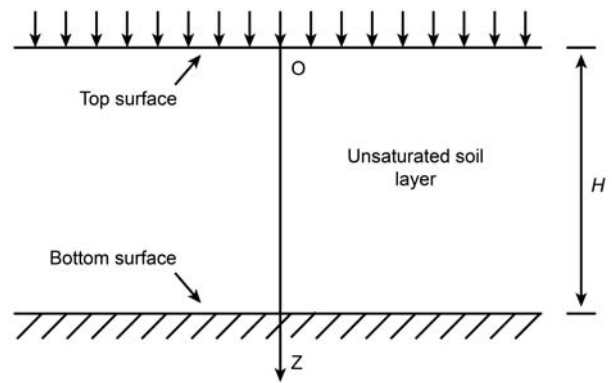


Figure 1. One-dimensional consolidation in unsaturated soils with a permeable top surface and an impermeable bottom base.

Hence, the initial conditions and boundary conditions are respectively expressed as

$$u_a(z, 0) = u_a^0, u_w(z, 0) = u_w^0 \quad (14)$$

$$\begin{cases} u_a(0, t) = u_a^0, u_w(0, t) = u_w^0 \\ \frac{\partial u_a(H, t)}{\partial z} = 0, \frac{\partial u_w(H, t)}{\partial z} = 0 \end{cases} \quad (15)$$

where u_a^0 and u_w^0 are the initial excess air and water pressures at $t = 0$, respectively. ($0 \leq z \leq H, t \geq 0$)

3. ANALYTICAL SOLUTION

3.1 THE ANALYTICAL SOLUTION OF THE EQUATIONS

The Eqs.(12)- (15) can now be rewritten in the dimensionless form as

$$\frac{C_1}{I^\alpha} \frac{\partial^2 \theta_w}{\partial \eta^2} (1 + \alpha C_0 \frac{\partial \theta_w}{\partial \eta}) = \frac{\partial \theta_w}{\partial \tau} + C_w C_2 \frac{\partial \theta_a}{\partial \tau} \quad (16)$$

$$C_3 \frac{\partial^2 \theta_a}{\partial \eta^2} = C_2 \frac{\partial \theta_a}{\partial \tau} + C_a \frac{\partial \theta_w}{\partial \tau} \quad (17)$$

subject to the initial and boundary conditions

$$\theta_a(\eta, 0) = 1, \theta_w(\eta, 0) = 1, \text{ in } 0 \leq \eta \leq 1 \quad (18)$$

$$\begin{cases} \theta_a(0, \tau) = 1, \theta_w(0, \tau) = 1 \\ \frac{\partial \theta_a(1, \tau)}{\partial \eta} = 0, \frac{\partial \theta_w(1, \tau)}{\partial \eta} = 0 \end{cases}, \text{ in } \tau \geq 0 \quad (19)$$

where, the dimensionless parameters are defined by

$$\theta_a = \frac{u_a}{u_a^0}, \theta_w = \frac{u_w}{u_w^0}, \eta = \frac{z}{H}, \tau = -\frac{k_w t}{\gamma_w m_{1k}^s H^2},$$

$$C_0 = \frac{u_w^0}{\gamma_w H}, C_1 = \frac{m_{1k}^s}{m_2^w}, C_2 = \frac{u_a^0}{u_w^0},$$

$$C_3 = \frac{k_a u_a^0}{k_w u_w^0} \frac{RT \gamma_w m_{1k}^s}{g \bar{u}_a^0 M(m_{1k}^a - m_2^a - (1-S)nu_{atm} / (\bar{u}_a^0)^2)}$$

3.2 SERIES SOLUTIONS GIVEN BY THE HAM

As a nonlinear analytical technique, the homotopy analysis method (HAM) is efficient in the selection of a series of basis functions and auxiliary linear operators, and easily makes the solution convergence. The technique is based on homotopy, which is an important part of topology. Using one interesting property of homotopy, we can transform any nonlinear problem into an infinite number of linear problems, no matter whether or not there exists a small or large parameter. These linear problems are not dependent on any small parameters, which is convenient for controlling the convergence region. After this transferring, a series solution to the nonlinear problem is then obtained by the HAM after the selection of auxiliary linear operator parameters. [13]

We chose the auxiliary linear operator,

$$L = \frac{\partial^2}{\partial \eta^2} \quad (20)$$

From Eq.(16), it is straightforward to define the nonlinear operator

$$N(\theta_w) = \frac{C_1}{I^\alpha} \frac{\partial^2 \theta_w}{\partial \eta^2} - \frac{\partial \theta_w}{\partial \tau} - C_w C_2 \frac{\partial \theta_a}{\partial \tau} \quad (21)$$

From Eq.(17), we define the operator

$$L_a(\theta_a) = C_3 \frac{\partial^2 \theta_a}{\partial \eta^2} - C_2 \frac{\partial \theta_a}{\partial \tau} - C_a \frac{\partial \theta_w}{\partial \tau} \quad (22)$$

and the initial approximation

$$\theta_0^w = \theta_0^a = 1 + \eta(1 - \eta)^2 \exp(-0.4\tau) + \eta(1 - \eta)^2 \exp(-0.2\tau) \quad (23)$$

The zero-order deformation equation is constructed as (Liao 2004)

$$(1 - p)L(\phi(\tau, \eta; p) - \theta_0^w) = pH H_f N(\phi_w(\tau, \eta; p)) \quad (24)$$

$$(1 - p)L(\phi_a(\tau, \eta; p) - \theta_0^a) = pH H_f L_a(\phi_a(\tau, \eta; p)) \quad (25)$$

subject to the conditions

$$\phi_i(\eta, 0) = 0, \text{ in } 0 \leq \eta \leq 1 \quad (26)$$

$$\begin{cases} \phi_i(0, \tau; p) = 0 \\ \frac{\partial \phi_i(1, \tau; p)}{\partial \eta} = 0 \end{cases}, \text{ in } \tau \geq 0 \quad (27)$$

where, $i = w, a$, $p \in (0, 1)$ is the embedding parameter, h is a non-zero auxiliary parameter, H_f is a auxiliary function, and ϕ is an unknown function of τ, η, p respectively. It is obviously that when $p = 0$ and $p = 1$, it respectively holds that $\phi_i(\tau, \eta, 0) = \theta_0^i, \phi(\tau, \eta, 1) = \theta_i(\tau, \eta)$. Then when p increases from 0 to 1, $\phi_i(\tau, \eta, p)$ varies from θ_0^i to $\theta_i(\tau, \eta)$. With respect to p due to the Taylors' series, $\phi_i(\tau, \eta, p)$ can be expanded, i.e.

$$\phi_i(\tau, \eta, p) = \sum_{k=0}^{+\infty} \theta_k^i(\tau, \eta) p^k \quad (28)$$

where

$$\theta_k^i(\tau, \eta) = \frac{1}{k!} \left. \frac{\partial^k \phi_i(\tau, \eta, p)}{\partial p^k} \right|_{p=0} \quad (29)$$

If h is chosen in such a way that this series is convergent at $p = 1$, so we have

$$\theta_i(\tau, \eta) = \sum_{m=0}^{+\infty} \theta_m^i(\tau, \eta) \quad (30)$$

Differentiating the zero-order deformation equations m times with respect to p , then dividing by $m!$, and finally setting $p = 0$, we have the m^{th} -order deformation equations, i.e.,

$$L(\theta_m^w(\tau, \eta) - \chi_m \theta_{m-1}^w(\tau, \eta)) = h H_f R_m^w(\tau, \eta) \quad (31)$$

$$L(\theta_m^a(\tau, \eta) - \chi_m \theta_{m-1}^a(\tau, \eta)) = h H_f R_m^a(\tau, \eta) \quad (32)$$

subject to the conditions

$$\theta_m^i(\eta, 0) = 0 \quad \text{in } 0 \leq \eta \leq 1 \quad (33)$$

$$\begin{cases} \theta_m^i(0, \tau) = 0 \\ \frac{\partial \theta_m^i(1, \tau)}{\partial \eta} = 0 \end{cases}, \quad \text{in } \tau \geq 0 \quad (34)$$

where

$$\chi_m = \begin{cases} 0, m \leq 1, \\ 1, m > 1 \end{cases} \quad (35)$$

and

$$R_m^w(\tau, \eta) = \frac{C_1}{I^\alpha} \frac{\partial^2 \theta_{m-1}^w}{\partial \eta^2} + \frac{\alpha C_0 C_1}{I^\alpha} \sum_{j=0}^{m-1} \frac{\partial^2 \theta_j^w}{\partial \eta^2} \frac{\partial \theta_{m-1-j}^w}{\partial \eta} - \frac{\partial \theta_{m-1}^w}{\partial \tau} - C_w C_2 \frac{\partial \theta_{m-1}^a}{\partial \tau} \quad (36)$$

$$R_m^a(\tau, \eta) = C_3 \frac{\partial^2 \theta_{m-1}^a}{\partial \eta^2} - C_2 \frac{\partial \theta_{m-1}^a}{\partial \tau} - C_a \frac{\partial \theta_{m-1}^w}{\partial \tau} \quad (37)$$

To satisfy the initial condition Eq.(33), we chose the auxiliary function as: $H_f = \tau$.

The solution to the above equations was obtained using Maple software. It was seen that θ_m^w, θ_m^a can be respectively expressed by

$$\theta_m^w = \sum_{i=0}^{2m+22m+32m+1} \sum_{j=0} \sum_{k=0} a_{ijk}^m(h) e^{-\frac{1}{5}i\tau} \eta^j \tau^k \quad (38)$$

$$\theta_m^a = \sum_{i=0}^{2m} \sum_{j=0}^{2m+3} \sum_{k=0}^{2m} b_{ijk}^m(h) e^{-\frac{1}{5}i\tau} \eta^j \tau^k \quad (39)$$

where $a_{ijk}^m(h), b_{ijk}^m(h)$ are dependent upon h . And $a_{ijk}^m(h), b_{ijk}^m(h)$ can be easily obtained, substituting Eqs. (38)–(39) into the m -order deformation Eqs. (31)–(35) and all coefficients a_{ijk}^m, b_{ijk}^m (see appendix A) of the solution can be obtained one by one from the first coefficients. The first coefficients were given by the initial approximation Eq.(23), i.e.,

$$\begin{aligned} a_{000}^0(h) = 1, a_{111}^0(h) = a_{131}^0(h) = 1, a_{211}^0(h) = a_{231}^0(h) = 1, \\ a_{121}^0(h) = a_{221}^0(h) = -2 \end{aligned} \quad (40)$$

So the solution can be given by

$$\theta_w(\tau, \eta) = \sum_{m=0}^{+\infty} \sum_{i=0}^{2m+22m+32m+1} \sum_{j=0} \sum_{k=0} a_{ijk}^m(h) e^{-\frac{1}{5}i\tau} \eta^j \tau^k \quad (41)$$

$$\theta_a(\tau, \eta) = \sum_{m=0}^{+\infty} \sum_{i=0}^{2m} \sum_{j=0}^{2m+3} \sum_{k=0}^{2m} b_{ijk}^m(h) e^{-\frac{1}{5}i\tau} \eta^j \tau^k \quad (42)$$

4 EXAMPLE AND VERIFICATION

It is important to ensure that the solution series can be converging. Fortunately, the convergence and the rate of approximation for the HAM solutions strongly depend on the values of the auxiliary parameter h . It is found that h must be negative ($h \in (-1, 0)$) to ensure that the solution series converges.

In order to validate the analytical solution of one-dimensional consolidation for unsaturated soil, a typical example is computed by using the analytical solution and a comparison is made between the analytical solution of the mathematic model and the numerical results obtained by the finite-difference method using the typical example. The material parameters for the example are adopted as the same parameters in Table 1 and Table 2 [3].

Table 1. The material parameters for the solution of the examples.

| | | |
|---|-----------------------|-----------------------|
| Layer thickness (m) | H | 10 |
| Initial pore-air pressure (kPa) | u_a^0 | 20 |
| Initial pore-water pressure (kPa) | u_w^0 | 40 |
| Porosity | n | 0.5 |
| Saturation | S | 0.8 |
| Coefficient of volume change (kPa ⁻¹) | m_{1k}^s | -2.5×10^{-4} |
| Ratio of two coefficients of volume change | m_2^s / m_{1l}^s | 0.4 |
| Ratio of two coefficients of volume change | m_{1k}^w / m_{1k}^s | 0.2 |
| Ratio of two coefficients of volume change | m_2^w / m_{1k}^w | 4 |

Table 2. The values of the parameters C_i ($i = 0, 1, 2, 3, w, a$).

| | | |
|--------------------------------------|-------|----------|
| Parameter of equation | C_0 | 0.4 |
| Parameter of equation | C_1 | 1.25 |
| Parameter of equation | C_2 | 0.5 |
| Parameter of equation | C_3 | 80.6 |
| Interactive constant for water phase | C_w | -0.75 |
| Interactive constant for air phase | C_a | -0.00775 |

Fig.2 and Fig.3 show that the change in the values of θ_w, θ_a at $\alpha = 2, I = 10, h = -0.001$ with τ under different η . From the dimensionless definitions of the parameters, i.e., the change in the values of pore water pressure and pore air pressure at $\alpha = 2, I = 10, h = -0.001$ with time under different depth z , we can find that the excess pore-water

pressure is gradually increasing at beginning. It reaches the highest value at about $\tau = 5$ (i.e., $t = 1250/k_w$) and then begins to dissipate. But the excess pore-air pressure reaches the highest value at about $\tau = 1$ (i.e., $t = 250/k_w$) and then begins to dissipate.

Fig.4 and Fig.5 show that the change in the values of θ_w , θ_a at $\alpha = 2$, $I = 10$, $h = -0.001$ with η under different τ . That is the excess pore-water pressure and the excess pore-air pressure increase initially, and then decrease with the depth.

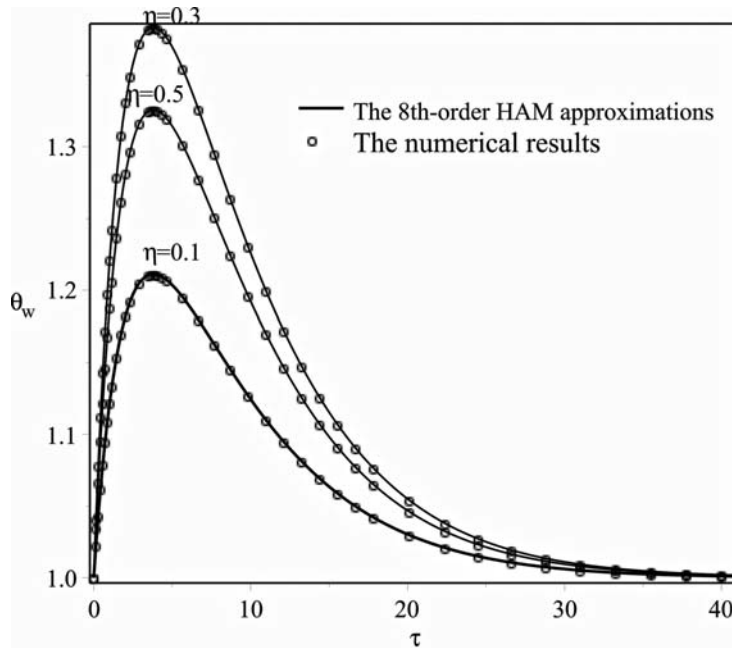


Figure 2. The 8th-order HAM approximations of θ_w at $\eta = 0.1, 0.3, 0.5$, $\alpha = 2$, $I = 10$, $h = -0.001$ open circle: the numerical results.

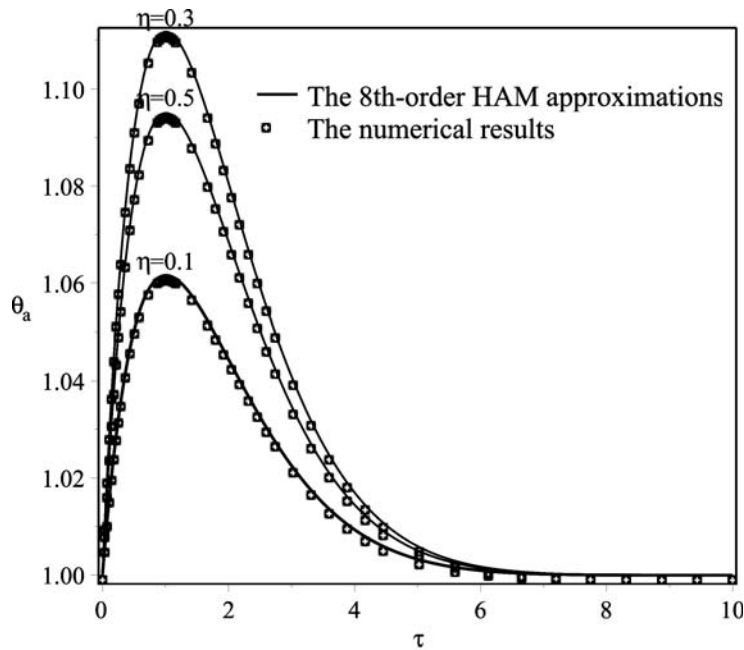


Figure 3. The 8th-order HAM approximations of θ_a at $\eta = 0.1, 0.3, 0.5$, $\alpha = 2$, $I = 10$, $h = -0.001$ open circle: the numerical results.

Figs. 2–5 show the comparison of the 8th-order HAM approximations and numerical solutions. It is clear that the computed results using the two methods are almost

the same, which proves that the analytical solution proposed in this paper is credible.

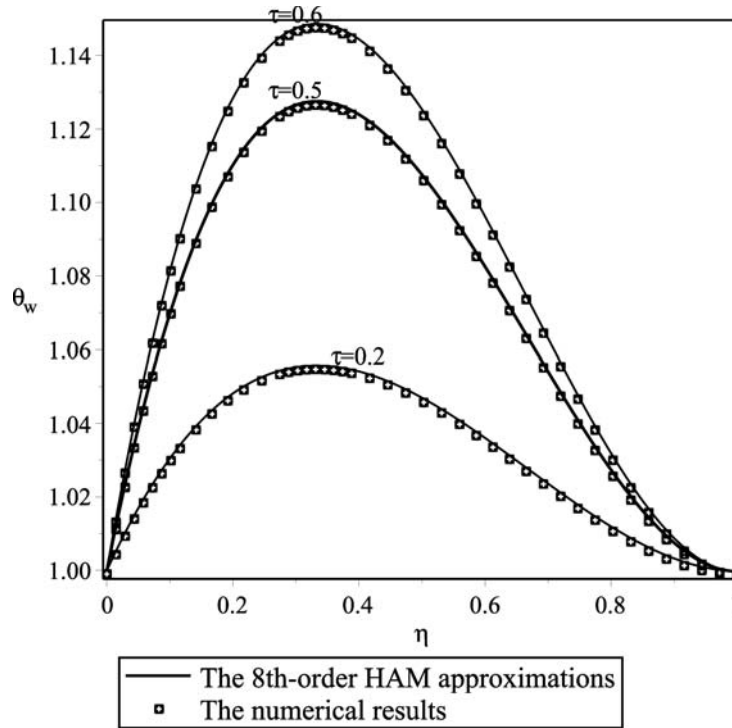


Figure 4. The 8th-order HAM approximations of θ_w at $\tau = 0.2, 0.5, 0.6, \alpha = 2, I = 10, h = -0.001$ open circle: the numerical results.

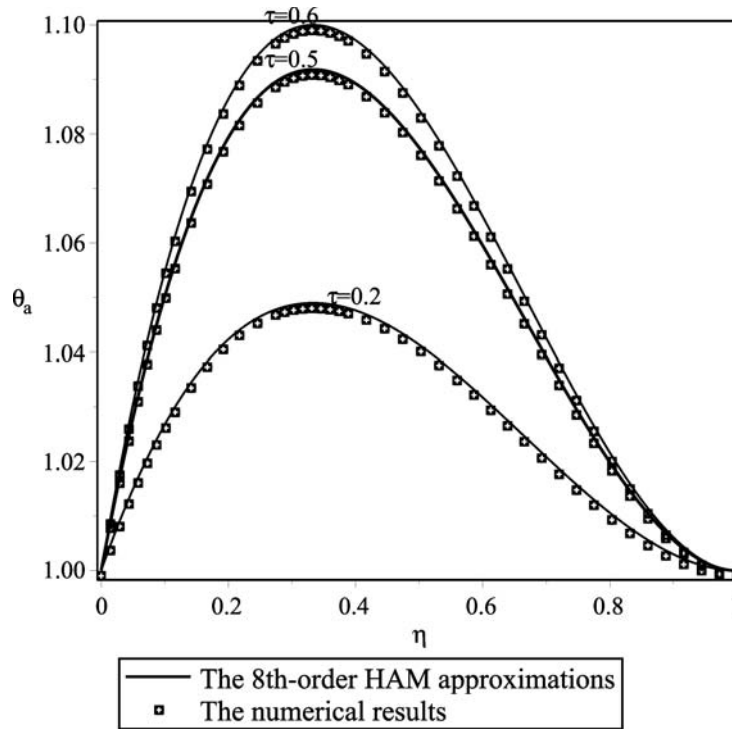


Figure 5. The 8th-order HAM approximations of θ_a at $\tau = 0.2, 0.5, 0.6, \alpha = 2, I = 10, h = -0.001$ open circle: the numerical results.

Figs. 6-7 show that the values of I have obvious effects on the dissipation values of the excess pore-water pressure. It indicates that for smaller I , there is a smaller excess

pore-water pressure. However, Fig. 6 shows that the values of I have no significant effect on the dissipation values of the excess pore-air pressure.

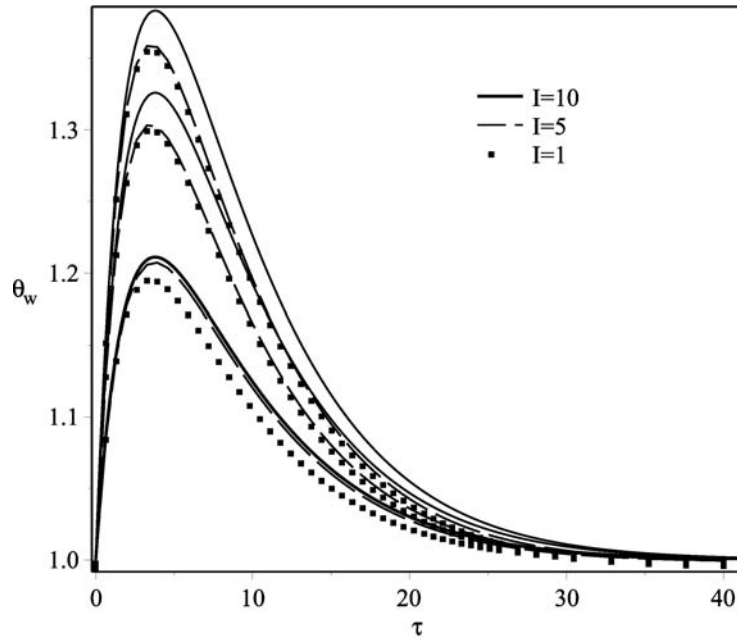


Figure 6. Change in θ_w with τ under different I at $\eta = 0.1, 0.3, 0.6$, respectively.

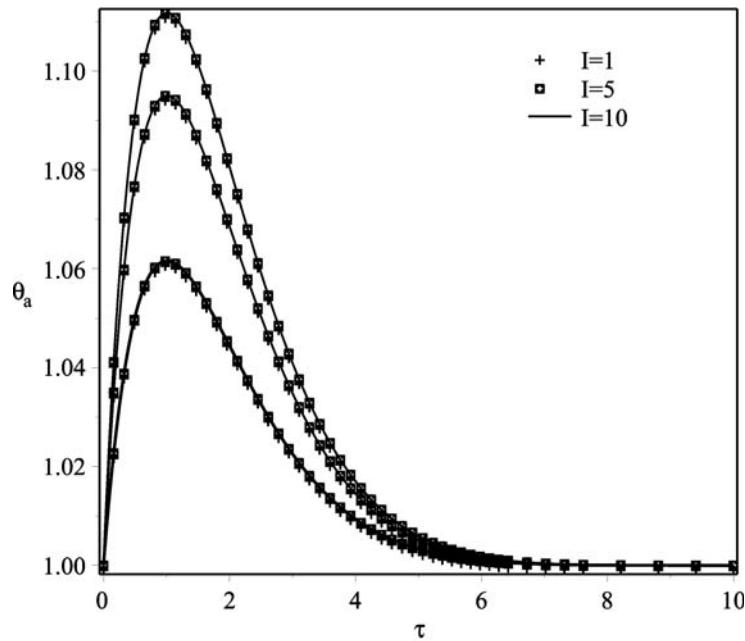


Figure 7. Change in θ_a with τ under different I at $\eta = 0.1, 0.3, 0.6$, respectively.

5 CONCLUSIONS

In this paper the water phase was assumed to obey the non-Darcy law. The simplified form of the governing equations for the one-dimensional consolidation of unsaturated soil was adopted. The series solutions based on the HAM for the excess pore-air pressure and the excess pore-water pressure were first obtained for the dimensionless consolidation in unsaturated soils. The solutions were applicable to the unsaturated soil layer with pore water and pore air pressure equivalent for the initial value at the top surface and the bottom impermeable to water and air. In addition, the validity of the present solutions was confirmed through a comparison with the numerical results.

Based on the solutions, the changes in the excess pore-air pressure and excess pore-water pressure with time were analyzed at different I and for different depths. In addition, it was found that the dissipation of air pressure was much faster than the dissipation of water pressure. Furthermore, the values of I had obvious effects on the dissipation values of the excess pore-water pressure but no significant effect on that of the excess pore-air pressure.

ACKNOWLEDGEMENTS

This research was supported by funding from the Natural National Science Foundation of China (41372296). In addition, partial support from the Doctoral Fund from the Ministry of Education of China (20100142110059) is acknowledged. A special note of appreciation is extended to the Ministry of National Science and Technology for their funding support (2012BAK10B00).

REFERENCES

- [1] Fredlund, D.G., Rahardjo, H. (1993). *Soil Mechanics for Unsaturated Soil*. John Wiley and Sons, New York.
- [2] Qin, A.F., Chen, G.J., Tan Y.W., Sun, D.A. (2008). Analytical solution to one-dimensional consolidation in unsaturated soils. *Appl. Math. Mech.*, 29:1329–1340.
- [3] Conte, E. (2004). Consolidation analysis for unsaturated soils. *Canadian Geotechnical Journal*, 41, 599–612.
- [4] Blight G.E. (1961). *Strength and consolidation characteristics of compacted soils*. Dissertation. England: University of London.
- [5] Scott, R.F. (1963). *Principles of soil mechanics*. Addison Wesley Publishing Company.
- [6] Barden L. (1965). Consolidation of compacted and unsaturated clays. *Geotechnique*, 15, 267–86.
- [7] Fredlund D.G., Hasan J.U. (1979). One-dimensional consolidation theory unsaturated soils. *Canadian Geotechnical Journal*, 17, 521–31.
- [8] Qin, A.F., Sun, D.A., Tan, Y.W. (2010). Analytical solution to one-dimensional consolidation in unsaturated soils under load varying exponentially with time. *Computers and Geotechnics*, 37, 233–238.
- [9] Shan, Z.D., Ling, D.S., Ding, H.J. (2012). Exact solutions for one dimensional consolidation of single layer unsaturated soil. *International Journal for Numerical and Analytical Methods in Geomechanics*, 36 (6), 708–722.
- [10] Cui, Y.J., Tang, A.M., Loiseau, C., Delage, P. (2008). Determining the unsaturated hydraulic conductivity of a compacted sand-bentonite mixture under constant-volume and free-swell conditions. *Phys. Chem. Earth*, 33, S462–S471.
- [11] Liu, H.H. (2011). A conductivity relationship for steady-state unsaturated flow processes under optimal flow conditions. *Vadose Zone J.*, 10, 736–740.
- [12] Liu, H.H., Jens, Birkholzer. (2012). On the relationship between water flux and hydraulic gradient for unsaturated and saturated clay. *Journal of Hydrology*, 475, 242–247.
- [13] Liao, S.J. (2003). *Beyond Perturbation: Introduction to Homotopy Analysis Method*. Chapman & Hall/CRC Press, Boca Raton.
- [14] Liao, S.J., Pop, I. (2004). Explicit analytic solution for similarity boundary layer equations, *Int. J. Heat Mass Transfer*, 47, 75–85.
- [15] Liao, S.J. (2005). A new branch of solutions of boundary-layer flows over an impermeable stretched plate. *Int. J. Heat Mass Transfer*, 48, 2529–2539.
- [16] Liao, S.J. (2006). An analytic solution of unsteady boundary-layer flows caused by an impulsively stretching plate. *Commun. Nonlinear Sci. Numer. Simul.*, 11, 326–339.
- [17] Swartzendruber, D. (1961). Modification of Darcy's law for the flow of water in soils. *Soil Sci.*, 93, 22–29 (*Soil Science Society of America Journal*, 69, 328–342.)
- [18] Fredlund, D.G., Morgenstern, N.R. (1976). Constitutive relation for volume change in unsaturated soils. *Canadian Geotechnical Journal*, 13, 386–396.

APPENDIX A

The values for $a_{ijk}^m(h), b_{ijk}^m(h)$ satisfy the recursive formula

$$L\left(\sum_{i=0}^{2m+2} \sum_{j=0}^{2m+3} \sum_{k=0}^{2m+1} a_{ijk}^m(h) e^{-\frac{1}{5}i\tau} \eta^j \tau^k - \chi_m \sum_{i=0}^{2m} \sum_{j=0}^{2m+1} \sum_{k=0}^{2m-1} a_{ijk}^m(h) e^{-\frac{1}{5}i\tau} \eta^j \tau^k\right) = hH_f \bar{R}_m^w(\tau, \eta)$$

$$L\left(\sum_{i=0}^{2m} \sum_{j=0}^{2m+3} \sum_{k=0}^{2m} b_{ijk}^m(h) e^{-\frac{1}{5}i\tau} \eta^j \tau^k - \chi_m \sum_{i=0}^{2m-2} \sum_{j=0}^{2m+1} \sum_{k=0}^{2m-2} b_{ijk}^m(h) e^{-\frac{1}{5}i\tau} \eta^j \tau^k\right) = hH_f \bar{R}_m^a(\tau, \eta)$$

where

$$\chi_m = \begin{cases} 0, m \leq 1, \\ 1, m > 1 \end{cases}$$

and

$$\begin{aligned} \bar{R}_m^w(\tau, \eta) &= \frac{C_1}{I^\alpha} \frac{\partial^2}{\partial \eta^2} \left(\sum_{i=0}^{2m} \sum_{j=0}^{2m+1} \sum_{k=0}^{2m-1} a_{ijk}^m(h) e^{-\frac{1}{5}i\tau} \eta^j \tau^k \right) \\ &+ \frac{\alpha C_0 C_1}{I^\alpha} \sum_{j=0}^{m-1} \frac{\partial^2 \theta_j^w}{\partial \eta^2} \left(\sum_{i=0}^{2j+2} \sum_{l=0}^{2j+3} \sum_{k=0}^{2j+1} a_{ijk}^m(h) e^{-\frac{1}{5}i\tau} \eta^l \tau^k \right) \frac{\partial \theta_{m-1-j}}{\partial \eta} \left(\sum_{i=0}^{2m-2} \sum_{l=0}^{2m-2} \sum_{k=0}^{2m-2} a_{ijk}^m(h) e^{-\frac{1}{5}i\tau} \eta^l \tau^k \right) \\ &- \frac{\partial}{\partial \tau} \left(\sum_{i=0}^{2m} \sum_{j=0}^{2m+1} \sum_{k=0}^{2m-1} a_{ijk}^m(h) e^{-\frac{1}{5}i\tau} \eta^j \tau^k \right) - C_w C_2 \frac{\partial}{\partial \tau} \left(\sum_{i=0}^{2m-2} \sum_{j=0}^{2m+1} \sum_{k=0}^{2m-2} b_{ijk}^m(h) e^{-\frac{1}{5}i\tau} \eta^j \tau^k \right) \end{aligned}$$

$$\begin{aligned} \bar{R}_m^a(\tau, \eta) &= C_3 \frac{\partial^2}{\partial \eta^2} \left(\sum_{i=0}^{2m-2} \sum_{j=0}^{2m+1} \sum_{k=0}^{2m-2} b_{ijk}^m(h) e^{-\frac{1}{5}i\tau} \eta^j \tau^k \right) - C_2 \frac{\partial}{\partial \tau} \left(\sum_{i=0}^{2m-2} \sum_{j=0}^{2m+1} \sum_{k=0}^{2m-2} b_{ijk}^m(h) e^{-\frac{1}{5}i\tau} \eta^j \tau^k \right) \\ &- C_a \frac{\partial}{\partial \tau} \left(\sum_{i=0}^{2m} \sum_{j=0}^{2m+1} \sum_{k=0}^{2m-1} a_{ijk}^m(h) e^{-\frac{1}{5}i\tau} \eta^j \tau^k \right) \end{aligned}$$

TVORJENJE MEZOPOR IN MIKROPOR V ELEKTRO-FILTRSKEM PEPELU ZEOLITA S TRI-STOPENJSKO AKTIVACIJO

BHAGWANJEE JHA IN D. N. SINGH

o avtorjih

Bhagwanjee Jha
Dr. B.B.A. Government Polytechnic, Karad (DP)
Dadra and Nagar Haveli, Indija
E-pošta: jha66b@yahoo.com

D. N. Singh
Indian Institute of Technology, Bombay, Powai,
Civil Engineering Department
Mumbai-400076, Indija
E-pošta: dns@civil.iitb.ac.in

izvleček

Raziskovalci so izčrpno opisali lastnosti bazno aktiviranega elektrofiltrskega pepela (ostanek) in potrdili njegove zeolitske lastnosti. Za vrednotenje njegovih uporabnih možnosti kot adsorbenta za dekontaminacijo odpadnih voda, so odločilni parametri večinoma ionska izmenjalna kapaciteta, mineralogija in morfologija. Vendar je študija lastnosti por (t.j. velikost in volumen) takšnih ostankov, še vedno osnova za predvidevanje o njihovi sposobnosti transporta onesneževalcev in pojavu difuzije. Pričujoča študija prikazuje razvoj por pri treh vrstah podobno sintetiziranih elektrofiltrskih pepelov po bazni aktivaciji in istočasno ta učinek na ostale lastnosti, t.j. specifično gravitacijo, specifično površino in ionsko izmenjalno kapaciteto. Na podlagi N₂ plinske absorpcije in infrardeče spektroskopije je dokazano, da so ostanki, pridobljeni v drugi in tretji stopnji aktivacije (vsak je bil v obdelavi 24 ur z uporabo filtratov 1,5M NaOH), bistveno obogateni z mezoporami in mikroporami v primerjavi s čistim in makro poroznim zeolitom 4A.

ključne besede

elektrofiltrski pepel, hidrotermalni postopek, tri-stopenjska aktivacija, lastnosti por

FORMATION OF MESO- AND MICRO-PORES IN FLY-ASH ZEOLITES USING A THREE-STEP ACTIVATION

BHAGWANJEE JHA and D. N. SINGH

about the authors

Bhagwanjee Jha
Dr. B.B.A. Government Polytechnic, Karad (DP)
Dadra and Nagar Haveli, India
E-mail: jha66b@yahoo.com

D. N. Singh
Indian Institute of Technology, Bombay, Powai,
Civil Engineering Department
Mumbai-400076, India
E-mail: dns@civil.iitb.ac.in

abstract

Researchers have comprehensively characterized alkali-activated fly-ash (the residue) and ascertained its highly zeolitic nature. In order to evaluate its potential for application as an adsorbent for the decontamination of waste water, the decisive parameters have mostly been the cation-exchange capacity, the mineralogy and the morphology of the residue. However, a study of the pore characteristics (e.g., the size and volume) of such residues is still warranted to anticipate their contaminant transport and the diffusion phenomena as a type of geotechnical engineering material. In this situation, the present study demonstrates the evolution of pores in the fly-ash after alkali activation up to three steps, and simultaneously, its effects on other characteristics (e.g., the specific gravity, specific surface area and the cation-exchange capacity) of three types of similarly synthesized residues (the first, produced by using a NaOH aqueous solution and the other two residues, the result of alkali activation using a NaOH spent solution, the filtrates). Based on N₂ gas absorption isotherms and infrared transmittance spectra, residues obtained from the second and third steps, each involving 24 hours of treatment using filtrates of 1.5-M NaOH, are established to be significantly enriched in the finer meso- and micro-pores, respectively, in comparison with a pure and macro-porous zeolite 4A.

keywords

fly-ash, hydrothermal treatment, three-step activation, pore characteristics

ABBREVIATIONS

| | |
|---------|---|
| AFA | alkali-activated fly-ash |
| BET | Brunauer-Emmett-Teller |
| EGME | ethylene glycol monoethyl ether |
| FAF | fly-ash filtrate |
| FAR | filtrate-activated residues |
| FEG-SEM | field-emission gun scanning electron microscopy |
| FT-IR | Fourier-transforms infrared |
| JCPDS | Joint Committee on Powder Diffraction Standards |
| MPA | micro-pore area |
| MPV | micro-pore volume |
| RZP | reference zeolite 4A powder |
| XRF | X-ray fluorescence |
| XRD | X-ray diffraction |

NOMENCLATURES

| | |
|---------------------|-----------------------------|
| CEC | cation-exchange capacity |
| G | specific gravity |
| M | molarity of NaOH |
| SSA | specific surface area |
| SSA _{BET} | surface area by BET method |
| SSA _{EGME} | surface area by EGME method |

1 INTRODUCTION

Alkali-activated fly-ash (AFA) is now an established synthetic material, as an adsorbent, for many industrial applications, e.g., waste-water and flue-gas treatment [1-6]. The credit goes to the cation-exchange capacity of the AFA, which has been thoroughly explored in the past for its likely use as a constituent for polycrystalline zeolites (the geotechnical composites) [1-8]. More specifically, the degree of coordination between [SiO₄]⁴⁻ and [AlO₄]⁵⁻ tetrahedra, present in such zeolites, governs the type of 3D framework and the creation of network of pores (e.g., voids and open spaces), which in turn affect the geotechnical application of such zeolites for waste-water or flue-gas decontamination (an

environmental cleanup project) [8]. In fact, the evolution of pores in the AFA, in general, and the presence of a distinct pore size and pore volume may be helpful in deciding their suitability for adsorbing the corresponding size of a heavy-metal contaminant (the cation) [5,8,11]. Accordingly, in the past BET analyses have been useful to quantify the pore size and the overall porosity of the AFA [8-10,12-15]. However, state-of-the-art information is limited to the zeolitic characteristics of the AFA obtained from the fly-ash–NaOH interaction by employing various hydrothermal techniques in: (1) a single step [1-7,10,11,13,16,], (2) two steps [17], and (3) three steps [18]. However, proper attention has not been given to a detailed investigation of the pore characteristics of the AFA, which is supposed to be of prime importance for the cation diffusion centric geotechnical application of such material [9]. Based on past reports on common fly-ash zeolites (e.g., Na-P1, hydroxysodalite, analcime, Na-A, Na-X and Na-Y etc.), facts about their pores have mostly been borrowed from standard data files of JCPDS (1994) [11,16], which deals with the pure form of these zeolites. To decide about the conformity of the ash zeolites to its pure zeolite counterpart, it still remains a challenging task to investigate the actual pore characteristics of the AFA, which can, in turn, be suitably evaluated for its contaminant diffusion and/or transport phenomenon, as a geotechnical engineering material [2-9,15,16]. In such a situation, the present study demonstrates how a three-step hydrothermal treatment of a fly-ash with NaOH or fly-ash filtrate (FAF) results in a remarkable growth of the pore sizes in the AFA. As such, the manuscript is framed to showcase these improvements in the AFA in detail. Also, attempts have been made to correlate the Brunauer-Emmett-Teller (BET) isotherms type with the specific gravity (G), the specific surface area (SSA), the cation exchange capacity (CEC), the Fourier transform infrared (FT-IR) transmittance bands, the X-ray fluorescence (XRF), the X-ray diffraction (XRD) studies and the field-emission-gun scanning electron microscopy (FEG-SEM) of the residues.

2 EXPERIMENTAL DETAILS

The original fly-ash (OFA) was procured from the hopper of an electrostatic precipitator of a thermal power plant in Maharashtra, India. The NaOH used for preparing its stock solution (molarity = 1.5- M) in deionized water was supplied by Thomas Baker, Mumbai, India. In order to activate the OFA and synthesize pure fly-ash zeolites, the liquid-to-solid ratio, i.e., a NaOH/OFA equal to 10, was maintained for preparing the fly-ash–NaOH slurry [7]. To investigate the residue-filtrate interaction (i.e., ignored by previous researchers

favoring a conventional hydrothermal treatment of the fly-ash–NaOH slurry only), the present manuscript addresses the hydrothermal treatment of the fly-ash up to three successive steps, in line with Jha and Singh (2013) [18], each of 24 hours at 100 °C. In particular, Step-2 and Step-3 were carried out by treating a mixture of the residue, AFA, and the filtrate, FAF of the previous step by maintaining the liquid-to-solid ratio, FAF/AFA equal to 10, in each case throughout the experiments. To evaluate the effect of these steps, each residue was characterized for physico-chemico-mineralogical, morphological and Fourier-transform infrared (FT-IR) characteristics [7-11,19,20]. For the sake of simplicity, the residue was designated by combining three parameters in a sequence: (i) a value of the molarity (M) of NaOH for the stock solution used in Step-1, and (ii) a designation for the step of the treatment and (iii) the time allowed in each step. For example, the designations 1.5-S1-24, 1.5-S2-24 and 1.5-S3-24 correspond to the residues obtained after the treatments by using 1.5- M NaOH in Step-1, Step-2 and Step-3, respectively, each for 24 hours. To ascertain the proximity of the residue to the pure zeolite, Na-A (i.e., zeolite 4A) was used as a reference zeolite powder (RZP) material for the comparative study.

3 CHARACTERIZATION

The specific gravity, G , of the sample was determined by employing an Ultra Pycnometer (Quanta chrome, USA), which works on the principle of the adsorption of helium gas [7]. The results of this analysis are presented in Table 1.

Table 1. Important parameters of fly-ash, activated fly-ashes and zeolite RZP.

| Parameter | OFA | 1.5-S1-24 | 1.5-S2-24 | 1.5-S3-24 | RZP |
|-----------------------------|------|-----------|-----------|-----------|------|
| G | 2.18 | 2.94 | 2.63 | 2.55 | 2.14 |
| SSA_{BET} (m^2/g) | 2.83 | 7.04 | 7.38 | 6.23 | 1.87 |
| SSA_{EGME} (m^2/g) | 7.0 | 33.9 | 110.5 | 155.6 | 94.5 |
| CEC (meq/100g) | 8 | 296 | 470 | 843 | 450 |

The Na^+ cation exchange capacity (CEC) of the residue was determined by following the ammonium acetate method [7,11]. The result for CEC is listed in Table 1. The investigations were carried out to study the micro-pore area (MPA) and the micro-pore volume (MPV) present in these samples. A BET set up (ASAP 2020 system V 3.01 H fitted with Micromeritics patented isothermal

jackets, Norcross, GA 30093-1877) was used and a set of standard procedures was followed for this purpose [12-15,18]. The analysis temperature was maintained at that of liquid N₂ (i.e., 195.489 °C). Also, the sample (maximum 1g) was degassed automatically under vacuum (5×10^{-3} mmHg) [19]. The results, e.g., the **SSA**, the pore volume and types of pore sizes e.g., micro-pores below 2 nm, meso-pores between 2 and 50 nm and macro-pores above 50 nm, are presented in Tables 1 to 2 and Figs. 1 to 2. The surface area, **SSA**, of the samples was also calculated by resorting to the ethyl-glycol-monoethyl ether (EGME) adsorption method [11] and the results of this analysis are presented in Table 1. Furthermore, a Fourier transform infrared (FT-IR) set up [17-19] was employed to generate the transmittance spectra of these samples by following procedures suggested by Jha and Singh (2011) [9]. The FT-IR spectra are presented in Fig. 3. The chemical compositions of the residues were investigated by carrying out quantitative analyses with the help of an XRF set up (Philips 1410, The Netherlands) [7]. The results of this analysis are presented in Table 2. Furthermore, the fly-ash and the residues were subjected to a field-emission-gun scanning electron microscopy (FEG-SEM) set up (JEOL JSM-7600F, Japan) to reveal their morphological details (e.g., surface pores and the shape and size of the crystals) [6,12,14,15]. The results of this analysis are presented in Fig. 4. Also, the mineralogy of the residue was investigated with the help of an X-ray diffraction spectrometer set up (Philips, Eindhoven, The Netherlands) and the results, as depicted in Fig. 5, were analyzed by using the JCPDS data files (1994) [20].

4 RESULTS AND DISCUSSION

In agreement with previous researchers' findings (Kolay and Singh, 2002) this study ascertains an increase in the specific gravity (**G**) and the specific surface area (**SSA**) from the fly-ash OFA to the residue 1.5-S1-24 obtained from the Step-1 treatment, as is clear from Table 1. It is also clear in this table that Step-2 results in filtrate

activated residues (FARs), which reduced the **G** and increased the **SSA** values, compared to the residues of Step-1. These changes in the FAR can be attributed to a significantly increased pore volume, from 0.01725 to 0.036 cm³/g (by 108%), as observed in Table 2. Incidentally, the Step-2 treatment is also effective in (i) the creation of smaller meso-pores (3 to 10 nm) by 6.94% (ii) a reduction in larger meso-pores, i.e., 10 to 50 nm by 5.56%, and (iii) a reduction in macro-pores by 1.4%. Accordingly, such an improvement in the pores in the Step-2 residue FAR can be responsible for the remarkably enhanced cation-exchange capacity (**CEC**) (refer to Table 1). This can be equally attributed to increased **SSA** values, in general; however, the **SSA** values obtained from the BET (N₂ gas relative pressure in between 0.05 and 0.3) correspond to the external pores, while that computed by the EGME adsorption corresponds to the total of the external and internal pores in the residues. Accordingly, Step-2 is believed to form more internal pores. Furthermore, from Table 3, quantities of SiO₂ and Al₂O₃ are found to increase due to the Step-2 treatment. This reveals that the silica dissolved during Step-1 in the filtrate is regained during the Step-2 treatment and in turn there could be (i) an improved coordination between the Si and Al tetrahedra and hence (ii) a better pore size distribution in the residue, as is apparent from Table 2.

Furthermore, it is interesting to note the characteristic changes in the residues obtained from Step-3, which results in an exceptionally high **SSA**_{EGME} value (refer Table 1). This is indicative of the formation of finer meso-pores (2–3 nm by 4.25% by volume). Most encouraging is that this step also creates some micro-pore volume by 2.1%, which can be attributed to the extraordinarily high **CEC** up to 843 meq/100g (i.e., higher than that of the reference zeolite RZP) of the residues 1.5-S3-24. In fact, the reason behind the relatively low **CEC** of the RZP could be its smaller surface area **SSA**, corresponding to macro-pores, as highlighted in Table 2. Furthermore, from Fig. 1 it is clear that the zeolite 4A exhibits more N₂ gas condensation at higher pressures than the fly-ash.

Table 2. Pore size distribution for fly-ash, activated fly-ashes based on a BET analysis.

| Sample | Total Pore volume (cm ³ /g) | Pore volume (%) contribution of various sizes (nm) | | | | |
|-----------|--|--|----------|-----------|----------|--------|
| | | < 2 | 2 to 3.0 | 3.0 to 10 | 10 to 50 | > 50 |
| | | Micro | Meso | | | Macro |
| OFA | 0.00195 | 0 | 0 | 0 | 35.89 | 64.10 |
| 1.5-S1-24 | 0.01725 | - | - | - | 33.33 | 66.67 |
| 1.5-S2-24 | 0.036 | - | - | 6.94 | 27.77 | 65.27 |
| 1.5-S3-24 | 0.0235 | 2.1 | 4.25 | 2.12 | 25.53 | 66.00 |
| RZP | 0.00325 | - | - | - | - | 100.00 |

Note: the dash indicates that the measurement is below the detection limit

Both these isotherms reveal fewer interconnected micropores, as is clear from the gap between the absorption and desorption isotherms and their open ends. Also, out of the three isotherms and the type-III hysteresis [12] for alkali-activated residues (the treated fly-ashes), 1.5-S2-24 undergo a remarkably high gas condensation in the capillaries between the meso-pores, which also exhibit a hysteresis lag between the two curves (absorption and desorption), commonly blamed for the pore blocking during desorption (referred to as the ink-bottle effect) in the residues. Such effects are relatively less noticeable in isotherms of residues 1.5-S3-24, which might be a revelation of well-interconnected micro- to meso-pores. More precisely, the dominant pore diameter in these samples was shown as black and red arrows on the $dV/[d\log(D)]$ versus pore diameter (D) curves corresponding to both adsorption and desorption, respectively, depicted in Fig. 2.

From this figure it is clear that the desorption curves terminate at smaller pore diameters than the adsorption curves. This can be attributed to (i) the reduced pore openings, which is an indication of gas condensation on the boundaries of the initial pores, (ii) the larger pores, i.e., the meso-pores get blocked and hence a reduced dominant pore diameter from the desorption trends. Such a pore-blocking effect is found to be very serious in the case of zeolite 4A, in which the desorption curve shifts remarkably to smaller pores. Exceptionally, only micropores are observable in the residue 1.5-S3-24, in which negligible pore blocking is possible for a pore diameter of less than 100 Å.

Slightly similar pore characteristics for these residues are observed from the FT-IR spectra, as indicated in Fig. 3.

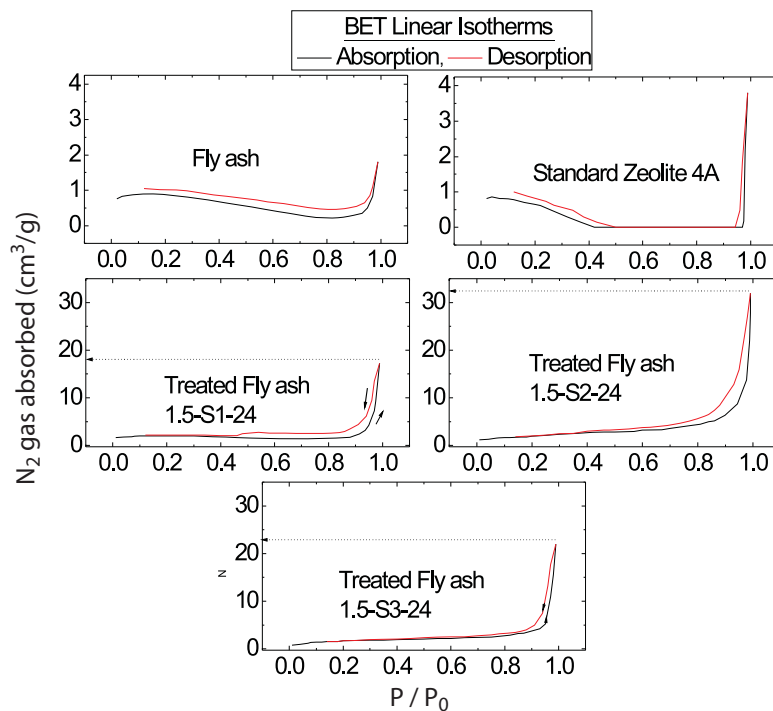


Figure 1. Variation in N_2 gas absorption with the P/P_0 ratio maintained in the BET analysis.

Table 3. Chemical composition of fly-ash, activated fly-ash residues and the zeolite RZP.

| Samples | Oxides (by Wt. %) | | | | | | | | | | | |
|-----------|-------------------|------|------|-----------|--------|------|---------|---------|----------|---------|------|---------|
| | Al_2O_3 | BaO | CaO | Fe_2O_3 | K_2O | MgO | MnO_2 | Na_2O | P_2O_5 | SiO_2 | SrO | TiO_2 |
| OFA | 26.05 | 0.14 | 1.88 | 5.14 | 0.66 | 0.39 | 0.16 | 0.054 | 10.5 | 63.85 | 0.25 | 1.52 |
| 1.5-S1-24 | 25.57 | 0.10 | 1.63 | 5.51 | 0.38 | 0.34 | 0.05 | 10.60 | NA | 48.71 | 0.04 | 1.51 |
| 1.5-S2-24 | 26.47 | 0.09 | 1.85 | 5.53 | 0.27 | 0.41 | 0.05 | 9.77 | 0.04 | 53.95 | 0.04 | 1.51 |
| 1.5-S3-24 | 34.55 | 0.09 | 1.86 | 3.60 | 0.30 | 0.39 | 0.05 | 8.57 | 0.05 | 49.13 | 0.04 | 1.40 |
| RZP | 46.04 | 0.03 | 0.22 | 0 | 0 | 0 | 0.02 | 16.87 | 0.02 | 36.57 | 0.01 | 0.24 |

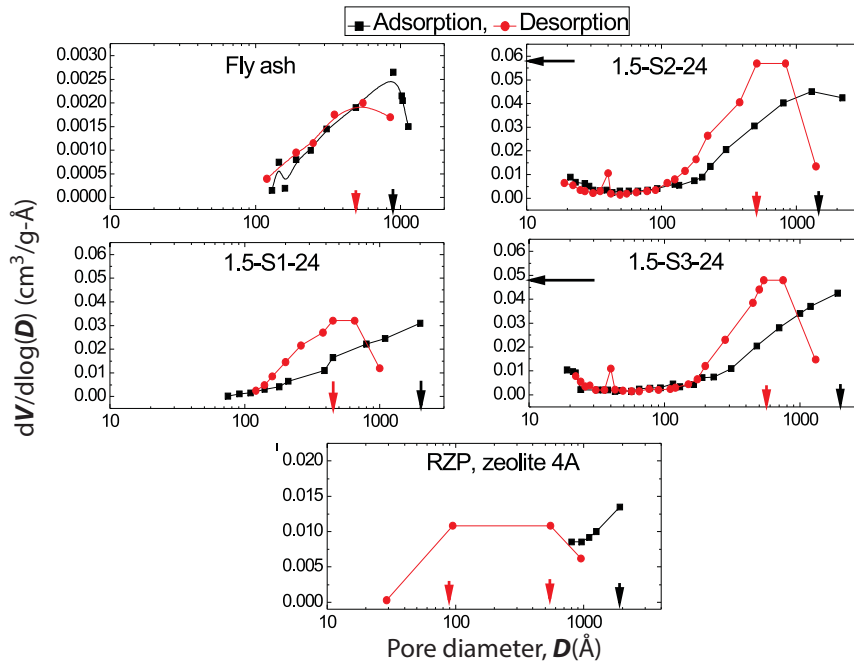


Figure 2. BJH sorption curves for the fly-ash, activated fly-ash residues and zeolite, where the black and red arrows represent the dominant pore diameters corresponding to N_2 gas adsorption and desorption, respectively.

From this figure the spectrum of zeolite 4A (designated as RZP) shows sharper bands than the residues 1.5-S2-24, which competes in the transmittance values up to nearly half of its counterpart at wave numbers, e.g., 3455, 1656, and 999 cm^{-1} . Based on the very sharp bands at 563 cm^{-1} , it is thought that the zeolite 4A is made up of a relatively more polymerized double-ring framework than the residues 1.5-S2-24 [20]. In contrast, the pore openings represented by the bands at 448 cm^{-1}

are similar for the residues 1.5-S2-24 and the zeolite RZP [7,17,18,20]. Surprisingly, the zeolite RZP and the residues 1.5-S3-24 display a negligible band at 1456 cm^{-1} (i.e., indicative of carbon or nitrogen to oxygen bonds), which might be beneficial for the residues to have a high CEC (refer Table 1). In addition, the sharper band in the spectrum of the residue 1.5-S3-24 at 448 cm^{-1} (i.e., an indication of micro-pores) is in agreement with the BET results, as is clear from Table 2).

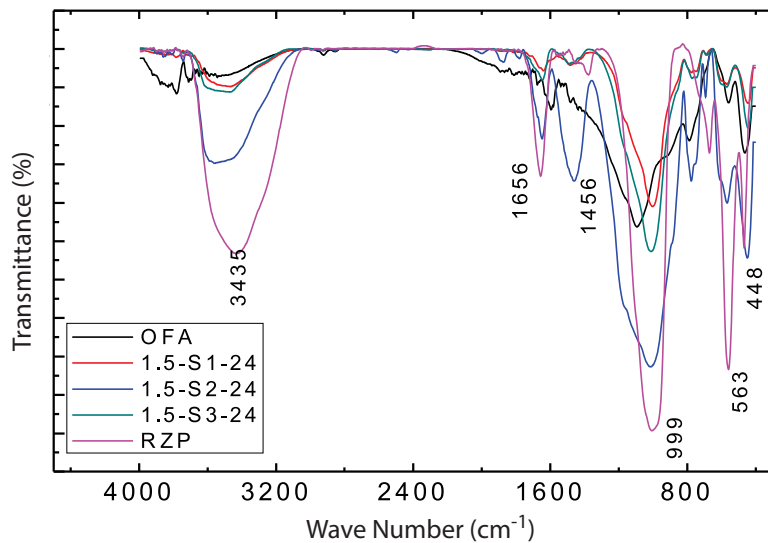


Figure 3. FT-IR spectra of the fly-ash OFA, its residues 1.5-S1-24, 1.5-S2-24, 1.5-S3-24 and the zeolite 4A.

To clarify the surface pores in these samples, Fig. 4 depicts the morphological transitions in these samples. As compared to the fly-ash OFA (i.e., a matrix of larger particles of quartz, mullite, small spherules of glass and cenospheres), the residue 1.5-S3-24 (i.e., agglomerates of spherules and cubic-to-cuboidal shaped crystals, conforming to those in the micrographs of zeolite RZP) exhibits significant changes in the particle morphology and pores (the opening between the crystals and also within their framework). A similarity between the zeolite RZP and the residues 1.5-S3-24 is also established from their XRD diffractograms, depicted in Fig. 5, which exhibits many new mineral peaks conforming to zeolite 4A, Na-P1 and X [20].

Incidentally, inactive minerals (e.g., quartz and mullite) present in the OFA are converted to zeolite Na-P1 after Step-1, which later exhibits higher intensity counts corresponding to Step- 2, and further upgraded to zeolite 4A, after the Step-3 activation. Accordingly, the increased intensity counts of zeolite Na-P1 and growth of zeolite 4A, present in 1.5-S3-24, are indicative of their

atomic-level packing and transition in pore characteristics, as well [15,20]. Thus, based on all the above discussions, the residues 1.5-S3-24 can be graded as a superior material, which is significantly enriched in *CEC*, highly porous and hydroxylated and hence a better material for waste-water decontamination.

5 CONCLUSIONS

The alkali-activated fly-ash obtained from Steps-2 and 3 became gradually enriched in smaller sizes of meso-pores (2 to 10 nm). Such pores are partially changed to micro-pores in the fly-ash residues 1.5-S3-24 obtained from Step-3 treatment using 1.5-*M* NaOH and an activation time of 24 hours. Also, a significant increase in the specific surface area, pore volume and the formation of the zeolites 4A and Na-P1 are responsible for a high cation-exchange capacity of this residue. These improvements in the residues of Steps-2 and 3 are in line with the major bands in their FT-IR spectra and FEG-SEM micrographs.

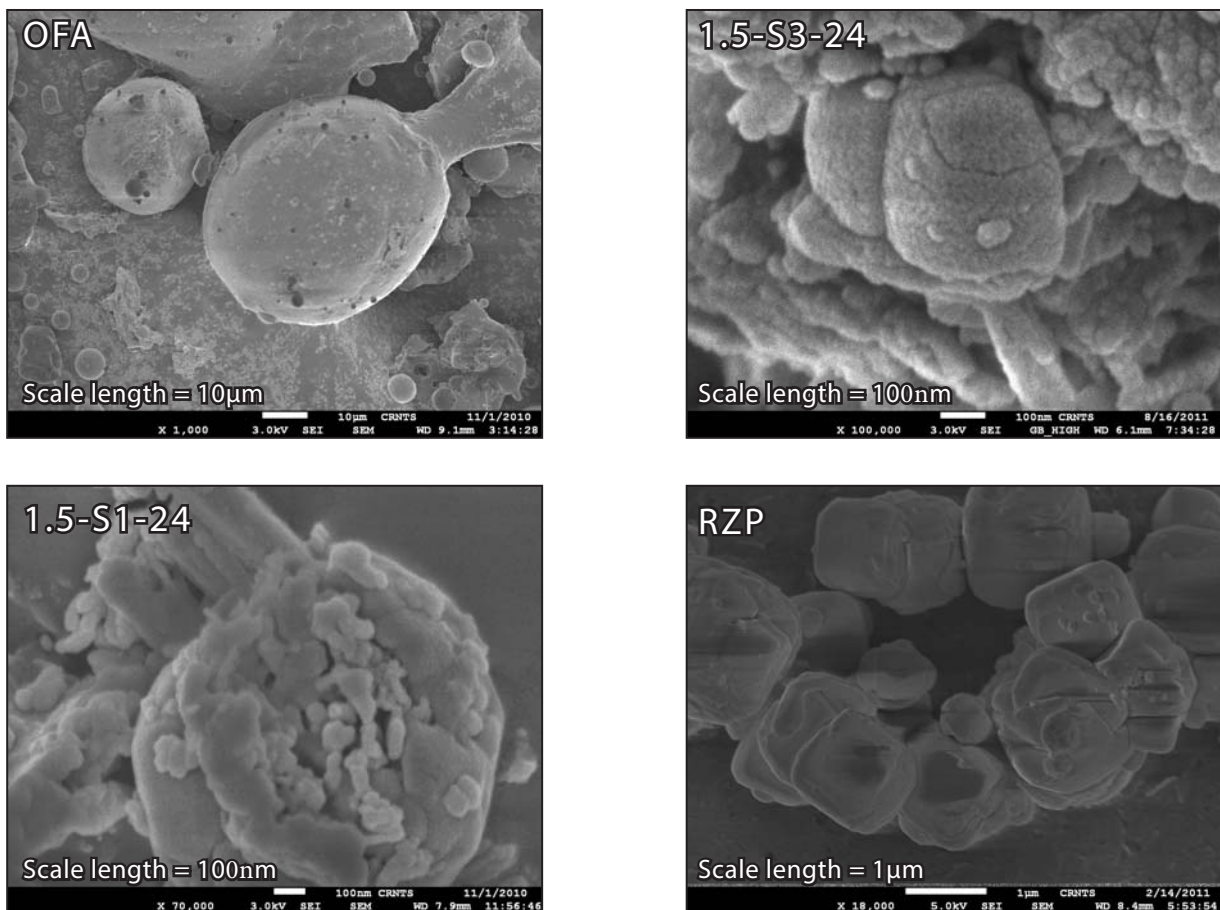


Figure 4. FEG-SEM micrographs of the fly-ash OFA, its conventional residue 1.5-S1-24, most porous residues 1.5-S3-24 and the RZP zeolite 4A.

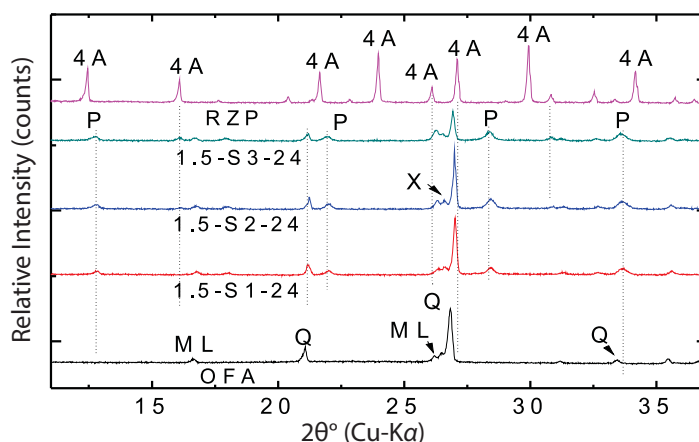


Figure 5. XRD diffractogram of the fly-ash OFA, its residues 1.5-S1-24, 1.5-S2-24, 1.5-S3-24 and zeolite 4A, where 4A, P, X, ML and Q designate zeolites 4A, Na-P1, Na-X, mullite and quartz, respectively.

REFERENCES

- [1] Lin, C.F., His, H.C. (1995). Resource recovery of waste fly-ash: synthesis of zeolite-like materials. *Environ. Sci. Technol.*, Vol. 29, pp. 1109-1117.
- [2] Berkgaut, V., Singer, A. (1996). High capacity cation exchanger by hydrothermal zeolitization of coal fly-ash. *Appl. Clay Sci.*, Vol. 10, pp. 369-378.
- [3] Kim, W., Seung-Hoon, Ahn, B.J. (1997). Synthesis of Na-P1 zeolite from coal fly-ash, *J. Ind. Eng. Chem.*, Vol. 3(3), pp. 185-190.
- [4] Kolay, P.K., Singh, D.N., Murti, M.V.R. (2001). Synthesis of zeolites from lagoon ash. *Fuel*, Vol. 80(5), pp. 739-745.
- [5] Querol, X., Moreno, N., Umana, J.C., Alastuey, A., Hernandez, E., Lopez-Soler, A., Plana, F. (2002). Synthesis of zeolites from coal fly-ash: an overview. *Int. J. Coal Geol.*, Vol. 50, pp. 413-423.
- [6] Medina, A., Gamero, P., Almanza, J.M., Vargas, A., Montoya, A., Vargas, G., Izquierdo, M. (2010). Fly-ash from a Mexican mineral coal. II. Source of W zeolite and its effectiveness in arsenic (V) adsorption. *J. Hazard. Mater.*, Vol. 181, pp. 91-104.
- [7] Jha, B., Singh, D.N. (2012). Zeolitization characteristics of fly-ashes from wet- and dry-disposal systems. *Acta Geotech. Slov.*, Vol. 9(2), pp. 63-71.
- [8] Tyrologou, P., Dudeney, A.W.L., Grattoni, C.A. (2005). Evolution of porosity in geotechnical composites. *Magn. Reson. Imaging*, Vol. 23, pp. 765-768.
- [9] Shekelford, C. (2013). The role of diffusion in environmental geotechnics. Proceedings of the 18th International Conference on Soil Mechanics and Geotechnical Engineering, Paris.
- [10] Franus, W. (2012). Characterization of X type zeolite prepared from coal fly-ash. *Pol. Environ. Stud.*, Vol. 21(2), pp. 337-343.
- [11] Jha, B., Singh, D.N. (2011). A review on synthesis, characterization and industrial application of fly-ash zeolites, *J. Mater. Educ.*, Vol. 33(1-2), pp. 65-132.
- [12] Gregg, S.J., Sing, K.S.W. (1982). Adsorption, surface area and porosity. Academic Press Inc, 2nd ed., London.
- [13] Ojha, K., Pradhan, N.C., Samanta, A.N. (2004). Zeolite from fly-ash synthesis and characterization. *Bull. Mater. Sci.*, Vol. 27, pp. 555-564.
- [14] ASAP 2020. Accelerated surface area and porosimetry system. Operator's Manual V3.0, Micromeritics Instrument Corporation, 2004-2006.
- [15] Neimark, A.V., Sing, K.S.W., Thommes, M. (2008) Surface area and porosity, Handbook of Heterogeneous Catalysis, Wiley.
- [16] Singh, D.N., Kolay, P.K. (2002). Simulation of ash water interaction and its influence on ash characteristics. *Prog. Energy Combust. Sci.*, Vol. 28 (3), pp. 267-299.
- [17] Jha, B., Nevin, K., Singh, D.N. (2014). Establishing two-stage interaction between fly-ash and NaOH by X-ray and infrared analyses, *Front. Environ. Sci. Eng.*, doi: 10.1007/s11783-014-0630-8.
- [18] Jha, B., Singh, D.N. (2013). A three step process for purification of fly-ash zeolites by hydrothermal treatment, *Appl. Clay Sci.*, <http://dx.doi.org/10.1016/j.clay.2013.12.035>.
- [19] Santen, R.A.V., Man, A.J.M.D., Kramer, G.J. (1992). Chemical bonding in zeolites, Zeolite Microporous Solids: Synthesis, Structure, and Reactivity, Kluwer Academic Publishers, Netherlands.
- [20] Joint committee on powder diffraction standards. (1994), Philadelphia-19103.

NAVODILA AVTORJEM

VSEBINA ČLANKA

Članek naj bo napisan v naslednji obliki:

- Naslov, ki primerno opisuje vsebino članka in ne presega 80 znakov.
- Izvleček, ki naj bo skrajšana oblika članka in naj ne presega 250 besed. Izvleček mora vsebovati osnove, jedro in cilje raziskave, uporabljeno metodologijo dela, povzetek izidov in osnovne sklepe.
- Največ 6 ključnih besed, ki bi morale biti napisane takoj po izvlečku.
- Uvod, v katerem naj bo pregled novejšega stanja in zadostne informacije za razumevanje ter pregled izidov dela, predstavljenih v članku.
- Teorija.
- Eksperimentalni del, ki naj vsebuje podatke o postavitvi preiskusa in metode, uporabljene pri pridobitvi izidov.
- Izidi, ki naj bodo jasno prikazani, po potrebi v obliki slik in preglednic.
- Razprava, v kateri naj bodo prikazane povezave in posplošitve, uporabljene za pridobitev izidov. Prikazana naj bo tudi pomembnost izidov in primerjava s poprej objavljenimi deli.
- Sklepi, v katerih naj bo prikazan en ali več sklepov, ki izhajajo iz izidov in razprave.
- Vse navedbe v besedilu morajo biti na koncu zbrane v seznamu literature, in obratno.

Dodatne zahteve

- Vrstice morajo biti zaporedno oštevilčene.
- Predložen članek ne sme imeti več kot 18 strani (brez tabel, legend in literature); velikost črk 12, dvojni razmik med vrsticami. V članek je lahko vključenih največ 10 slik. Isti rezultati so lahko prikazani v tabelah ali na slikah, ne pa na oba načina.
- Potrebno je priložiti imena, naslove in elektronske naslove štirih potencialnih recenzentov članka. Urednik ima izključno pravico do odločitve, ali bo te predloge upošteval.

ENOTE IN OKRAJŠAVE

V besedilu, preglednicah in slikah uporabljajte le standardne označbe in okrajšave SI. Simbole fizikalnih veličin v besedilu pišite poševno (npr. v , T itn.). Simbole enot, ki so sestavljene iz črk, pa pokončno (npr. Pa, m itn.). Vse okrajšave naj bodo, ko se prvič pojavijo, izpisane v celoti.

SLIKE

Slike morajo biti zaporedno oštevilčene in označene, v besedilu in podnaslovu, kot sl. 1, sl. 2 itn. Posnete naj

bodo v katerem koli od razširjenih formatov, npr. BMP, JPG, GIF. Za pripravo diagramov in risb priporočamo CDR format (CorelDraw), saj so slike v njem vektorske in jih lahko pri končni obdelavi preprosto povečujemo ali pomanjšujemo.

Pri označevanju osi v diagramih, kadar je le mogoče, uporabite označbe veličin (npr. v , T itn.). V diagramih z več krivuljami mora biti vsaka krivulja označena. Pomen oznake mora biti razložen v podnaslovu slike.

Za vse slike po fotografskih posnetkih je treba priložiti izvirne fotografije ali kakovostno narejen posnetek.

PREGLEDNICE

Preglednice morajo biti zaporedno oštevilčene in označene, v besedilu in podnaslovu, kot preglednica 1, preglednica 2 itn. V preglednicah ne uporabljajte izpisanih imen veličin, ampak samo ustrezne simbole. K fizikalnim količinam, npr. t (pisano poševno), pripišite enote (pisano pokončno) v novo vrsto brez oklepajev. Vse opombe naj bodo označene z uporabo dvignjene številke¹.

SEZNAM LITERATURE

navedba v besedilu

Vsaka navedba, na katero se sklicujete v besedilu, mora biti v seznamu literature (in obratno). Neobjavljeni rezultati in osebne komunikacije se ne priporočajo v seznamu literature, navedejo pa se lahko v besedilu, če je nujno potrebno.

oblika navajanja literature

V besedilu: Navedite reference zaporedno po številkah v oglatih oklepajih v skladu z besedilom. Dejanski avtorji so lahko navedeni, vendar mora obvezno biti podana referenčna številka.

Primer: »..... kot je razvidno [1,2]. Brandl and Blovsky [4], sta pridobila drugačen rezultat...«

V seznamu: Literaturni viri so oštevilčeni po vrstnem redu, kakor se pojavijo v članku. Označimo jih s številkami v oglatih oklepajih.

Sklicevanje na objave v revijah:

- [1] Desai, C.S. (2007). Unified DSC constitutive model for pavement materials with numerical implementation. Int. J. of Geomech., Vol. 7, No. 2, pp. 83-101.

Sklicevanje na knjigo:

- [2] Šuklje, L. (1969). Rheological aspects of soil mechanics. Wiley-Interscience, London

Sklicevanje na poglavje v monografiji:

- [3] Mettam, G.R., Adams, L.B., 1999. How to prepare an electronic version of your article, in: Jones, B.S., Smith, R.Z. (Eds.), Introduction to the Electronic Age. E-Publishing Inc., New York, pp. 281–304.

Sklicevanje na objave v zbornikih konferenc:

- [4] Brandl, H. and Blovsky, S. (2005). Slope stabilization with socket walls using the observational method. Proc. Int. conf. on Soil Mechanics and Geotechnical Engineering, Bratislava, pp. 2485-2488.

Sklicevanje na spletne objave:

- [5] Kot najmanj, je potrebno podati celoten URL. Če so poznani drugi podatki (DOI, imena avtorjev, datumi, sklicevanje na izvirno literaturo), se naj prav tako dodajo.

PODATKI O AVTORJIH

Članku priložite tudi podatke o avtorjih: imena, nazive, popolne poštne naslove, številke telefona in faksa,

naslove elektronske pošte. Navedite kontaktno osebo.

SPREJEM ČLANKOV IN AVTORSKE PRAVICE

Uredništvo si pridržuje pravico do odločanja o sprejemu članka za objavo, strokovno oceno mednarodnih recenzentov in morebitnem predlogu za krajšanje ali izpopolnitev ter terminološke in jezikovne korekture. Z objavo preidejo avtorske pravice na revijo ACTA GEOTECHNICA SLOVENICA. Pri morebitnih kasnejših objavah mora biti AGS navedena kot vir.

Vsa nadaljnja pojasnila daje:

Uredništvo
ACTA GEOTECHNICA SLOVENICA
Univerza v Mariboru,
Fakulteta za gradbeništvo
Smetanova ulica 17, 2000 Maribor, Slovenija
E-pošta: ags@uni-mb.si

INSTRUCTIONS FOR AUTHORS

FORMAT OF THE PAPER

The paper should have the following structure:

- A Title, which adequately describes the content of the paper and should not exceed 80 characters;
- An Abstract, which should be viewed as a mini version of the paper and should not exceed 250 words. The Abstract should state the principal objectives and the scope of the investigation and the methodology employed; it should also summarise the results and state the principal conclusions;
- Immediately after the abstract, provide a maximum of 6 keywords;
- An Introduction, which should provide a review of recent literature and sufficient background information to allow the results of the paper to be understood and evaluated;
- A Theoretical section;
- An Experimental section, which should provide details of the experimental set-up and the methods used to obtain the results;
- A Results section, which should clearly and concisely present the data, using figures and tables where appropriate;
- A Discussion section, which should describe the relationships shown and the generalisations made possible by the results and discuss the significance of the results, making comparisons with previously published work;

- Conclusions, which should present one or more conclusions that have been drawn from the results and subsequent discussion;
- A list of References, which comprises all the references cited in the text, and vice versa.

Additional requirements for manuscripts

- Use double line-spacing.
- Insert continuous line numbering.
- The submitted text of Research Papers should cover no more than 18 pages (without Tables, Legends, and References, style: font size 12, double line spacing). The number of illustrations should not exceed 10. Results may be shown in tables or figures, but not in both of them.
- Please submit, with the manuscript, the names, addresses and e-mail addresses of four potential referees. Note that the editor retains the sole right to decide whether or not the suggested reviewers are used.

UNITS AND ABBREVIATIONS

Only standard SI symbols and abbreviations should be used in the text, tables and figures. Symbols for physical quantities in the text should be written in Italics (e.g. *v*, *T*, etc.). Symbols for units that consist of letters should be in plain text (e.g. Pa, m, etc.).

All abbreviations should be spelt out in full on first appearance.

FIGURES

Figures must be cited in consecutive numerical order in the text and referred to in both the text and the caption as Fig. 1, Fig. 2, etc. Figures may be saved in any common format, e.g. BMP, JPG, GIF. However, the use of CDR format (CorelDraw) is recommended for graphs and line drawings, since vector images can be easily reduced or enlarged during final processing of the paper.

When labelling axes, physical quantities (e.g. v , T , etc.) should be used whenever possible. Multi-curve graphs should have individual curves marked with a symbol; the meaning of the symbol should be explained in the figure caption. Good quality black-and-white photographs or scanned images should be supplied for the illustrations.

TABLES

Tables must be cited in consecutive numerical order in the text and referred to in both the text and the caption as Table 1, Table 2, etc. The use of names for quantities in tables should be avoided if possible: corresponding symbols are preferred. In addition to the physical quantity, e.g. t (in Italics), units (normal text), should be added on a new line without brackets.

Any footnotes should be indicated by the use of the superscript¹.

LIST OF REFERENCES

citation in text

Please ensure that every reference cited in the text is also present in the reference list (and vice versa). Any references cited in the abstract must be given in full. Unpublished results and personal communications are not recommended in the reference list, but may be mentioned in the text, if necessary.

reference style

Text: Indicate references by number(s) in square brackets consecutively in line with the text. The actual authors can be referred to, but the reference number(s) must always be given:

Example: "... as demonstrated [1,2]. Brandl and Blovsky [4] obtained a different result ..."

List: Number the references (numbers in square brackets) in the list in the order in which they appear in the text.

Reference to a journal publication:

- [1] Desai, C.S. (2007). Unified DSC constitutive model for pavement materials with numerical implementation. *Int. J. of Geomech.*, Vol. 7, No. 2, pp. 83-101.

Reference to a book:

- [2] Šuklje, L. (1969). *Rheological aspects of soil mechanics*. Wiley-Interscience, London

Reference to a chapter in an edited book:

- [3] Mettam, G.R., Adams, L.B. (1999). How to prepare an electronic version of your article, in: Jones, B.S., Smith, R.Z. (Eds.), *Introduction to the Electronic Age*. E-Publishing Inc., New York, pp. 281–304.

Conference proceedings

- [4] Brandl, H. and Blovsky, S. (2005). Slope stabilization with socket walls using the observational method. *Proc. Int. conf. on Soil Mechanics and Geotechnical Engineering*, Bratislava, pp. 2485-2488.

Web references:

- [5] As a minimum, the full URL should be given and the date when the reference was last accessed. Any further information, if known (DOI, author names, dates, reference to a source publication, etc.), should also be given.

AUTHOR INFORMATION

The following information about the authors should be enclosed with the paper: names, complete postal addresses, telephone and fax numbers and E-mail addresses. Indicate the name of the corresponding author.

ACCEPTANCE OF PAPERS AND COPYRIGHT

The Editorial Committee of the Slovenian Geotechnical Review reserves the right to decide whether a paper is acceptable for publication, to obtain peer reviews for the submitted papers, and if necessary, to require changes in the content, length or language.

On publication, copyright for the paper shall pass to the ACTA GEOTECHNICA SLOVENICA. The AGS must be stated as a source in all later publication.

For further information contact:

Editorial Board
ACTA GEOTECHNICA SLOVENICA
University of Maribor,
Faculty of Civil Engineering
Smetanova ulica 17, 2000 Maribor, Slovenia
E-mail: ags@uni-mb.si

NAMEN REVIJE

Namen revije ACTA GEOTECHNICA SLOVENICA je objavljjanje kakovostnih teoretičnih člankov z novih pomembnih področij geomehanike in geotehnike, ki bodo dolgoročno vplivali na temeljne in praktične vidike teh področij.

ACTA GEOTECHNICA SLOVENICA objavlja članke s področij: mehanika zemljin in kamnin, inženirska geologija, okoljska geotehnika, geosintetika, geotehnične konstrukcije, numerične in analitične metode, računalniško modeliranje, optimizacija geotehničnih konstrukcij, terenske in laboratorijske preiskave.

Revija redno izhaja dvakrat letno.

AVTORSKE PRAVICE

Ko uredništvo prejme članek v objavo, prosi avtorja(je), da prenese(jo) avtorske pravice za članek na izdajatelja, da bi zagotovili kar se da obsežno razširjanje informacij. Naša revija in posamezni prispevki so zaščiteni z avtorskimi pravicami izdajatelja in zanje veljajo naslednji pogoji:

fotokopiranje

V skladu z našimi zakoni o zaščiti avtorskih pravic je dovoljeno narediti eno kopijo posameznega članka za osebno uporabo. Za naslednje fotokopije, vključno z večkratnim fotokopiranjem, sistematičnim fotokopiranjem, kopiranjem za reklamne ali predstavitvene namene, nadaljnjo prodajo in vsemi oblikami nedobičkonosne uporabe je treba pridobiti dovoljenje izdajatelja in plačati določen znesek.

Naročniki revije smejo kopirati kazalo z vsebino revije ali pripraviti seznam člankov z izvlečki za rabo v svojih ustanovah.

elektronsko shranjevanje

Za elektronsko shranjevanje vsakršnega gradiva iz revije, vključno z vsemi članki ali deli članka, je potrebno dovoljenje izdajatelja.

ODGOVORNOST

Revija ne prevzame nobene odgovornosti za poškodbe in/ali škodo na osebah in na lastnini na podlagi odgovornosti za izdelke, zaradi malomarnosti ali drugače, ali zaradi uporabe kakršnekoli metode, izdelka, navodil ali zamisli, ki so opisani v njej.

AIMS AND SCOPE

ACTA GEOTECHNICA SLOVENICA aims to play an important role in publishing high-quality, theoretical papers from important and emerging areas that will have a lasting impact on fundamental and practical aspects of geomechanics and geotechnical engineering.

ACTA GEOTECHNICA SLOVENICA publishes papers from the following areas: soil and rock mechanics, engineering geology, environmental geotechnics, geosynthetic, geotechnical structures, numerical and analytical methods, computer modelling, optimization of geotechnical structures, field and laboratory testing.

The journal is published twice a year.

COPYRIGHT

Upon acceptance of an article by the Editorial Board, the author(s) will be asked to transfer copyright for the article to the publisher. This transfer will ensure the widest possible dissemination of information. This review and the individual contributions contained in it are protected by publisher's copyright, and the following terms and conditions apply to their use:

photocopying

Single photocopies of single articles may be made for personal use, as allowed by national copyright laws. Permission of the publisher and payment of a fee are required for all other photocopying, including multiple or systematic copying, copying for advertising or promotional purposes, resale, and all forms of document delivery.

Subscribers may reproduce tables of contents or prepare lists of papers, including abstracts for internal circulation, within their institutions.

electronic storage

Permission of the publisher is required to store electronically any material contained in this review, including any paper or part of the paper.

RESPONSIBILITY

No responsibility is assumed by the publisher for any injury and/or damage to persons or property as a matter of product liability, negligence or otherwise, or from any use or operation of any methods, products, instructions or ideas contained in the material herein.